

TO MUM AND DAD

THE WEAR OF POLYMERS DURING SLIDING
UNDER FLUID-CONTAMINATED CONDITIONS

By

WAYNE LINDSAY SKELCHER, B.Sc.

A thesis submitted for the degree of

DOCTOR OF PHILOSOPHY

THE UNIVERSITY OF ASTON IN BIRMINGHAM

JANUARY 1982

SUMMARY

THE WEAR OF POLYMERS DURING SLIDING UNDER FLUID-CONTAMINATED CONDITIONS

By WAYNE LINDSAY SKELCHER

A thesis submitted for the degree of

DOCTOR OF PHILOSOPHY

1982

Polymer-based dry bearings are widely used in the aircraft industry. In many applications, these materials may fail to achieve their required performances as a result of contamination by fluids, such as, water, fuel, oils and greases. The purpose of this project is to examine in detail some of the fundamental mechanisms underlying the effects produced by contaminants.

Meaningful measurements of wear are only possible when elastohydrodynamic effects are negligible and the surfaces remain in solid contact within the boundary lubrication regime. A rotating pin-on-ring apparatus has been built to measure the friction and wear of polymers under these conditions. The polymer used was Polyphenylene Oxide (PPO) and the lubricants were polydimethyl siloxane silicone fluids of different viscosities. The worn surfaces of the polymer were examined for the presence of silicon by Electron Probe Microanalysis and Rutherford backscattering. A depth of silicon to approximately $8\mu\text{m}$ was found in samples worn under boundary-lubricated sliding conditions. When the external lubricant was removed, one might expect the coefficient of friction to rise from its value under boundary-lubricated sliding to its value under dry sliding conditions after about $8\mu\text{m}$ of wear. In fact, the rise in friction did not occur until several hundred microns of wear of the polymer. Scanning electron microscopy was used to identify any change in the surface and an indentation experiment was devised to detect changes in mechanical properties of the surface layers.

The general conclusion from the experimental results is that a plasticised layer is formed on the surface of the polymer, which migrates further into the polymer during wear under starved lubrication conditions, still maintaining a low coefficient of friction.

Finally, an attempt is made to quantify the changes in some of the mechanical properties of the polymer which have occurred as a result of sliding under boundary-lubricated conditions, using a theory of boundary lubrication.

Polymer / Boundary Lubrication / Friction / Wear / Silicone Fluid

ACKNOWLEDGEMENTS

I would like to acknowledge my supervisor, Dr. T.F.J. Quinn (Physics Department, Aston University) for his help during the work contained in this thesis. I am indebted to my other supervisor, Dr. J.K. Lancaster (R.A.E. Farnborough) for the many valuable discussions and for his useful advice. Thanks are due to Mr. J.L. Sullivan (Physics Department, Aston University) for his help, interest and encouragement in the final stages of completing this thesis.

I am grateful to the staff of the Physics Workshop, in particular to Frank Lane for his effort and interest shown in the apparatus and to Howard Arrowsmith for his practical assistance. Thanks are also due to Mr. R. Howell (Metallurgy Department, Aston University) for instruction in the use of the Electron Probe Microanalyser, and also to Dr. L. Earwaker and Mr. A. Bentley (Radiation Centre, Birmingham University), for their help with the Rutherford backscattering experiments.

Financial assistance for the project was provided by the Science Research Council and by the Royal Aircraft Establishment, Farnborough.

Finally, I would like to thank Professor S.E. Hunt, Head of the Department of Physics, in whose laboratories, the majority of the work was carried out.

CONTENTS

	PAGE
CHAPTER 1 : INTRODUCTION	1
1.1 Polymeric Materials	2
1.2 Friction of Polymers	7
1.3 Wear of Polymers	8
1.4 Friction and Wear of Dry Bearing Materials	10
1.5 Lubrication of Polymers	11
1.6 Research Program	16
CHAPTER 2 : EXPERIMENTAL EQUIPMENT AND PROCEDURE	
2.1 Boundary Lubrication Apparatus	19
2.1.1 Introduction	19
2.1.2 Design Principle	20
2.1.3 The Wear Counterface	20
2.1.4 Wear Pins and Holder	26
2.1.5 Measurement of Wear	31
2.1.6 Measurement of Friction	31
2.1.7 Load Application	32
2.1.8 Rotary Motion of the Pin and Wear Counterface	34
2.1.9 Lubricants and Application	34
2.2 Electron Probe Microanalysis (E.P.M.A.)	35
2.3 Rutherford Backscattering (R.B.S.)	37
2.4 Indentation Tests	44
2.4.1. Introduction	44
2.4.2 Experimental Details of Indentation Tests	45
2.5 X-Ray and Electron Diffraction	48
2.6 Differential Thermal Analysis	49

CHAPTER 3 : EXPERIMENTAL RESULTS		
3.1	Friction and Wear	50
	3.1.1 Establishing Conditions for Boundary Lubrication	50
	3.1.2 Measurements	50
3.2	Electron Probe Microanalysis (E.P.M.A.)	61
3.3	Rutherford Backscattering (R.B.S.)	75
	3.3.1 Results	75
	3.3.2 Computer Simulation of Results	81
3.4	Scanning Electron Microscopy (S.E.M.)	87
3.5	Indentation Results	94
	CHAPTER 4 : DISCUSSION	100
	CHAPTER 5 : CONCLUSIONS AND FURTHER WORK	119
	APPENDIX 1	123
	REFERENCES	124

TABLES

		PAGE
Table 1.1	MAIN POLYMERS OF INTEREST FOR BEARINGS.	5
Table 1.2	MAIN FILLERS OF INTEREST FOR BEARINGS.	5
Table 4.1	VALUES FOR μ_D , μ_L^s , μ_L^e AND μ_{-L} FOR VARIOUS SPEEDS WITH A LOAD OF 11N AND 10CS VISCOSITY SILICONE FLUID.	112

FIGURES

Fig. 1.1	Diagram of the Tornado Swing-wing Aircraft showing the Positions of Dry Bearings (Reproduced by Kind Permission of R.A.E. Farnborough).	3
Fig. 1.2	Diagram of Lynx Helicopter showing the Positions of Dry Bearings (Reproduced by Kind Permission of R.A.E. Farnborough).	4
Fig. 1.3	(a), (b) and (c) Representation of Linear, Branched and Crosslinked Polymers.	6
Fig. 1.4	Lubrication Regimes.	12
Fig. 1.5	Stribeck Curve.	14
Fig. 2.1	Schematic Diagram to show the Design Principle.	21
Fig. 2.2	Some Important Features of the Boundary Lubrication Apparatus.	22
Fig. 2.3	Rear-side View of Apparatus showing the Axis of Rotation.	23

Fig. 2.4	Details of Wear Counterface (Detachable from the Apparatus).	24
Fig. 2.5	Details of Wear Counterface, Wear Pin and Gear Assembly.	25
Fig. 2.6	Ring Extractor.	27
Fig. 2.7	Wear Pin and Wear Pin Holder.	28
Fig. 2.8	(a) and (b) Structure of Polyphenylene Oxide and Silicone Fluid.	29
Fig. 2.9	Schematic Diagram of Wear Pin Holder.	30
Fig. 2.10	Diagram to show the Application of Load using Coil Springs.	33
Fig. 2.11	Mounting of Specimens for Electron Probe Microanalysis.	36
Fig. 2.12	Schematic Diagram of the Experimental Apparatus used for Rutherford Backscattering.	38
Fig. 2.13	Representation of Conservation of Momentum.	40
Fig. 2.14	The Dependence of α -particle Recoil Energy with Atomic Mass.	41
Fig. 2.15	Idealised Spectrum showing the Yield Variation for Equal Numbers of Atoms of Each Element.	43
Fig. 2.16	Indentation Tester.	46
Fig. 2.17	Practical Details of Indentation Tester.	47
Fig. 3.1	Variation of Coefficient of Friction with Speed for Different Loads and Viscosities.	51

Fig. 3.2	Variation of Coefficient of Friction versus the Dimensionless Parameter $\frac{\eta N}{P}$.	52
Fig. 3.3	Coefficient of Friction versus Speed for a Load of 11N (Dry and Lubricated with 10cs Silicone Fluid).	53
Fig. 3.4	Wear Rates versus Speed for a Load of 11N, for Dry Conditions and Lubricated with 10cs Silicone Fluid.	55
Fig. 3.5	Typical Chart Recorder Trace showing Friction and Wear.	56
Fig. 3.6	Two Typical Chart Recorder Traces for the Speed of 0.021ms^{-1} , showing Induction and Dwell Periods.	57
Fig. 3.7	Depth of Wear before Rise in Friction to Dry Value versus Duration of Lubricated Sliding, for Three Different Speeds of Sliding, 0.0037ms^{-1} , 0.021ms^{-1} and 0.25ms^{-1} .	59
Fig. 3.8	Critical Period of Lubricated Sliding versus Speed.	60
Fig. 3.9	(a), (b) and (c) X-Ray Distributions of Ag and Si and Electron Micrograph of the Transverse Section through a Polymer Pin Worn under Conditions of Boundary Lubrication (Speed 0.0037ms^{-1} , 10cs Viscosity Silicone Fluid, 11N Load), Magnification X1000.	62
Fig. 3.10	(a), (b) and (c) X-Ray Distributions of Ag and Si and Electron Micrograph of the Transverse Section through a Polymer Pin Worn under the same Conditions as in Fig. 3.9, Magnification X1000.	63
Fig. 3.11	(a), (b) and (c) X-Ray Distributions of Ag and Si and Electron Micrograph of the Transverse Section through a Polymer Pin Worn under Conditions of Boundary Lubrication (Speed 0.021ms^{-1} , 10cs Viscosity Silicone Fluid, 11N Load), Magnification X1000.	64

Fig. 3.12	(a) and (b) A Typical Example of the X-Ray Distribution of Si and Electron Micrograph of the Transverse Section through a Polymer Pin Worn under the same Conditions as in Fig. 3.9, except for 7,000 Revolutions of Lubricated Sliding, (using the later method of specimen preparation), Magnification X1000.	65
Fig. 3.13	(a) and (b) X-Ray Distribution of Si and Electron Micrograph of the Transverse Section through a Polymer Pin Worn under the same Conditions as in Fig. 3.12, Magnification X1000.	66
Fig. 3.14	(a), (b) and (c) X-Ray Distributions of Ag and Si and Electron Micrograph from an area on the edge of the Specimen used in Fig. 3.9 which was not in Sliding Contact, Magnification X1000.	68
Fig. 3.15	(a) and (b) A Typical Example of the X-Ray Distribution of Si and Electron Micrograph for an Unworn Pin, Magnification X1000.	69
Fig. 3.16	(a) and (b) A Typical Example of the X-Ray Distribution of Si and Electron Micrograph for an Unworn Pin, Magnification X1000.	70
Fig. 3.17	A Line-profile of Si across the Surface of a Polymer Pin worn under Boundary-lubricated Sliding Conditions (Speed 0.021ms^{-1} , 10cs Viscosity Fluid, 11N Load), Magnification X120, Total Distance of Scan is 0.8mm.	71
Fig. 3.18	A Line-profile of Si across a Section of the same Pin as used in Fig. 3.17, Magnification X750, Total Distance of Scan is 0.14mm.	72
Fig. 3.19	(a) and (b) Two Electron Micrographs with Different Exposures of the Area over which the Line-profile was taken in Fig. 3.17, Magnification X120.	73

Fig. 3.20	(a) and (b) Two Ideal Spectra for a Single Element (a) and for Two Elements (b) from a Rutherford Backscattering Experiment.	76
Fig. 3.21	Rutherford Backscattering Spectrum for an Unworn Pin of PPO.	78
Fig. 3.22	Rutherford Backscattering Spectrum from a Microtomed Granule of PPO.	79
Fig. 3.23	Rutherford Backscattering Spectrum from a Microtomed Unworn Pin of PPO.	80
Fig. 3.24	Rutherford Backscattering Spectrum from a Worn Pin of PPO (Speed 0.0037ms^{-1} , 10cs Viscosity Fluid, 11N Load).	82
Fig. 3.25	(a) and (b) Two Computer Simulations of Rutherford Backscattering Spectra for (a) the Pure Granule of PPO and (b) the Worn Pin of PPO.	83
Fig. 3.26	An Energy Dispersive Analysis of the Surface of a Worn Pin of PPO.	85
Fig. 3.27	Representation of the Variation of the Ratio of Silicone Fluid to Polymer Molecules with Depth, derived from Rutherford Backscattering Computer Simulation Results.	86
Fig. 3.28	Rutherford Backscattering Spectrum from a Microtomed Pin of PPO, worn under Boundary Lubrication Conditions (Speed 0.0037ms^{-1} , 10cs Viscosity Silicone Fluid, 11N Load). The Depth of Microtoming is approximately 10 μm .	88
Fig. 3.29	Fig. 3.23 superimposed on Fig. 3.24.	89
Fig. 3.30	Fig. 3.22 superimposed on Fig. 3.28.	90

Fig. 3.31	A Scanning Electron Micrograph of a Pin Worn under Boundary Lubrication Conditions, Magnification X1200.	91
Fig. 3.32	(a) and (b) Two Scanning Electron Micrographs showing a Large Region of Plasticised Polymer, (a) Magnification X200 and (b) an Area within this Region, Magnification X4900.	93
Fig. 3.33	Results from Indentation Tests at Different Temperatures for a Worn Pin.	95
Fig. 3.34	Results from Indentation Tests at Different Temperatures for an Unworn Pin.	96
Fig. 3.35	Indentation Depth versus Temperature, (A), (B)-Unworn Samples of PPO, (C)-Worn Pins (Speed 0.0037ms^{-1} , 10cs Viscosity Fluid, 11N Load).	97
Fig. 3.36	Result from Thermomechanical Analyser, giving a Tg of 147°C .	99
Fig. 4.1	(a) and (b) Two Scanning Electron Micrographs of PPO sliding against Stainless Steel in the presence of Methanol under Boundary Lubrication Conditions, (a) Magnification X1500 and (b) Magnification X2000. (Reproduced from Evans (24)).	106
Fig. 4.2	Variation of α , (The Fraction of the Real Area of Contact at which Polymer/Metal Contact occurs) with Sliding Speed.	113
Fig. 4.3	Variation of S , (the Shear Strength of the Polymer) with Sliding Speed.	114
Fig. 4.4	Variation of S_L , (the Shear Strength of the Lubricant) with Sliding Speed.	115
Fig. 4.5	Variation of μ_L^e , (the Coefficient of Friction at the end of a Lubricated Experiment) with Sliding Speed.	116

CHAPTER ONE

INTRODUCTION

The applications of unlubricated-'dry'-bearing materials has increased in recent years. The advantages of using this type of bearing occur when maintenance is difficult or costly, when contamination arises and where fluid lubrication is impossible (e.g. at high or low temperatures) (1,2).

The requirements of a dry bearing material are that it must be able to support an applied load in a given environment without significant distortion, deformation or loss in strength and possess a low coefficient of friction and wear rate, which are preferably unaffected by small changes in the environment (1). Four groups of materials satisfy all, or most of these requirements. The main group is that of composites, i.e. synthetic polymers to which fillers or reinforcements are added to improve mechanical properties. The second group comprises, carbons and graphites (with additives) which are important for applications at higher temperatures than are normally possible with composites. The third group is solid film lubricants, based on Polytetrafluoroethylene (PTFE) or lamellar solids such as graphite or Molybdenum Disulphide (MoS_2). These materials are used in conjunction with suitable metallic or non-metallic substrates when a particularly low coefficient is required. The last group consists of hard metals, ceramics and cermets, either in bulk form or as coatings on a metallic substrate, and are used for high temperature applications - above about 400°C .

This dissertation is relevant to the first group, i.e. the polymer-based dry bearing materials. Polymer-based dry bearings are used extensively in military and civil aircraft. Examples of the more crucial uses in the Tornado swing-wing aircraft and

Lynx helicopter, are shown in Fig. 1.1 and Fig. 1.2 respectively. Dry bearings do not always operate in dry conditions. They may be greased on assembly, either by accident or design, they may operate whilst 'lubricated' by process fluids, or they may be contaminated in service. Contamination by fluids may result in the failure of materials chosen for optimum friction and wear to reach the required performance. The wear of polymers during lubricated or contaminated conditions has not so far, been widely examined. The purpose of this research is to examine in detail, some of the fundamental mechanisms underlying these effects.

1.1 Polymer Materials

There are many polymers commercially available but only a small proportion of these are used in dry bearing applications. These are listed in Table 1.1 under the classification of thermoplastics and thermosets (1). Linear and branched polymers can be induced to flow with the application of heat and/or stress or can be dissolved in suitable solvents, (see Fig. 1.3(a) and Fig. 1.3(b)) (3). This property enables them to be moulded. Hence, these polymers are referred to as thermoplastics. Thermoplastics can possess varying degrees of crystallinity, but are seldom, if ever, completely crystalline or completely amorphous. Crystallinity in polymers develops through spherulitic growth, at various heterogeneous nuclei. The growth occurs in a radial fashion with ribbonlike lamellae which become more distorted with distance from the nucleus of growth. The lamellae are about 100Å thick and consist of chains which are folded and packed close to one another. In crosslinked polymers, molecular flow and separation by solution are prevented by strong primary valence forces (3). A crosslinked polymer is depicted in Fig. 1.3(c). Crosslinked polymers cannot be moulded and are known as thermosets.

In comparison with the thermal and mechanical properties of mild steel, the tensile strengths of polymers are lower by a factor of about 10, their elastic moduli and thermal conductivities are lower by a factor of 100, and their thermal coefficients

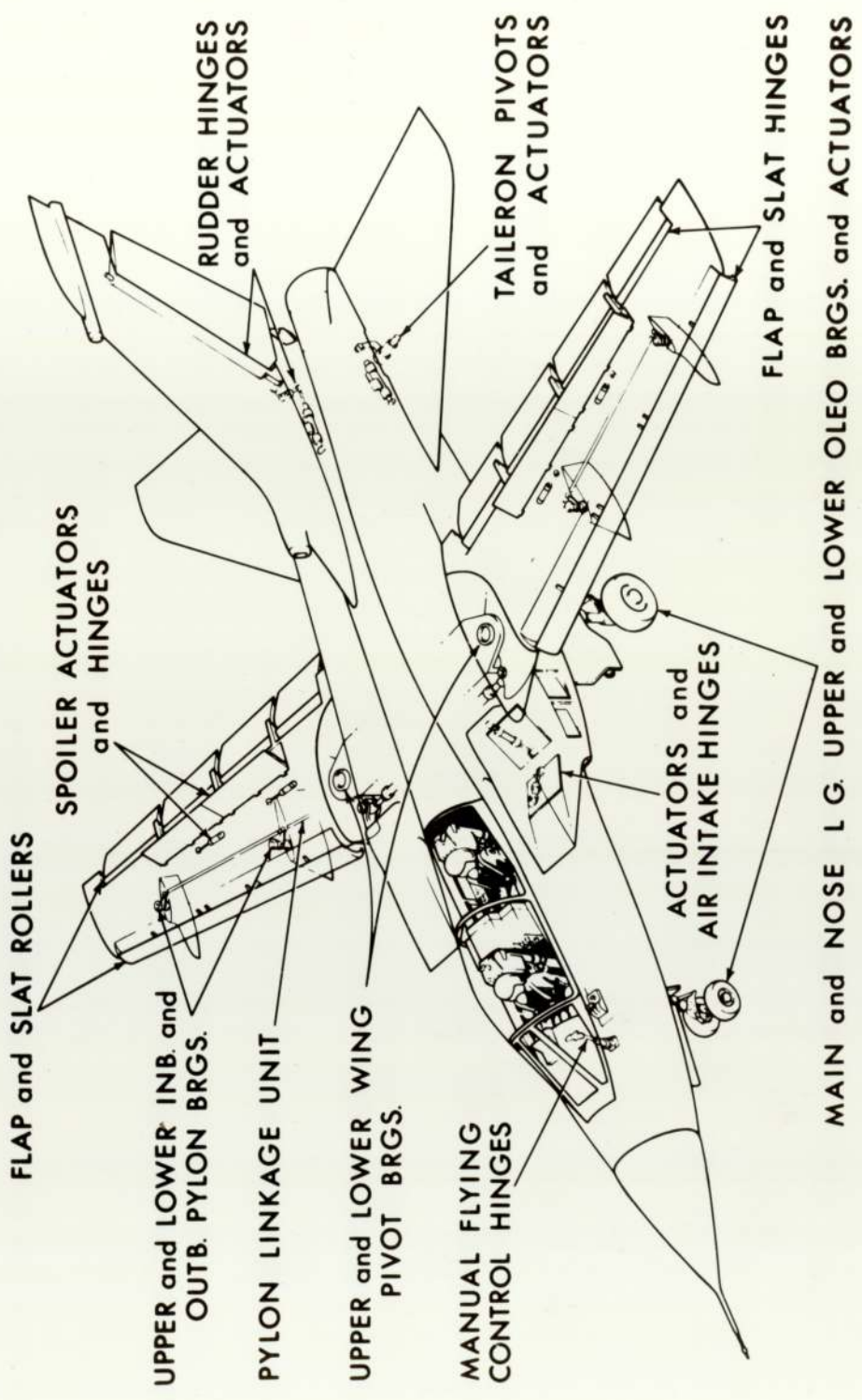


Fig.1.1 Diagram of the Tornado Swing-wing Aircraft showing the Positions of Dry Bearings.

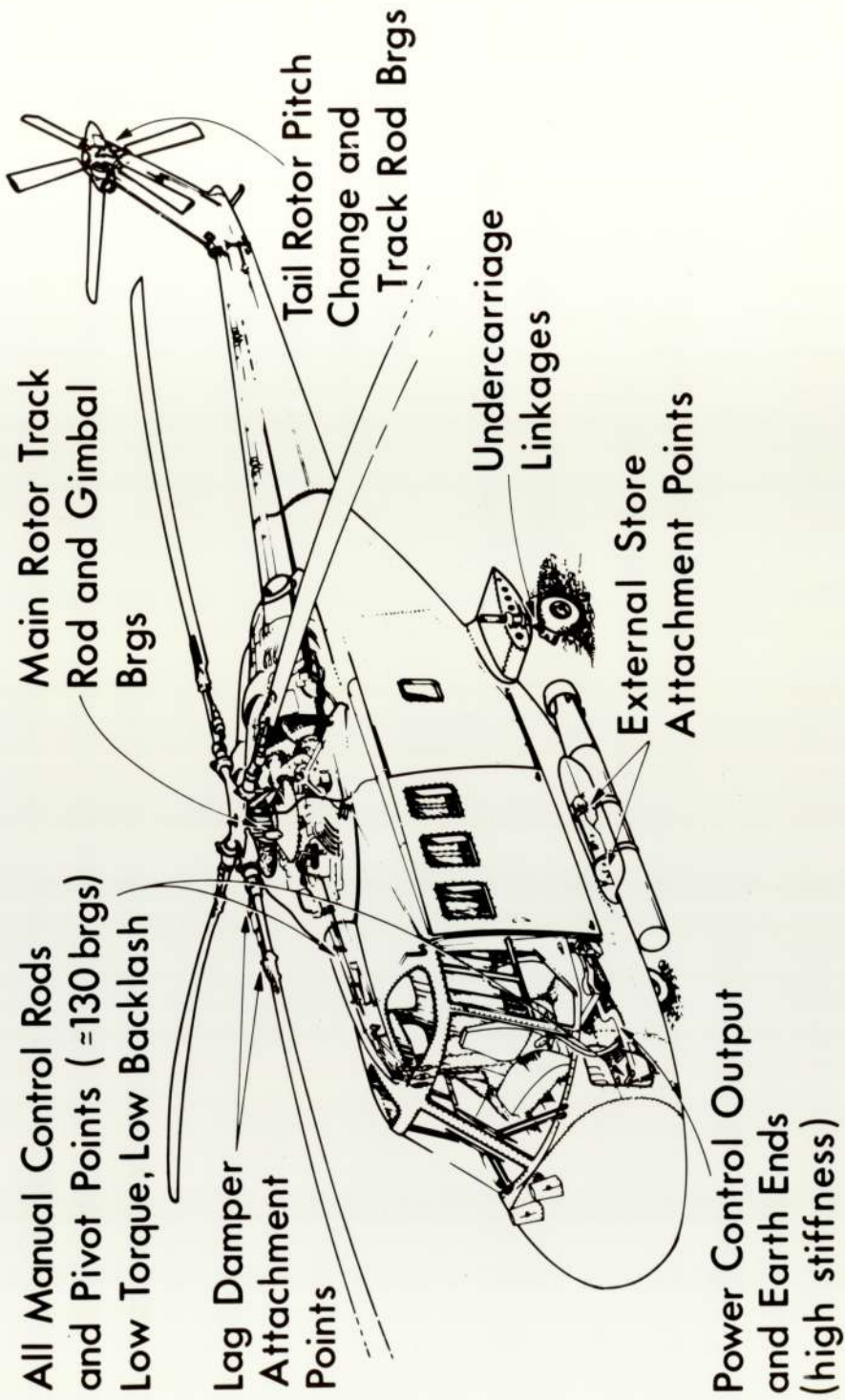


Fig.1.2 Diagram of Lynx Helicopter showing the Positions of Dry Bearings.

TABLE 1.1

MAIN POLYMERS OF INTEREST FOR BEARINGS

Thermoplastics

Polyethylene-high molecular wt.

Acetal-homo- and co-polymer

Polyamides (Nylon 6, 6.6, and 11)

PTFE

Polyphenylene Oxide

Polycarbonate

Thermosetting Resins

Phenolics

Polyesters

Epoxies

Silicones

Polyimides

TABLE 1.2

MAIN FILLERS OF INTEREST FOR BEARINGS

Improve Mechanical Properties

Asbestos

Glass

Carbon

Textile Fibres

Mica

Metals and oxides

Reduce Friction

Graphite

MoS₂

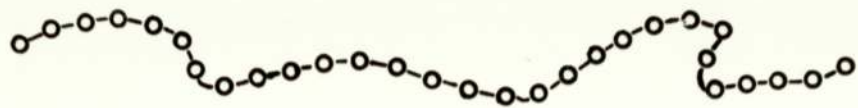
PTFE (particles or fibre)

Improve Thermal Properties

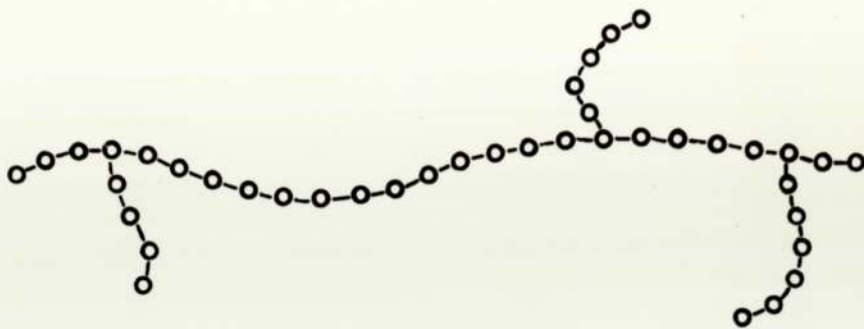
Bronze

Silver

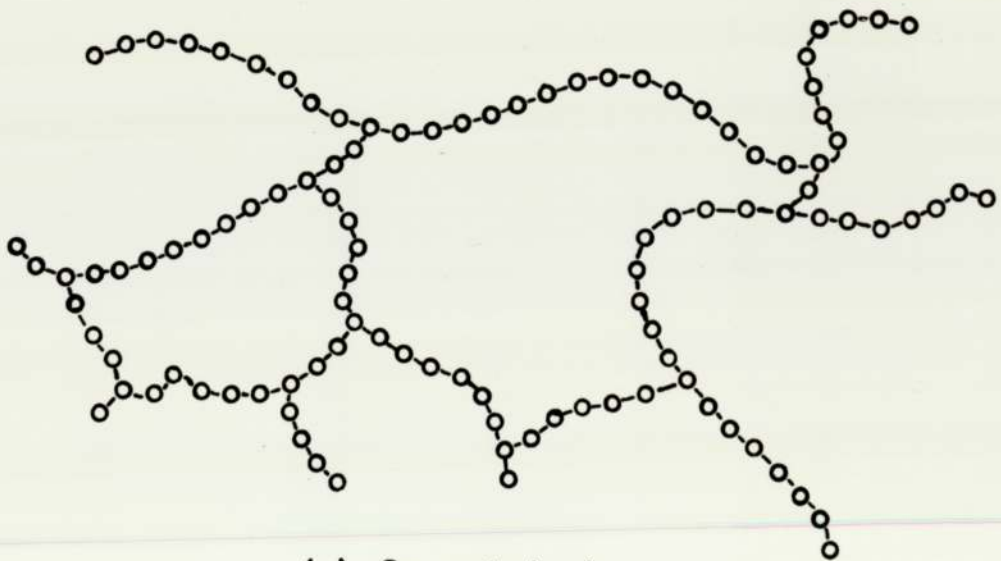
Carbon/Graphite



(a) Linear



(b) Branched



(c) Crosslinked

Fig.1.3(a),(b)and(c) Representation of Linear, Branched and Crosslinked Polymers.

of expansions are greater by a factor of about 10. These properties can be improved by using fillers or reinforcing fibres. A list of typical fillers is given in Table 1.2(3). The particular filler used in composites will depend on the exact use of the bearing.

Before continuing with a review of composite materials, it is useful to describe the possible ways in which friction and wear may arise with polymers under dry sliding conditions.

1.2 Friction of Polymers

The two main components of friction are adhesion and deformation ('ploughing'), at localised areas of contact. As with metals, the adhesive component of friction is given by $F = As$, where A is the real area of contact and s is the shear strength of the junctions formed by contacting asperities. For polymers, these junctions are thought to arise mainly from Van der Waals forces (4,5), possibly supplemented by electrostatic forces (6). It is possible to make the assumption that localised plastic flow will occur, and then the load will be supported by the real area of contact, giving $A = \frac{L}{P}$ where L is the total load and P is the flow pressure of the polymer. Now $\mu = \frac{F}{L} = \frac{As}{L} = \frac{Ls}{PL} = \frac{s}{P}$. However, most polymers undergo mainly elastic and only a small amount of plastic deformation at the asperities (7). Mainly elastic deformation occurs because of the low moduli of elasticity of polymers. These can be of the order of $\frac{1}{100}$ - $\frac{1}{10}$ th those of metals where mainly plastic deformation occurs. If the strength of the interfacial junctions exceed that of the polymer itself, shear will occur within the polymer (i.e. cohesive failure), leading to transfer. There is evidence of polymer transfer on an atomic level (8) and on a more macroscopic level with transfer onto metal or glass surfaces (9,10,11,12). Transfer is most common for crystalline thermoplastics (13). For amorphous thermoplastics and thermosets, failure is more usually at the junction itself and transfer does not occur (14).

The deformation component of friction is most easily described by considering the elastic deformation occurring during the rolling of a rigid sphere over a polymer. Adhesive effects are small, and the energy dissipated can be calculated in terms of the hysteresis losses occurring during each deformation cycle (15). When sliding occurs it is no longer possible to say which of the two components predominates in the measurement of friction.

1.3 Wear of Polymers

At the onset of sliding, wear rates tend to be high. However, the metal counterface can be modified by transfer of the polymer and this generally leads to a smoother counterface and the wear rate decreases to a steady value. In many wear situations, after an initial 'running-in' period, it is found that the volume of wear V , becomes proportional to time, or sliding distance S , directly proportional to the load L , and almost independent of the apparent area of contact. A wear rate may therefore be defined as $\frac{V}{S}$, the units of which are m^3/m or a specific wear rate may be defined as $\frac{V}{SL}$, in m^3/Nm . The type of wear occurring initially is often abrasive. Abrasive wear of rigid polymers occurs when harder surface asperities penetrate the polymer and remove material by shearing or cutting. This leads to the relationship $\frac{V}{S} = \frac{KL}{H} \left(\frac{2}{\pi} \tan \alpha \right)$ where H is the indentation hardness and α is the base angle of the indenting asperity (16). K is a constant accounting for the fact that only a proportion of the polymer undergoing deformation appears as loose wear debris. For abrasive wear to occur, deformation of the asperities must be plastic rather than elastic, and two criteria are available to define this condition. Halliday (17) suggested that critical values of α are given by $\tan \alpha = C \left(\frac{H}{E} \right) (1-\nu^2)$, where ν is Poisson's ratio, E is Young's modulus and the constant $C = 0.8$ for the onset of plasticity and $C = 2$ for full plasticity. Greenwood and Williamson (18) have defined a 'plasticity index' $\left(\frac{E}{H} \right) \left(\frac{\sigma}{\beta} \right)^{\frac{1}{2}}$, where σ is the standard deviation of the asperity heights and β is their average radius of curvature; plasticity begins when the ratio is equal to unity. Inserting typical values of E and H into the first

criterion, plastic deformation and abrasive wear occurs with metals for $\alpha \simeq 1^\circ$, but for polymers, α is of the order of 5-10°. The higher angles are only likely to be encountered on very rough surfaces of the order of 1.25 μmRa or greater, or on abrasive papers (19).

A simple theory for the wear of polymers against abrasive paper has been derived by Ratner et al. (20). In this theory, the volume of wear, V , per unit sliding distance, S , is related to polymer properties — $\frac{V}{S} = \frac{\mu L}{Hse}$, where μ is the coefficient of friction, s is the ultimate breaking strength and e is the elongation at break. The theory is based on the assumption that three stages are involved in the production of a wear particle: plastic deformation to give a real area of contact inversely proportional to the hardness H , relative motion opposed by a frictional force $F = \mu L$, and disruption of material involving work equivalent to the area under the stress-strain curve at fracture. This work can be approximated to the product of the breaking strength and the elongation at break, se . The elongation at break is given as a percentage increase in length.

Localised elastic deformation of a polymer during sliding becomes significant with decreasing elastic modulus and/or counterface roughness, and under these conditions, fatigue is thought to become more important in the wear process. Adhesion between a polymer and metal can only result in transfer of the polymer if the shear strength of a junction exceeds that of the subsurface layer of the polymer. This situation can arise either because an adhesive junction becomes very strong, or because the subsurface layer becomes very weak. When a junction is formed, its strength will be influenced by the oxide or adsorbed films present on the two surfaces. It is difficult to imagine the strength of an adhesive junction ever exceeding the shear strength of the polymer. The process more likely to occur, is one whereby the surface layer becomes progressively weaker as a result of repeated contacts on a relatively smooth counterface, until, eventually even weak adhesion across a junction can become strong enough to detach a fragment

and transfer it to the opposite face (21).

Transfer from polymers with high elongations, such as PTFE, acetals or nylons, leads to smoother counterfaces and hence lower wear rates. Transfer from the more brittle polymers, such as polyesters, some epoxies, or polystyrene is often in the form of irregular lumps, which has the effect of increasing the surface roughness and hence the wear rates.

1.4 Friction and Wear of Dry Bearing Materials.

When fillers are incorporated in a polymer as a reinforcement, the strength, s , increases by a factor of, typically, 1.5-4, but the elongation at break may decrease by a factor up to 100. So the parameter se is reduced when fillers are used and this results in an increase in abrasive wear. However, abrasion may give rise to modification of the metal counterface. Other ways of modifying the metal surface include transfer from the polymer or filler, and abrasion by contaminants in the surrounding environment. In most cases, a smoother counterface is produced and the wear rate gradually decreases to a constant value. PTFE, graphite and MoS_2 are all fillers used to reduce friction and produce a transfer film (1). In some polymer composites filled with carbon/graphite particles or fibres for example, the transferred film can be destroyed by the addition of water. This results in a dramatic increase in the wear rate and could well account for the service failure of many dry bearing materials in contaminated environments.

Reinforced thermosetting laminates are anisotropic in their mechanical properties. Their strengths and stiffnesses however, can still be much greater than filled or reinforced thermoplastics. Reinforced thermosets are most suitable for use in bearings where the frictional heating can be dissipated or minimised by reducing the coefficient of friction. One of the ideal applications of this type of bearing is in marine engineering; the temperature is reduced by the water acting as a

coolant, and which may also result in a lower coefficient of friction. There is an added problem here, and that is the corrosiveness of sea water towards metals (22,23). When operating in dry conditions, thermosets usually contain some form of solid lubricant such as PTFE, graphite or MoS_2 . The wear rates of these materials are still quite high in comparison with PTFE composites, but they can be used at higher temperatures even when thermal or oxidative degradation occurs of the resin or reinforcement. The rates of wear tend to increase with temperature but not as dramatically as do the wear rates for reinforced thermoplastics near their softening points.

1.5 Lubrication of Polymers

As mentioned earlier, it is possible for dry bearing materials to be contaminated during production or in use. Such contaminants could be water, or oils and grease present in the working environment. If this occurs, the conditions of operation can no longer be classed as dry, but now must be considered as operating under a particular regime of lubrication (24).

The various lubrication regimes which exist for the lubrication of metals are shown in Fig.1.4. Fluid film conditions are generally produced when the sliding velocity is relatively high and the loads relatively light, and friction then arises from the shearing of the lubricant film. Elastohydrodynamic conditions occur when high pressures transferred through the lubricant result in deformation of the surfaces and an increase in viscosity of the lubricant itself. A fluid film is still maintained. Mixed lubrication involves a breakdown of the fluid film and the occasional asperity contacts result in wear of the surfaces. Boundary lubrication occurs under conditions of low speeds and high loads which lead to considerably more metal-metal contact. Good boundary lubrication of metals is obtained by the absorption of polar molecules where metal-metal contact is prevented (25,26). This is often achieved in practice by the addition to a lubricating fluid of polar molecules such

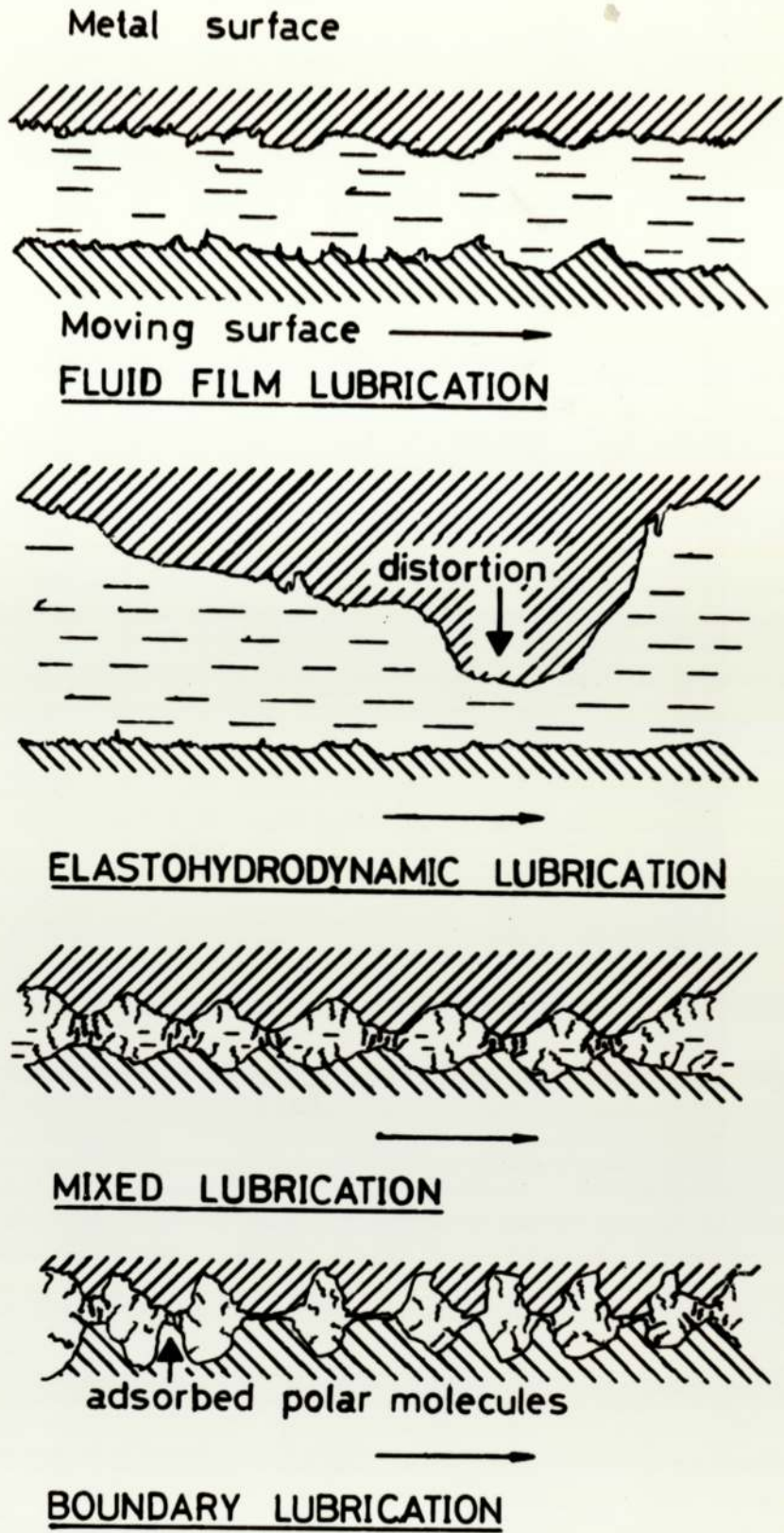


Fig.1.4 Lubrication Regimes.

as long-chain organic acids or esters. The variation of the coefficient of friction with the dimensionless parameter, $\eta U/P$ is shown in Fig. 1.5 (27), where η is the viscosity of the lubricant, U , the sliding speed and P is the pressure. This plot is generally known as a Stribeck curve (28) which gives a convenient summary of the phenomena observed in lubrication. The lubrication regimes shown in Fig. 1.4 can be identified with different parts of this curve. When comparing the boundary lubrication of metals with the boundary lubrication of polymers, certain essential differences exist. The reductions in coefficients of friction for metals can be from unity down to about 0.05-0.1 (26,29,30). With polymers, however, the reductions in the coefficient of friction are much smaller because of the inability of long-chain organic molecules to form fully-condensed monolayers on the low energy polymer surfaces (31,32). Because of their lower moduli of elasticity, polymers may undergo fluid film lubrication in conditions which, with metals, would lead to metal-metal contact (33). Under these conditions, polymers will tend to suffer less wear than metals. With the elastohydrodynamic lubrication of metals, the lubricant viscosity increases considerably in the regions of high contact pressures, whereas with polymers, the localised stresses cannot become sufficiently high to cause an increase in the viscosity of the lubricant. The coefficients of friction are therefore lower (34). However, when polymers slide against metals in the presence of conventional boundary lubricants, the reductions in friction are generally greater than with polymer - polymer systems due to the interaction of the lubricant with the metal (35,36). It is also possible for a metal surface to suffer loss in strength due to the adsorption of surface active species. This is known as the Rehbinder effect (37).

Polymers are known to be influenced by the action of fluids in two ways - wettability (38,39,40) and plasticisation (38,41). The coefficient of friction is reduced appreciably when the surface tension of the fluid falls below the critical value for wetting of the polymer. Yet attempts to correlate this reduction in friction with the wettability, contact angle or the reduction of surface energies

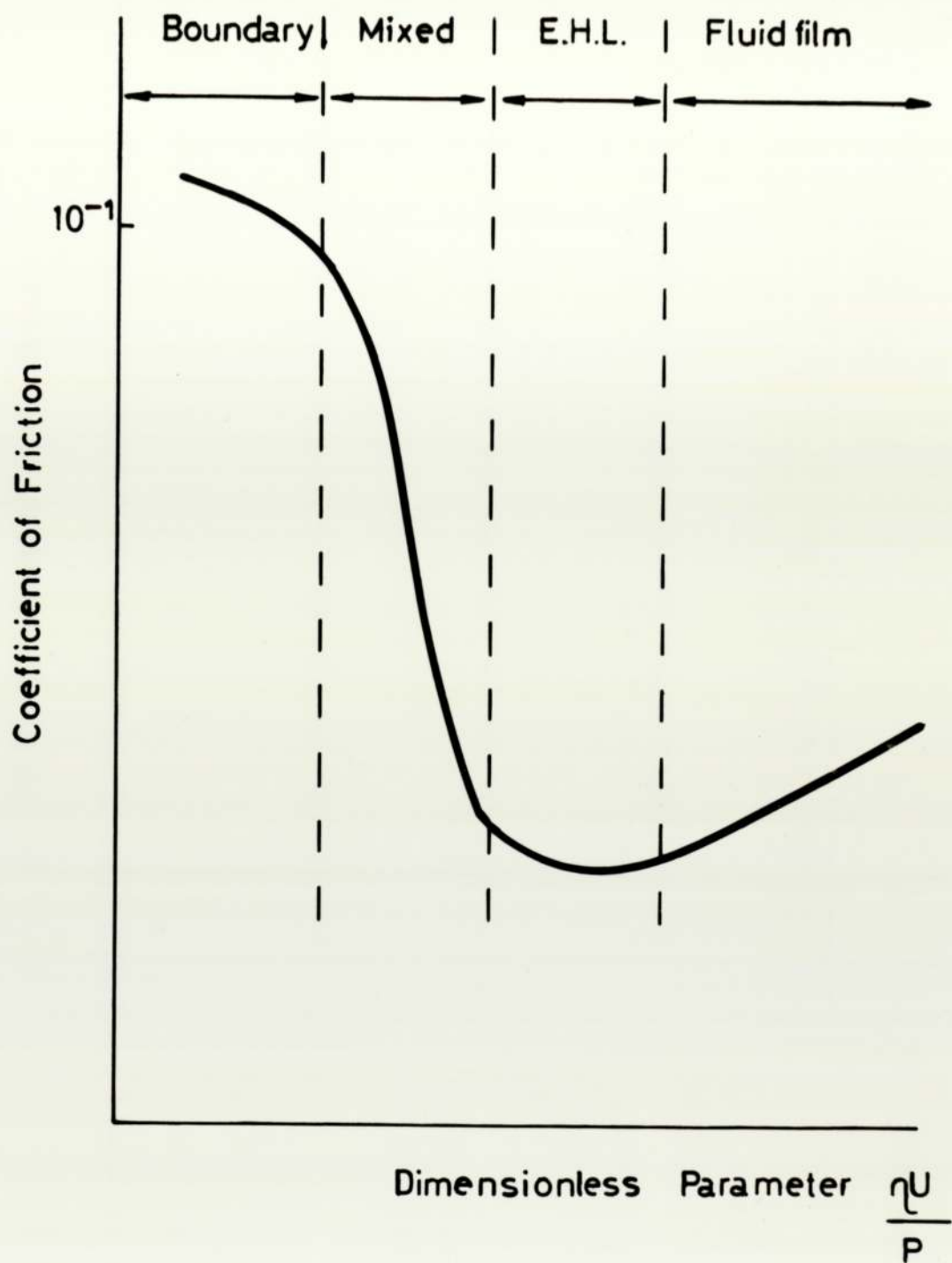


Fig.1.5 Stribeck Curve.

have proved inconclusive for any one polymer in different fluids (40) or for different polymers in one fluid (42). Plasticisation is a term referring to the process of making a material more susceptible to plastic flow. The effect of this is to decrease hardness and increase flexibility. This can occur with some polymer-fluid sliding systems and results in the absorption of fluid into the surface layers of the polymer (41,43). Plasticisation only effects the amorphous regions in a polymer. Absorption of fluid can also lead to:

- (i) a reduction in strength and modulus of elasticity and an increase in the elongation to break.
- (ii) swelling of the surface layers, leading to differential expansion and possible stress concentrations.
- (iii) cracking or crazing of amorphous polymers under stress. Cracks tend to form along the direction of sliding whereas crazes, which are crack-like features tend to form perpendicular to the direction of sliding and consist of porous polymer. (44)

For composites sliding under boundary lubrication conditions, the wear rates tend to be higher than the dry wear rates, because the formation of transfer films on a counterface, or back-transferred films on the composite itself, are inhibited by the fluid. The lubricated wear rates of crystalline polymers, however, are often the same or lower than the dry value. Liquids are not readily absorbed by these polymers and so the effectiveness of the lubricant depends on its ability to act as a boundary lubricant.

An interesting feature of some polymers not mentioned so far, is their ability to undergo lubrication with only small amounts of fluid. Booser, Scott and Wilcock (45) have shown that following pre-lubrication by a small amount of hydrocarbon oil, a

nylon-metal combination will exhibit low wear for at least 100 times as long as a metal-metal combination in the same conditions. Similar results have been reported by Pratt (46). This observation has been exploited practically by the incorporation of very small amounts of fluid into the bulk structure of polymers. The fluid reaches the sliding interface either by diffusion or as a result of wear. Various fluids have been examined including fatty acids and amides (47,43), low molecular weight fluorocarbons (49), mineral oils (50) and silicones (51,52,53). Reduction in wear rates by fluid incorporation has also been found by Pascoe and Dzhankmedov (54) and Abouelwafa et al. (55).

1.6 Research Program

Improvements in dry bearing materials are needed to reduce production costs, to increase wear-life, and obtain greater reliability in performance. The overall aims of any research program into these aspects must be:-

- (i) to determine the main factors influencing life and reliability.
- (ii) to understand the fundamental ways in which these factors influence friction and wear.
- (iii) to develop improved products based on the information from (i) and (ii).

The aims of this project are concerned with (i) and (ii) above. There is information already available on (i) (1,2), which shows fluid contamination to be a very significant parameter, usually leading to shorter bearing lives (i.e. higher wear rates). The intention of the research is to concentrate on (ii) using a polymer about which experimental information is available and is known to be sensitive to particular fluids (24). The polymer chosen for this work was Poly 2,6-dimethyl 1,4-

phenylene oxide (PPO) and the fluid was polydimethyl siloxane (silicone fluids) of different viscosities. The possible mechanisms relevant to wear are examined by sliding experiments and the changes in the surface layers induced by sliding are characterised using various physical and surface analytical technique.

As already discussed, the presence of a fluid in a dry bearing application can lead to boundary lubrication, full fluid film lubrication or a mixture of the two can result. A polymer-metal system can undergo the transition to elastohydrodynamic lubrication more easily than a metal-metal system. If partial elastohydrodynamic lubrication occurs, then the proportion of the load supported by the fluid is unknown and the effect of load, viscosity, temperature, sliding speed and surface roughness is unknown also. It is therefore impossible to compare and interpret friction coefficients and wear rates for different materials and fluids in terms of surface changes and mechanical properties in any lubrication conditions other than boundary.

Experiments designed to assess the friction and wear of polymers in the boundary lubrication regime generally involve the use of 'pin-on-ring' or 'pin-on-disc' machines. Wear is measured by using, for example, a conically- or hemispherically-shaped wear specimen. By measuring the diameter of the specimen periodically it is possible to calculate a wear rate. However, it is possible for a hydrodynamic fluid film to be formed with these specimen geometries, which is produced by a combination of the wear and elastic deflection of the assembly supporting the specimen (24). For the present work, an apparatus was designed to reduce the effects of hydrodynamic or elastohydrodynamic film formation. To overcome these effects, nominal Hertzian line-contact conditions were maintained throughout the experiment, irrespective of wear. The plane surface of a rotating metal ring was mounted between centres on a commercially-available lathe. Line-contact conditions were maintained by slowly rotating the polymer wear specimen about its cylindrical axis. With suitable loads, sliding speeds and viscosities of

fluid, boundary lubrication conditions could be achieved. This apparatus is described in the next chapter.

CHAPTER TWO

EXPERIMENTAL EQUIPMENT AND PROCEDURE

2.1 Boundary Lubrication Apparatus

2.1.1 Introduction

The basic design criteria of the boundary lubrication apparatus were that:-

- (a) it should provide rotation of a wear counterface at variable speeds
- (b) the polymer wear specimen should rotate
- (c) friction needs to be measured
- (d) wear needs to be measured continuously (since a non-conforming geometry is used)
- (e) a lubricant should be applied
- (f) a range of loads should be available.

How these criteria were achieved and combined together into one apparatus is described in the first part of this chapter. Once the experimental conditions of boundary lubrication had been derived from the apparatus, then various polymer wear specimens could be generated for analysis. These polymer wear specimens were examined for changes in mechanical or chemical properties which might have occurred in the uppermost surface layers, during boundary lubrication. The techniques used to determine these changes are described in the rest of the chapter.

2.1.2 Design Principle

A schematic view of the apparatus is shown in Fig. 2.1. It was designed so that the

whole assembly could rotate about an axis projecting out from the centre of the head bearing of a lathe. This rotation is required to measure the friction force generated between the polymer and its counterface. Rotation is restricted to a few minutes of arc by a tensile/compressive load transducer which functions both as a buffer and measures the friction force. The weight above the projected axis is counterbalanced exactly by the weight below. Fig. 2.2 shows the friction transducer and Fig. 2.3 indicates the axis of rotation of the apparatus. The friction transducer is described in more detail in a later section in this chapter. Inertial effects have been minimised by keeping the bulk of the apparatus as close to the axis of rotation as possible. There are bearings at both the front and rear of the apparatus, and the distance between them has been minimised to reduce the possibility of mis-alignment of the bearings, which could affect the friction measurements.

2.1.3 The Wear Counterface

The wear counterface used in all the experimental work was the outer race of a commercially-available bearing made from EN31 steel ($\approx 1\%C, \approx 1.5\%Cr$) hardened to ≈ 700 V.P.N. It was chosen originally because of its convenient size and its ability to fit onto an existing piece of apparatus used for polishing. The counterface surfaces were randomly abraded first on 180 grade silicon carbide paper (particle size $74\mu m$) to remove the previous wear track and then 240 grade silicon carbide paper (particle size $53\mu m$) to a C.L.A. (Centre-line-average) roughness of $0.1\mu m$. The rings were ultrasonically cleaned in acetone to remove any surface debris from the polishing process and washed in petroleum ether before use. The wear counterface is an interference fit onto a notched holder, which in turn is mounted onto a Morse taper using a washer and cap nut. The taper then fits into the headstock of the lathe. The other end of the taper fits into the front bearing in the main frame of the apparatus, see Fig. 2.2, Fig. 2.4 and Fig. 2.5.

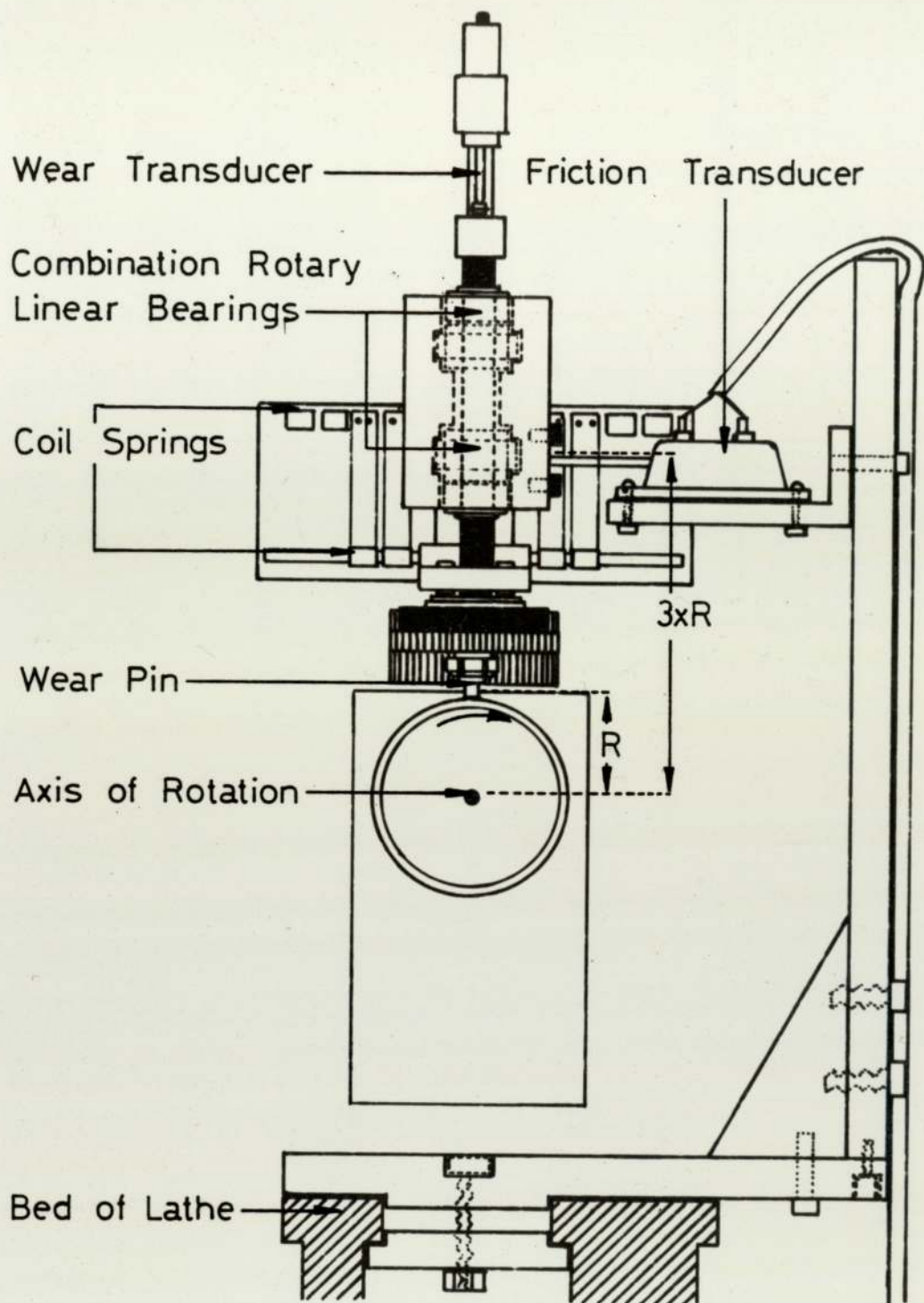


Fig.2.1 Schematic Diagram to show the Design Principle .

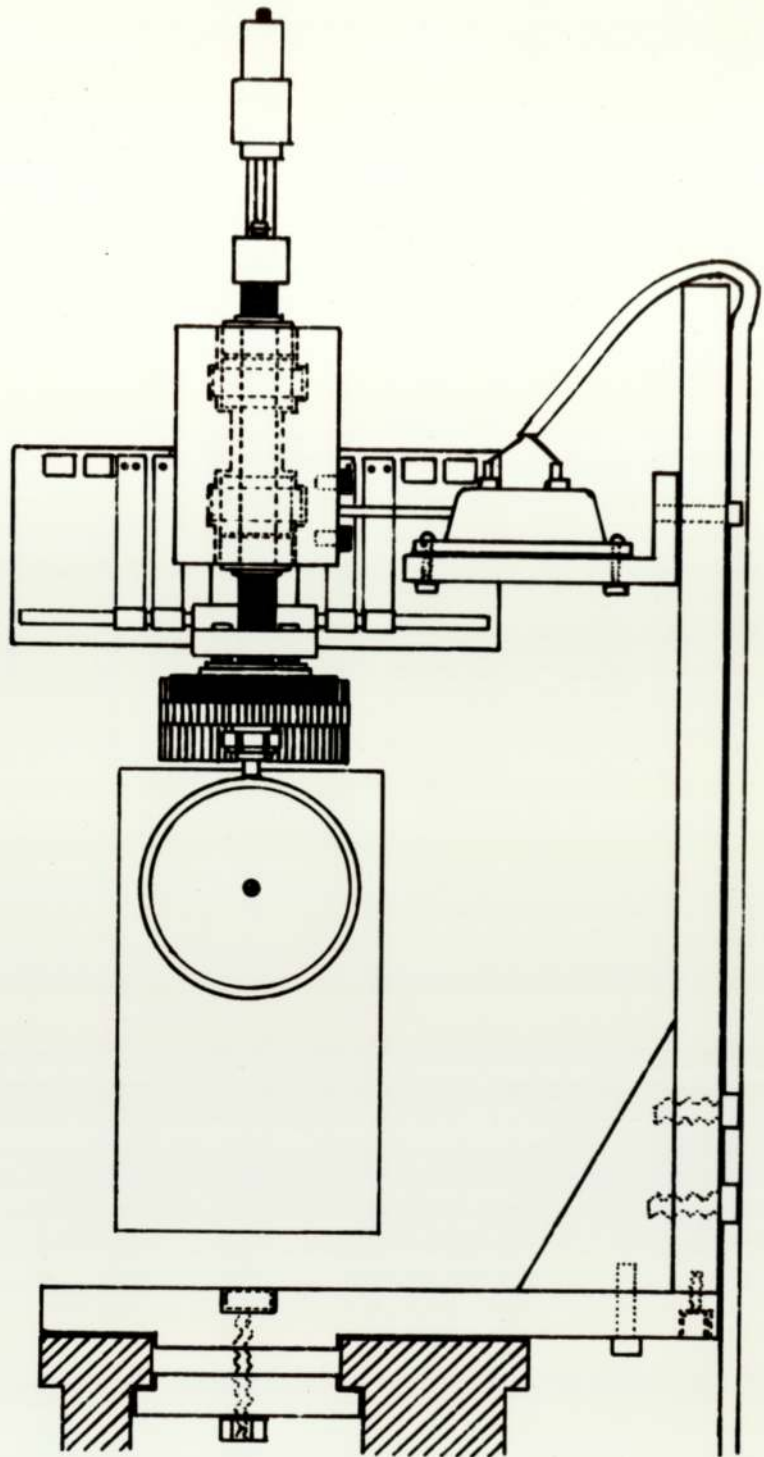


Fig.2.1 Schematic Diagram to show the Design Principle .

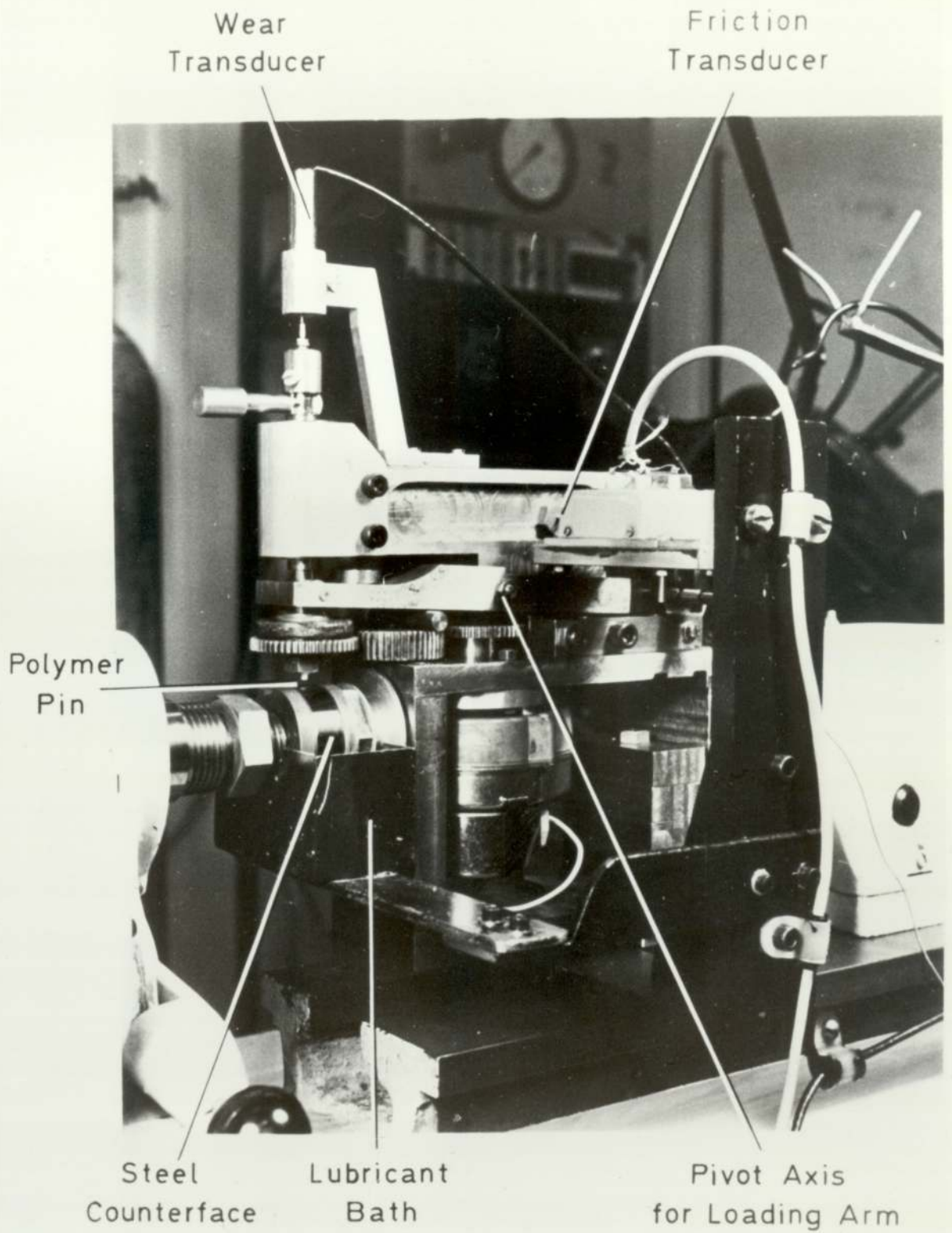


Fig.2.2 Some Important Features of the Boundary Lubrication Apparatus.

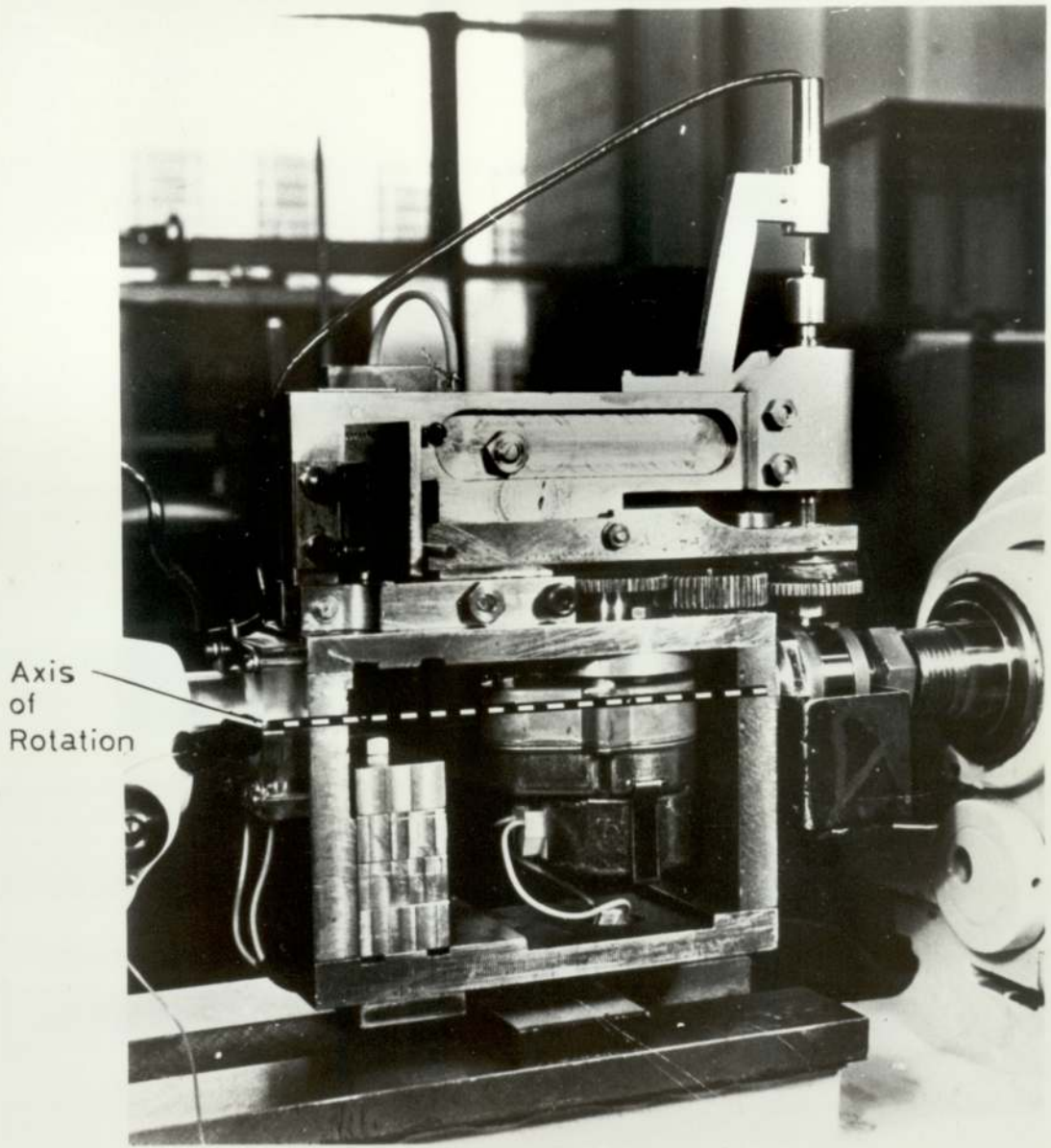


Fig.2.3 Rear-side View of Apparatus showing the Axis of Rotation.

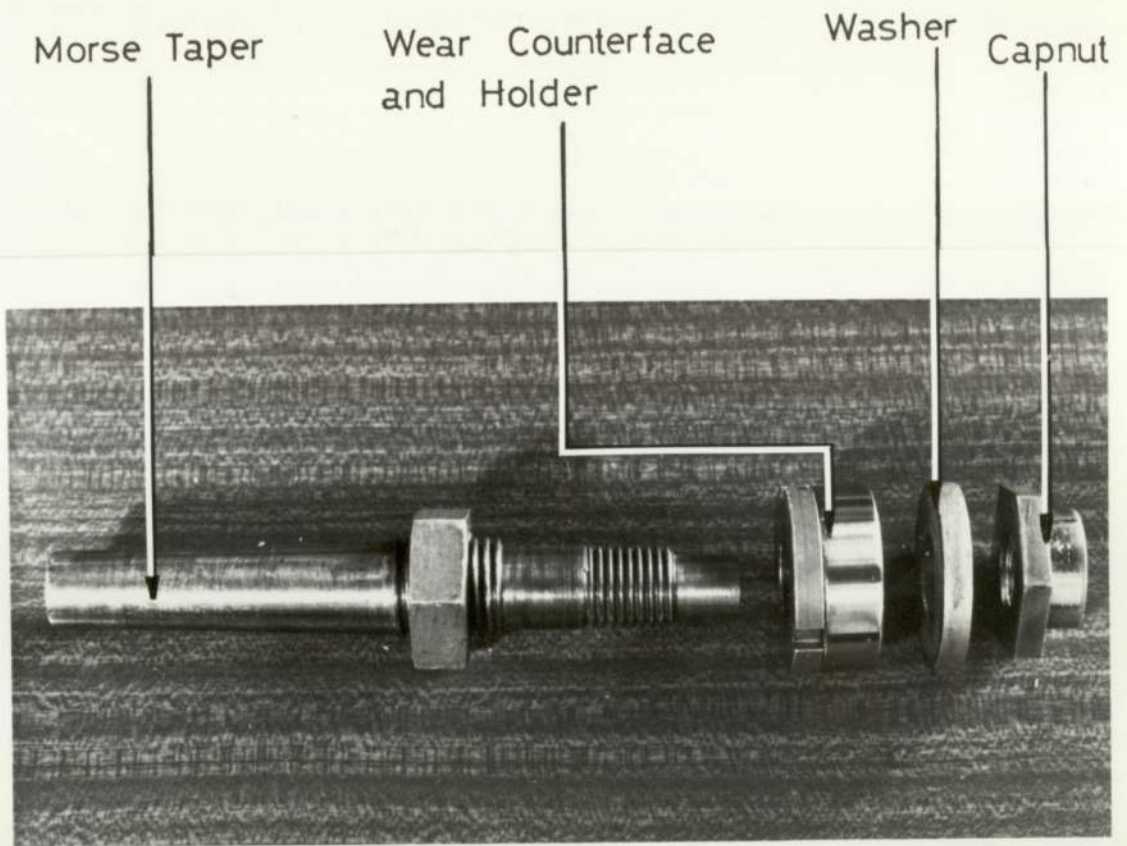


Fig.2.4 Details of Wear Counterface(detachable from the Apparatus).

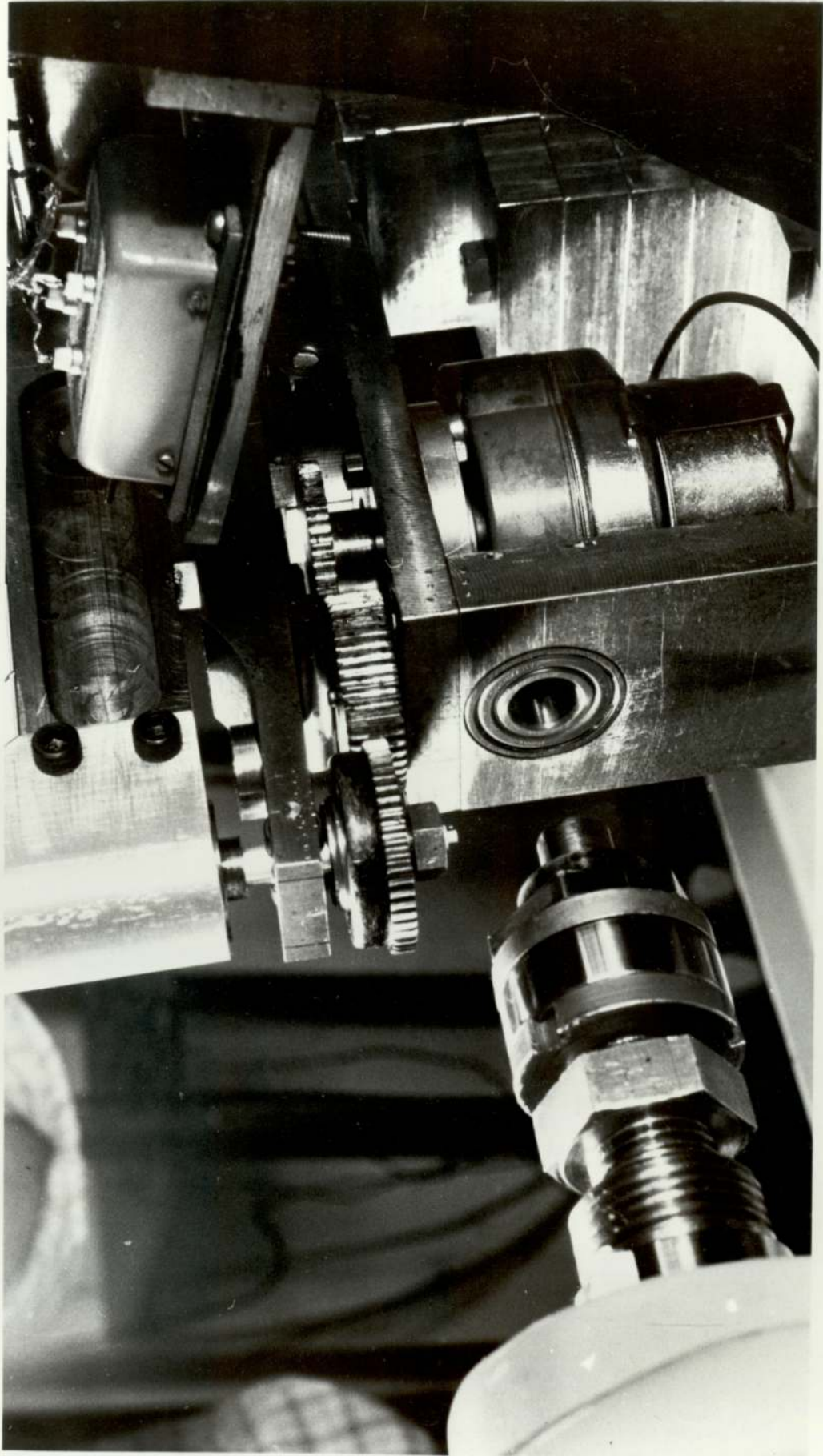


Fig.2.5 Details of Wear Counterface,Wear Pin and Gear Assembly.

A splash washer also fits onto the cap nut to protect the front bearing from any lubricant. An extractor, to permit removal of the ring without contaminating the wear surface is shown in Fig. 2.6.

2.1.4 Wear Pins and Holder

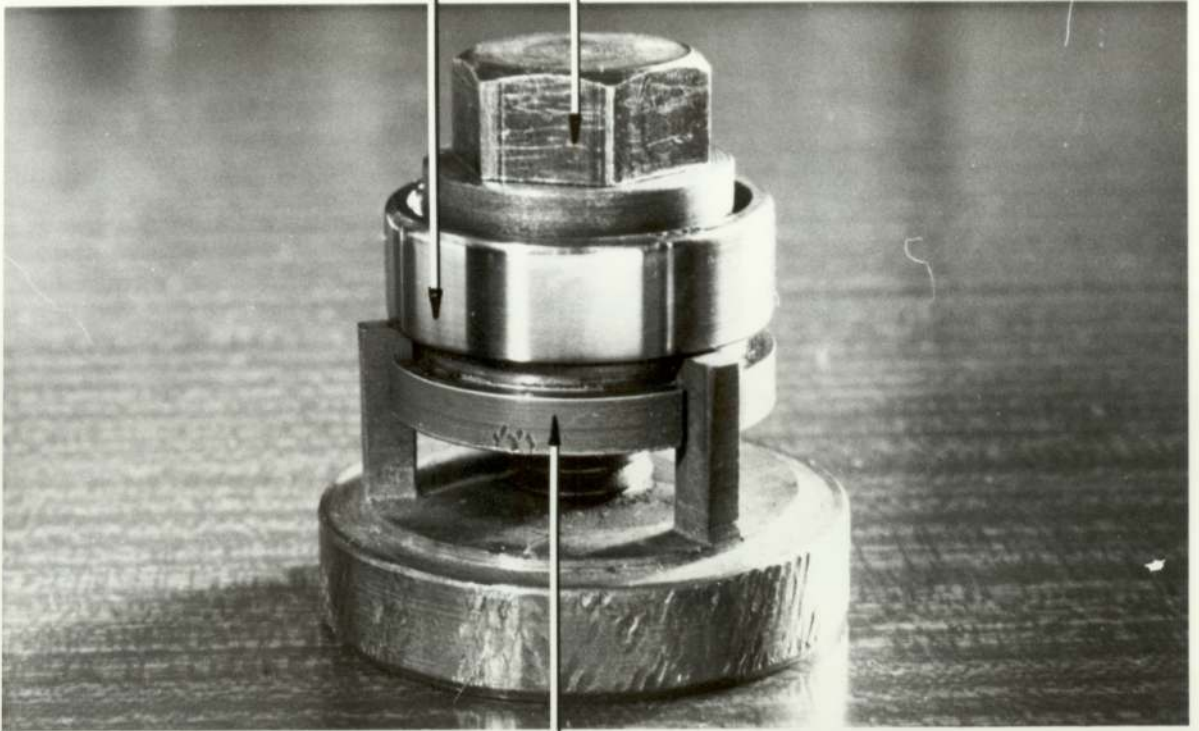
The PPO was originally supplied in the form of granules which are difficult to mould under compression. To offset this, approximately 40g of PPO granules were dissolved in 1200 ml of toluene, using a magnetic stirrer and precipitated back out in about 10 litres of methanol, using only a few hundred ml of the toluene/PPO solution at a time. The excess toluene was removed and the precipitate washed using a Buchner funnel with methanol and finally water. This was dried in an oven to constant weight and the particle aggregates broken down using a rotary bladed cutting device. The moulding temperature was approximately 250°C. The polymer wear pins were turned on a lathe from these compression-moulded blocks. The shape of the wear pin is shown in Fig. 2.7, together with the wear pin holder. The structure of PPO is shown in Fig. 2.8(a).

A schematic diagram is shown in Fig. 2.9, giving details of the pin holder, gear and thrust washer assembly. The rear end of the pin holder is machined to a close fit onto the end of the shaft (shown by the diagonal shading). This is tapered on the outside to allow the gear and thrust washer housing to clamp the pin holder to the end of the shaft. The gear and thrust housing were machined from a solid piece of metal and the inside of this was tapered also to achieve the clamping action. This was considered to be the best way of attaching the pin holder to the shaft. Another method would have been to use a screw-clamp device, but this would then have resulted in an eccentric rotation of the pin. The thrust washer consisted of a cage of ball bearings between two washers and was a loose fit within the housing.

As can be seen from Fig. 2.7 and Fig. 2.9, the pins have been machined into a 3-tier

Wear Counterface

Bolt screws down



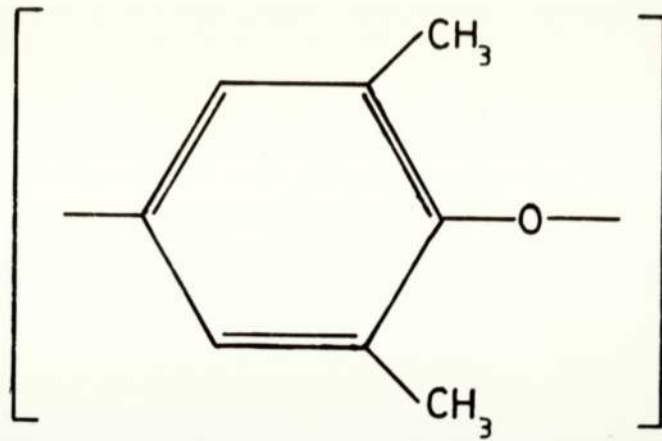
Wear Counterface

Holder moves down

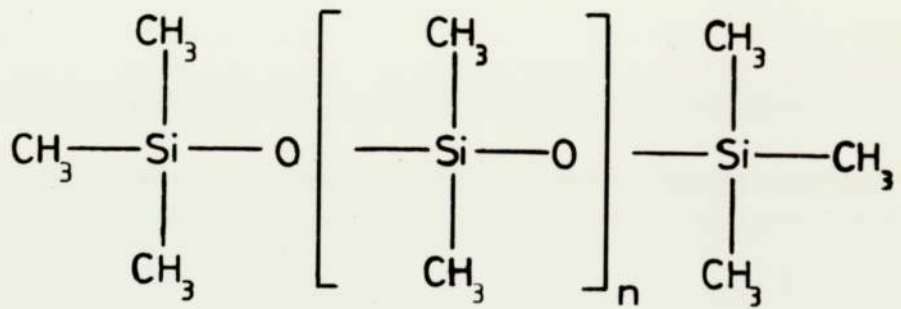
Fig.2.6 Ring Extractor.



Fig.2.7 Wear Pin and Wear Pin Holder.



(a) Poly(2,6-Dimethyl 1,4-Phenylene Oxide)



(b) Polydimethylsiloxane

Fig. 2.8(a) and (b) Structure of Polyphenylene Oxide and Silicone Fluid.

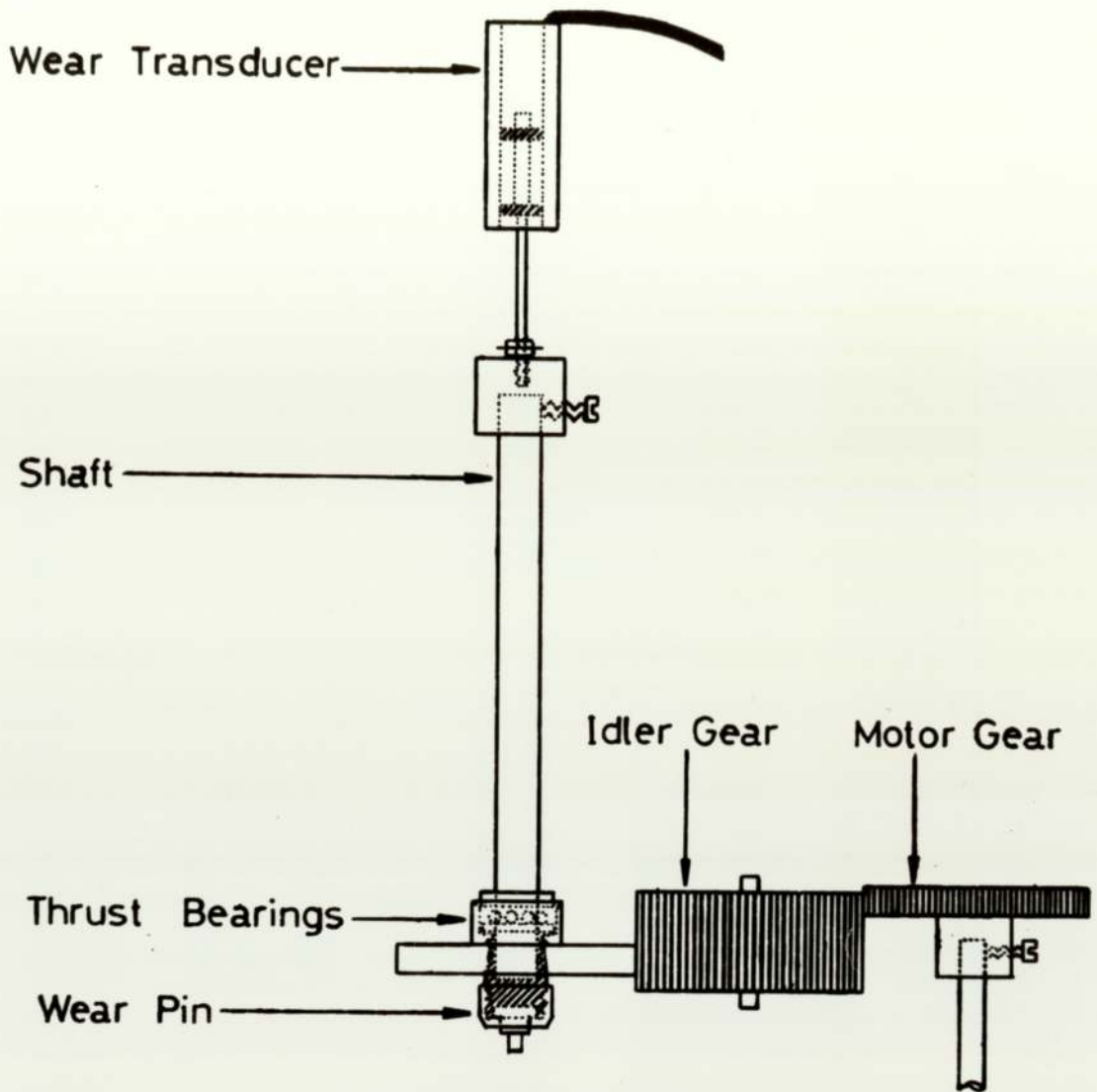


Fig.2.9 Schematic Diagram of Wear Pin Holder.

shape. The largest tier fitted into the wear pin holder and is used to attach the pin to the holder via a cap nut. The final tier is the wearing surface and the second tier is merely for strengthening purposes. The rotating shaft is hardened and ground, and fits into a combination bearing set (see later section). The thrust washer allows the load to be applied (via a pivot and fork mechanism) whilst the shaft and pin rotate.

2.1.5 Measurement of Wear

The wear of the polymer pins was monitored continuously using a Linear Displacement Transducer, which was linear over 1mm movement. The error was rated at 0.3%. The stylus of this device was 'free-moving', within two plastic bushes, i.e. it can rotate and move linearly at the same time. The wear transducer is shown in Fig. 2.9. The transducer is mounted directly above the rotating shaft connected to the wear pin. On top of the shaft is a brass cap, held on by a horizontal nylon screw. The inside of the cap is threaded to the same pitch as the transducer stylus. Two small nuts above the brass cap keep the stylus in place. The transducer stylus can now rotate and descend as the pin wears. The attachment of the transducer to the apparatus is shown in Fig. 2.2 and Fig. 2.3. It is important to align the centres of the shaft, polymer pin and transducer to enable an accurate measurement of wear to be made. Note that the wire from the transducer was fixed as close as possible to the axis of the lathe, to reduce inertial effects and maintain balance. The transducer is connected to an oscillator demodulator unit with adjustable span and zero controls. The output signal was fed into one input of a double channel chart recorder. The chart recorder was usually used at its slowest speed of 1mm/min.

2.1.6 Measurement of Friction

The friction force generated between the polymer and counterface is measured by

a commercially-available Tensile/Compressive Load Transducer. The type of transducer used is one designed to measure steady and rapidly fluctuating tensile or compressive forces. It consists of an unbonded strain-gauge element. The transducer is mounted in an horizontal position, using an upright support connected to the bed of the lathe, as is shown in Fig. 2.1 and Fig. 2.2. The output signal from the strain-gauge bridge is connected to an amplifier and then to the second input of the chart recorder previously mentioned. This gives a continuous friction trace. The range of the transducer is $\pm 450\text{g}$, and the maximum excursion of the sensing armature is $40\mu\text{m}$ (at maximum load). The transducer just rests against the side of the apparatus when it is in a vertical position. The transducer is positioned a distance of three times the radius of the wear counterface above the axis of rotation. To calculate the friction force between the polymer and counterface, the measured friction from the chart recorder must thus be multiplied by a factor of three. There is a slight amount of friction produced in the front and rear bearings of the apparatus. This is measured by suspending the pin above the wear counterface (so no load is applied) and setting the lathe in motion. The friction value obtained in this way is taken as the 'zero' and over the whole range of speeds used amounts to 0.4 to 4% of the contact friction.

2.1.7 Load Application

Constant-force, commutator-brush springs were used for loading purposes. These springs are unlike ordinary ones in that, varying the extension does not produce any variation in the load output. Compression springs are unsuitable since as the pin wears, the extension will change and thus alter the load. Fig. 2.10 shows how they are applied on the apparatus. This set-up was arrived at after experimentation with various configurations. Various sizes and spring loads are available and it is possible to vary the load from 1N up to 31N in steps of 1N, if required. The springs are easily interchanged by passing the rod, (shown in Fig. 2.10) through the centre of the coiled part of the spring. A small brass ring is placed in the centre of the

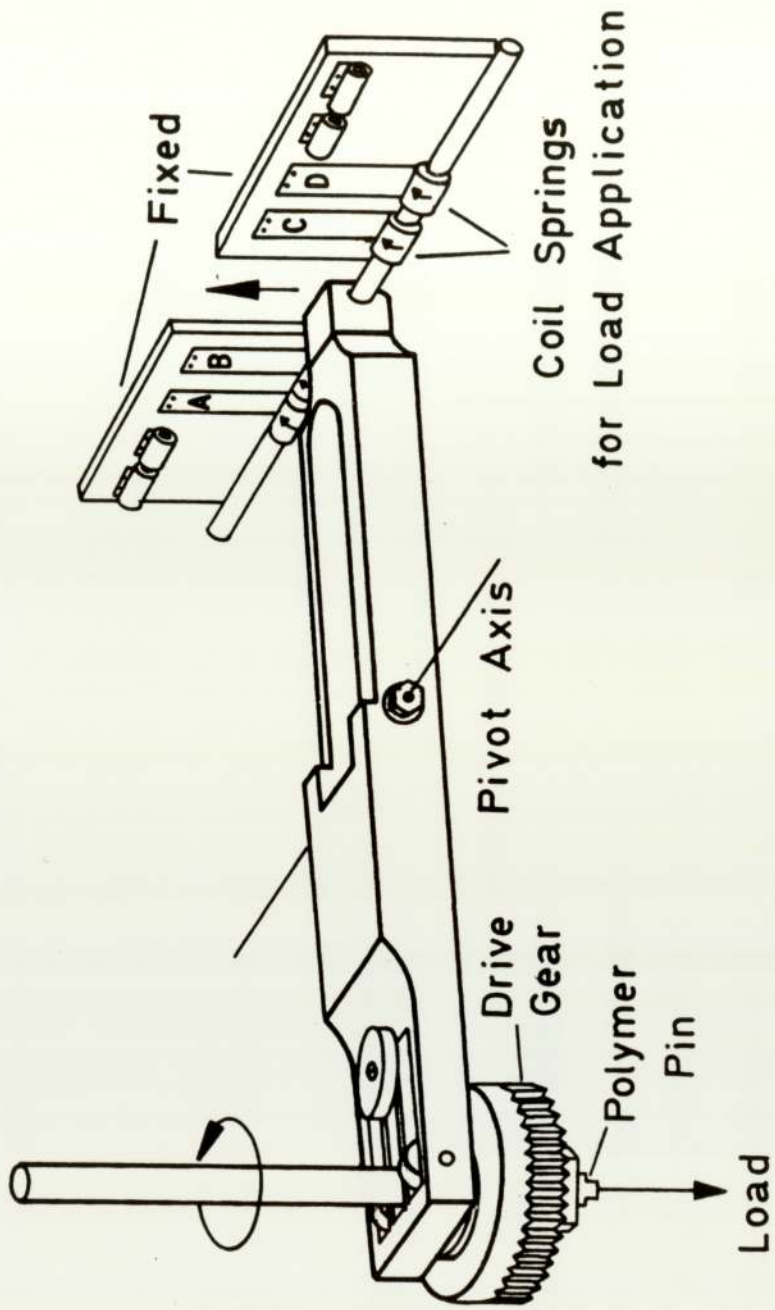


Fig.2.10 Diagram to show the Application of Load using Coil Springs.

coil of the spring to facilitate its recoil. The load is applied to the wear pin using a pivot and fork mechanism. With no springs in use, the load is made exactly 1N, by using a lead weight on top of the pin holder, gear and shaft assembly (shown in Fig. 2.1). The fork is balanced exactly about the pivot axis, so that it does not contribute to the loading. There are two small plain bearings mounted horizontally at the end of the fork, either side of a channel which allows the shaft to pass through. These two bearings press down on top of the thrust washer, allowing the pin to rotate. The shaft has been hardened and ground and passes through two combination bearings, so that the shaft can drop and rotate at the same time, with the minimum of friction on the shaft. The approximate positions of these combination bearings are shown in Fig. 2.1.

2.1.8 Rotary Motion of the Pin and Wear Counterface

The lathe was modified by the addition of a 0.25KW, 1400r.p.m., D.C. motor and thyristor speed controller to give a continuously variable range of speeds from 0.001ms^{-1} to 10ms^{-1} , using a pulley and gearing system already in the lathe.

The wear pin is rotated using a 1:1 gear ratio with an idler gear in between and a 5 r.p.m. synchronous motor. The gear arrangement is shown in Fig. 2.9. With the continued use of the apparatus, it was thought possible that the motor gear could wear a groove in the idler gear and so interfere with the descent of the shaft gear as the pin wears. This potential problem was overcome, however, by arranging that the lower horizontal face of the motor gear was always well above the upper horizontal face of the shaft gear.

2.1.9 Lubricants and Application

The lubricant in all experiments was applied by allowing the lower part of the rotating counterface to be immersed in a bath of fluid. The lubricant was

commercially-available polydimethyl siloxane (silicone fluid) and the structure is shown in Fig. 2.8(b). This fluid was chosen because it is available in a range of different viscosities. They are chemically identical but vary only in molecular weight (i.e. number of repeat units). The range of viscosities used was 1-1000cs.

2.2 Electron Probe Microanalysis (E.P.M.A.)

One of the main reasons for choosing silicone fluids as lubricants is that the silicon atoms present in the main chain are readily detectable by several surface analytical techniques.

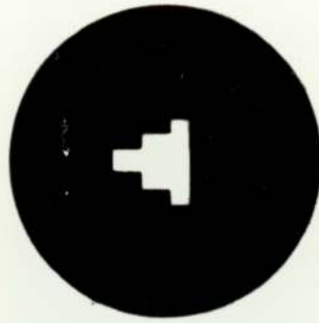
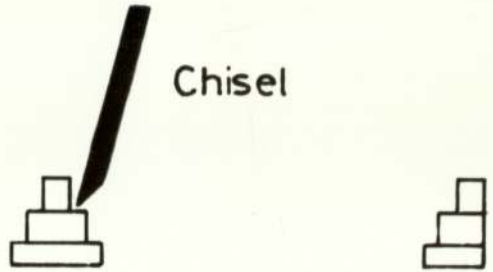
PPO pins worn under boundary lubrication conditions with silicone fluid were examined in the electron probe microanalyser (E.P.M.A.) by mounting the wear specimens in transverse sections. If the silicone fluid has penetrated the worn PPO surfaces to any significant depth, then this could be detected from the presence of the characteristic X-Rays of silicon. Details of the principles involved in the E.P.M.A. can be found elsewhere (56). In the method of mounting the worn specimens, part of the second and third tiers were removed by a small sharp chisel, being careful to avoid contact with the first tier (i.e. the worn surface). In an initial set of experiments, it was found that the conductive mounting medium, a phenolic resin, also contained silicon atoms, making it difficult to detect the edge of the worn surface. This problem was overcome by coating the top of the specimen with silver conducting paint. By obtaining a silver X-Ray intensity picture, the edge of the specimen could then be seen with ease. Without moving the specimen, the Bragg angle was varied to obtain a silicon X-Ray intensity picture. If there is any silicon present below this edge, it must then be in the surface layers of the worn specimen. A further improvement on this method of mounting was to make two angled cuts in the mounting medium very close to the specimen and 'chip' this portion away, leaving the edge of the wear surface of the specimen exposed. This method of mounting is summarized in Fig. 2.11. All the mounted sections of the

Wear Surface to be examined

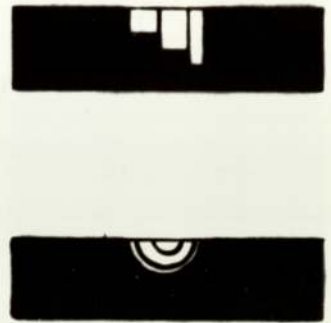


Wear Pin

Chisel



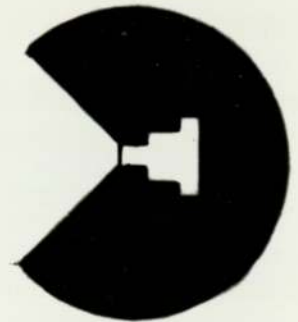
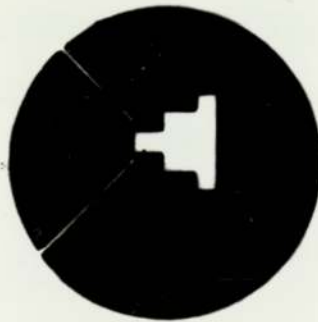
Top View



Side View

MOUNTED SPECIMEN

Cuts



Finished Specimen
(Coated with Carbon)

Fig.2.11 Mounting of Specimens for Electron Probe Microanalysis.

polymer pins were polished in the same way using various grades of papers, finishing finally on $6\mu\text{m}$ and $1\mu\text{m}$ diamond pastes. The specimens were then given a conductive coating of carbon to dissipate electrostatic charging effects under the electron beam.

2.3 Rutherford Backscattering (R.B.S.)

Rutherford backscattering is a comparatively new technique for surface examination which does not, so far, appear to have been used for the analysis of worn surfaces. It is therefore, pertinent to describe the principles involved in the technique. Three distinct physical properties of 'thin layer' targets can be determined: the elemental masses within the target; the amounts of each element in the target; the concentration versus depth profiles of each element in the upper layers of the target.

The basic experimental arrangement is shown in Fig. 2.12 (57). The sample was mounted in a vacuum chamber, connected to the beam tube of the Dynamitron accelerator. The Dynamitron is a high-current machine, which can operate at voltages up to three million volts and accelerate either electrons or positive ions, such as deuterons, protons and α -particles. The beam produced can be either continuous or pulsed and of energy in the range of 1-3MeV. In the present experiments, the Dynamitron was used to provide a continuous monoenergetic beam of α -particles (${}^4\text{He}^{2+}$), of 2MeV energy which impinged on the sample. This beam energy was chosen such that it was well below the nuclear reaction threshold. Most of the beam penetrates deep into the sample (of the order of $10\mu\text{m}$) with only a few ions undergoing large-angle collisions with target nuclei. These backscattered ions were detected by a silicon surface barrier detector in conjunction with a charge sensitive pre-amplifier and main amplifier, followed by a multi-channel analyser which is capable of determining the energy of the ions with a resolution of 15keV.

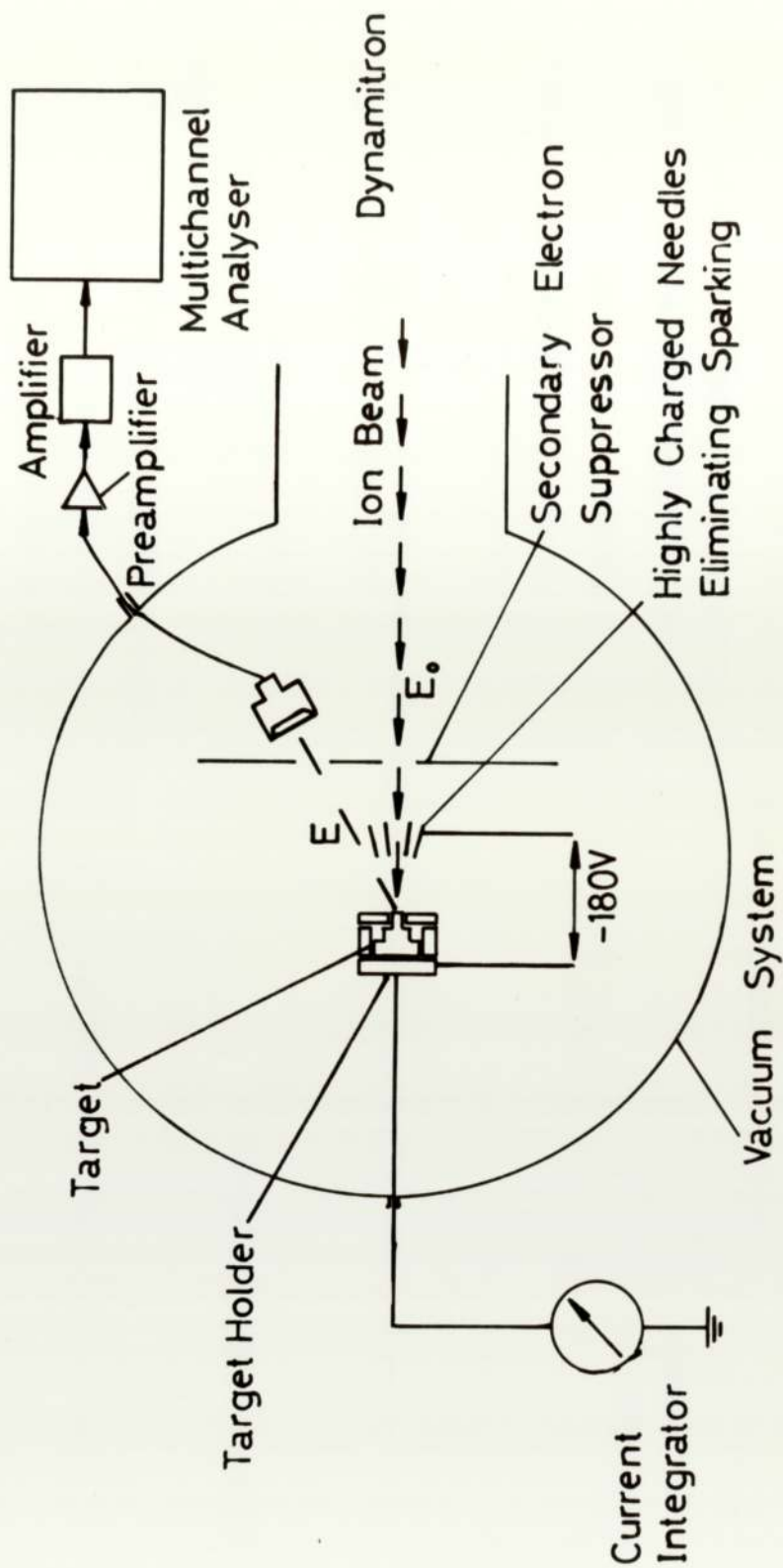


Fig.2.12 Schematic Diagram of the Experimental Apparatus used for Rutherford Backscattering.

The incident ions undergo 'billiard ball' type collisions if they pass close enough to a target nucleus (within 10^{-5} to 10^{-6} nm). Elastic scattering occurs due to simple Coulombic electrostatic repulsion. When this occurs, both energy and momentum are conserved and the incident ion rebounds with an energy characteristic of the mass of the target atom. The physical principle of the technique is shown in Fig. 2.13. If the incident ion collides with a very heavy target nucleus, this nucleus will absorb very little energy and so the backscattered α -particle will retain most of its original energy. If, however, the ion is scattered from a light target nucleus, then most of the projectile's energy will be absorbed and the ion's final energy is substantially reduced. The energy of the backscattered ion, E , is always less than its original energy E_0 and is given by the equation $E = KE_0$ where K is the Kinematic factor of the collision and can be obtained from the classical conservation laws of energy and momentum. K is given by:

$$\frac{M_p^2 (\cos \theta_s + M_p ((M_t^2 / M_p^2) - \sin^2 \theta_s)^{\frac{1}{2}})^2}{(M_t + M_p)^2}$$

where M_p is the mass of the α -particle

M_t is the mass of the target atom

and θ_s is the scattered angle of the α -particle.

Thus, by analysing the energies of the backscattered ion, it is possible to identify the different elements in the specimen. The dependence of percentage α -particle recoil energy with atomic mass is shown in Fig. 2.14(58). The energy separation of adjacent masses, is not linear, but decreases as the mass of the target elements increases. This means that the resolution of adjacent light elements e.g. oxygen and fluorine (energy difference of 131keV) is better than that of e.g. platinum and gold (energy difference of 1.4keV)(57).

The yield of backscattered α -particles from a given element depends on the

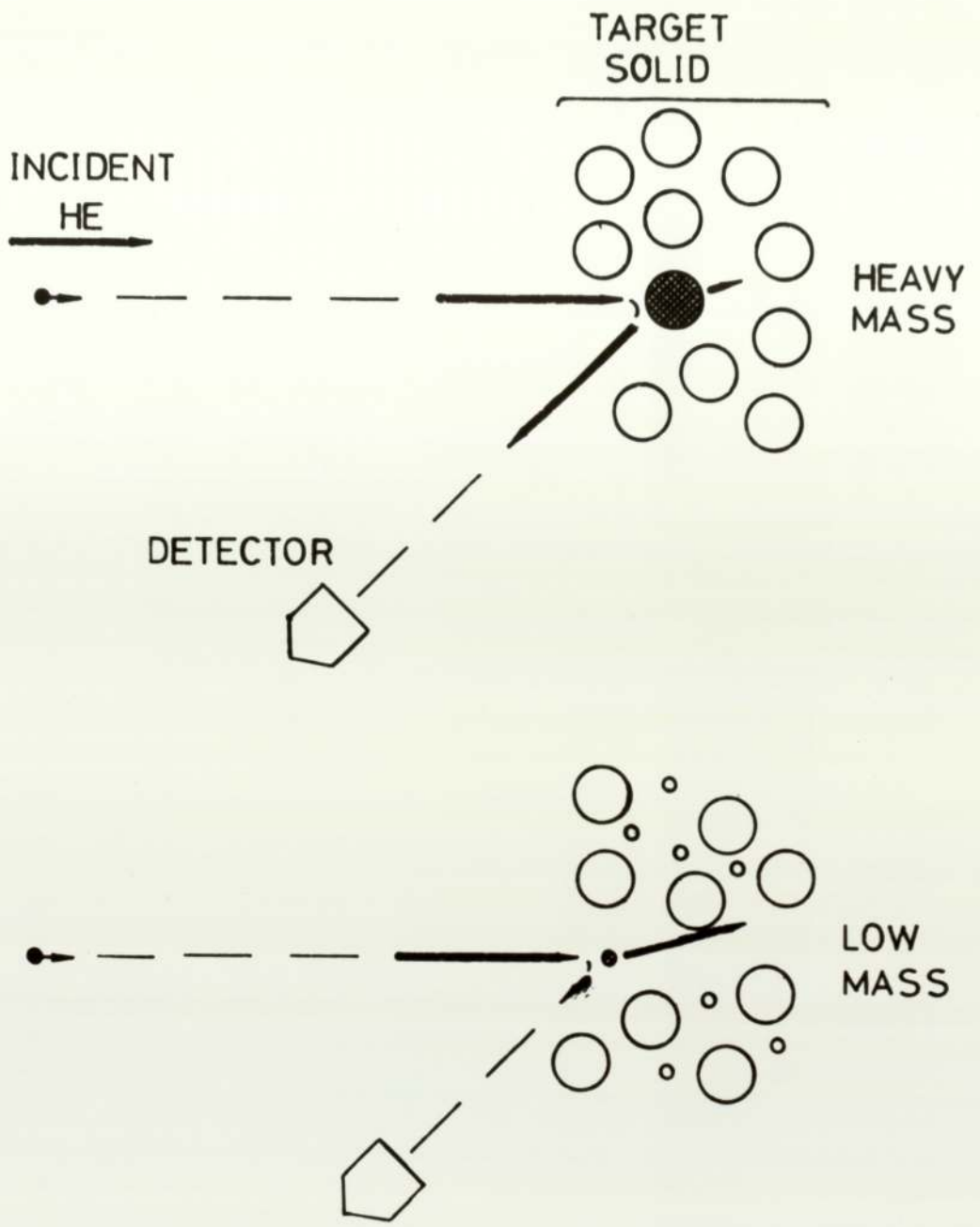


Fig.213 Representation of Conservation of Momentum.

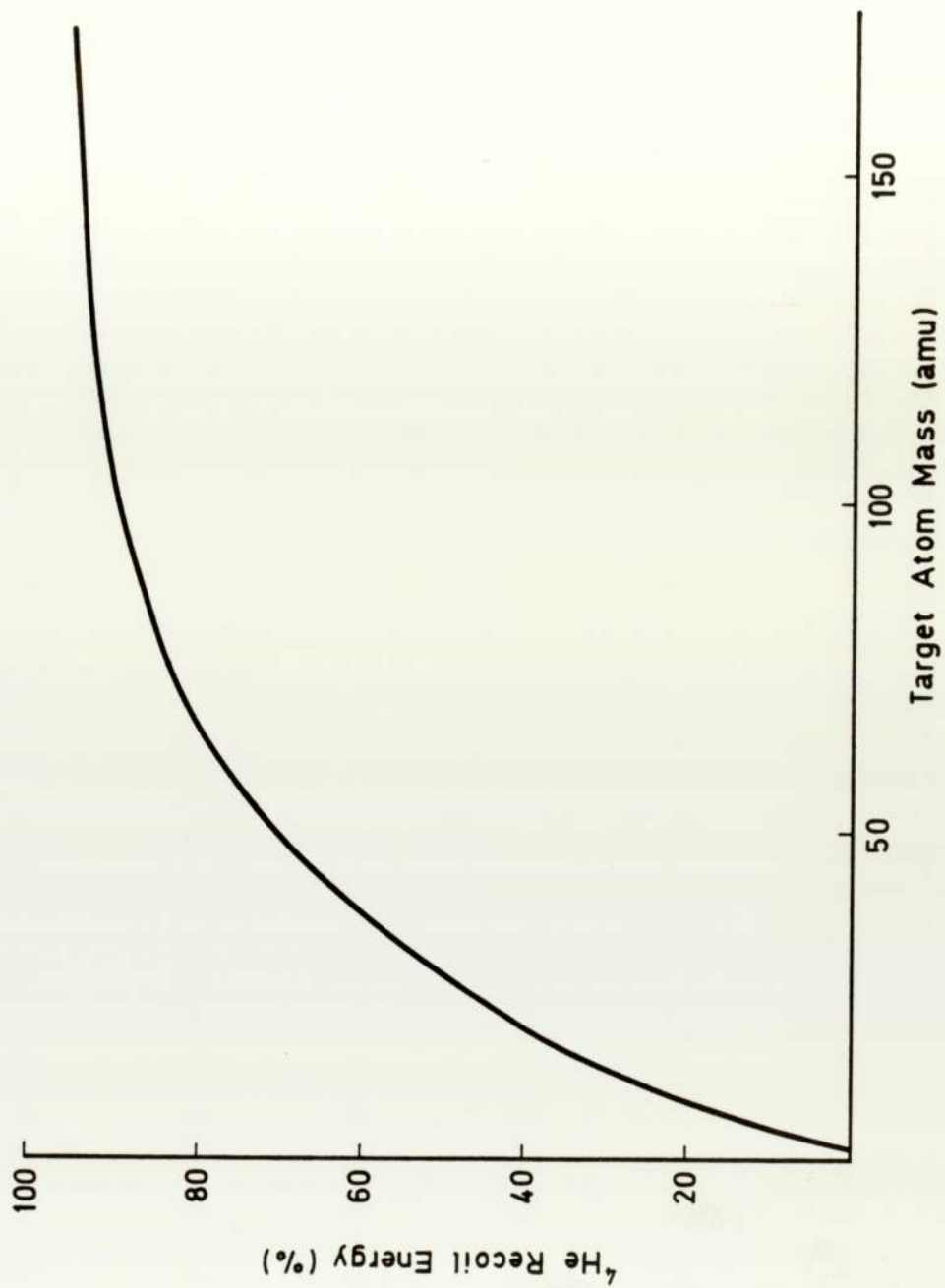


Fig.2.14 The Dependence of α -particle Recoil Energy with Atomic Mass.

probability of a scattering event occurring between the α -particle and that element. The differential scattering cross-section can be written:

$$\sigma(\theta_s) = \left[\frac{Z_p Z_t e^2}{2E \sin^2 \theta_s} \right]^2 \frac{(\cos \theta_s + (1 - (M_p / M_t) \sin^2 \theta_s)^{1/2})^2}{(1 - (M_p / M_t) \sin^2 \theta_s)^{1/2}}$$

where M_p is the mass of the α -particle

M_t is the mass of the target atom

Z_p is the atomic number of the α -particle

Z_t is the atomic number of the target atom

E is the energy of the α -particle immediately before scattering

and θ_s is the scattered angle of the α -particle.

Because of the factor Z_t^2 , the yield of backscattered α -particles varies rapidly with the mass of the target elements. This effect is shown in Fig. 2.15 for the same number of atoms of each element. In other words, small amounts of heavy elements are easier to detect than the same quantity of light elements. The yield Y , of α -particles scattered into a solid angle at a given energy and detection angle is related to the number of atoms per unit area N , of an element by

$$Y = Q \sigma(\theta_s) \Omega N$$

where Q is the number of α -particles

and $\sigma(\theta_s)$ is the average differential scattering cross-section, taken over a finite solid angle Ω , spanned by the detector.

So this shows the second important feature of the technique; the ability to analyse quantitatively different elements on or near the surface of the specimen.

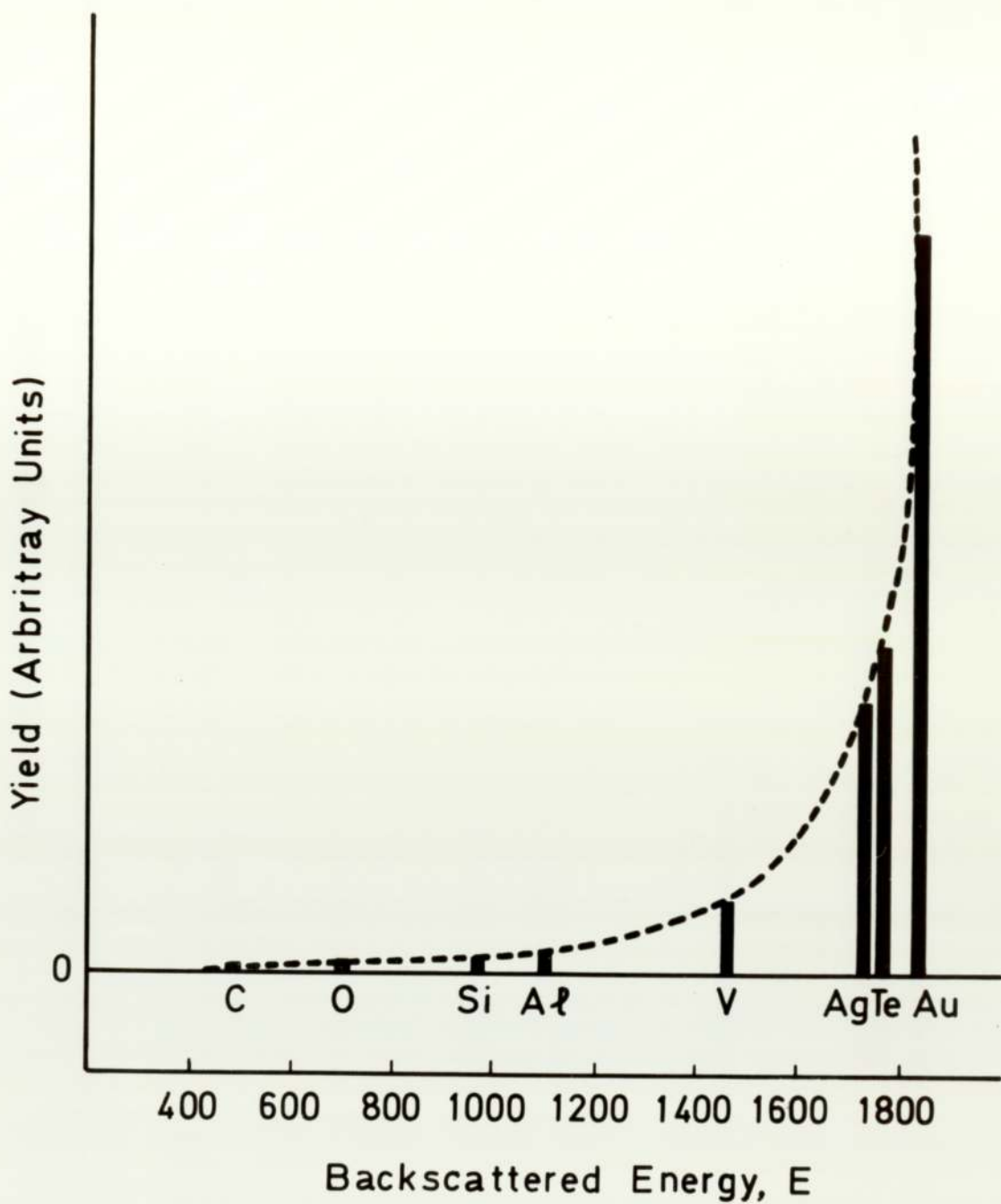


Fig.2.15 Idealised Spectrum showing the Yield Variation for Equal Numbers of Atoms of Each Element.

When the α -particles penetrate the target, they lose energy to the electrons of the target atoms by ionization and excitation. Thus, the further the α -particle penetrates into the target, the more energy it will lose by these effects. If a Rutherford elastic collision occurs, the energy of the α -particle is reduced by an amount defined by the Kinematic factor and reduced even more during its return to the surface (again by ionization and excitation effects). By measuring this energy loss, it is possible to determine the depth of penetration of these α -particles into the sample, i.e. concentration gradients for elements within the target can be found.

E.P.M.A. and R.B.S. can both be used to establish the presence, distribution and concentrations of any new elements which may have appeared in the surface layers of the polymer specimens as a consequence of wear under boundary lubrication conditions. They will both also detect any changes in the elements already present before wear. However, these two techniques do not yield any information on the changes, if any, in mechanical properties which may have occurred during wear. An experimental technique designed to investigate this last aspect of polymer friction and wear under boundary lubrication conditions, is described in the next section.

2.4 Indentation Tests

2.4.1 Introduction

One of the properties of the amorphous regions of a polymer is that as its temperature is raised, there is a sharp transition from glass-like behaviour to a soft, rubbery behaviour. The particular temperature at which this effect occurs is known as the Glass Transition Temperature (T_g). At the T_g , there is a decrease in hardness of the polymer. An indentation experiment was devised to determine whether any change in T_g of the PPO had occurred in the upper few microns of the

polymer as a consequence of wear under boundary lubrication conditions. This experiment assumes that the depth of indentation is inversely proportional to the hardness of the polymer.

2.4.2 Experimental Details of Indentation Tests

The Linear Displacement Transducer (described in Ch 2.1.5) and associated circuitry readily resolves displacements of the order of $0.1 \mu\text{m}$. For the indentation experiments, the free-moving stylus of the transducer was connected to a flat-ended indenter. The load was applied using an ordinary flat disc 10g (0.1N) weight with a 'V-shape' cut from it to facilitate placement of the disc on top of the indenter, see Fig. 2.16 and Fig. 2.17. The total weight of stylus, indenter and load was 0.12N. This produced an indentation of two or three microns at room temperature on the surface of an unworn pin. The pin surface was heated and indentations made at various temperatures for both unworn and worn specimens. For every different temperature of indentation, a new specimen was used. The pins were set in a thermally-insulating block of asbestos fibre and cement compound, so that only the top surface was exposed. A hot filament coupled to an air compressor allowed just the surface of the pin to be heated. The pins were drilled from the back to within $50 \mu\text{m}$ of the top surface. The diameter of this hole was 0.5mm, just wide enough to allow a 36 S.W.G. (0.19mm) copper-constantan thermocouple junction to be inserted, so that it was as close to the heated surface as possible. The last 2mm of outer covering was removed from the copper and constantan thermocouple wires, twisted together and coated with silver conducting paint, which also acted as an 'adhesive' to form the junction. To ensure that a good junction had been produced and unaffected by the silver conducting paint, the thermocouple was calibrated against a platinum resistance thermometer. The coated thermocouple was placed in an insulated, resistance-heated, copper block while the other end was maintained at 0°C . The e.m.f. of the thermocouple was compared to the standard copper-constantan values and it was found that the

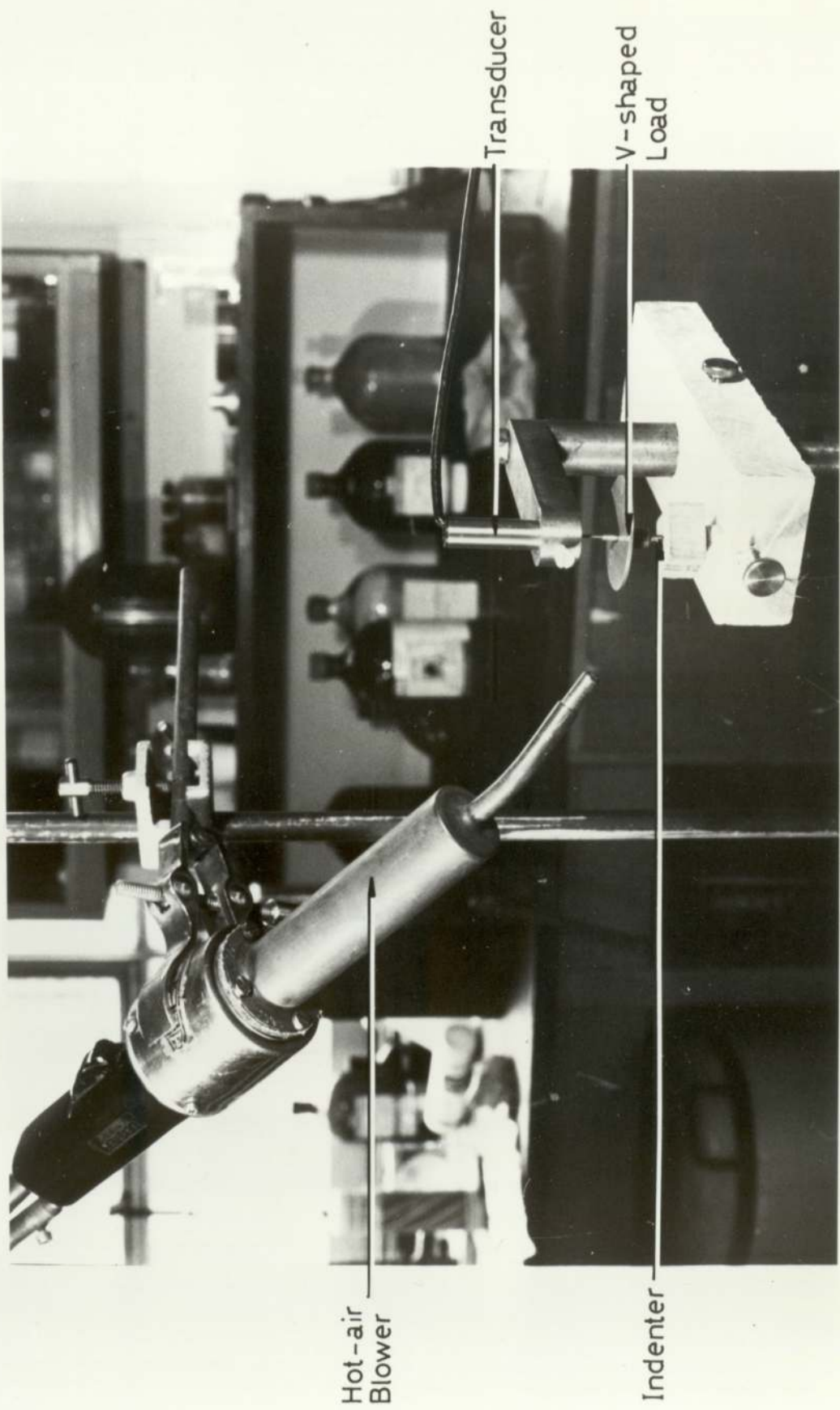


Fig.2.16 Indentation Tester

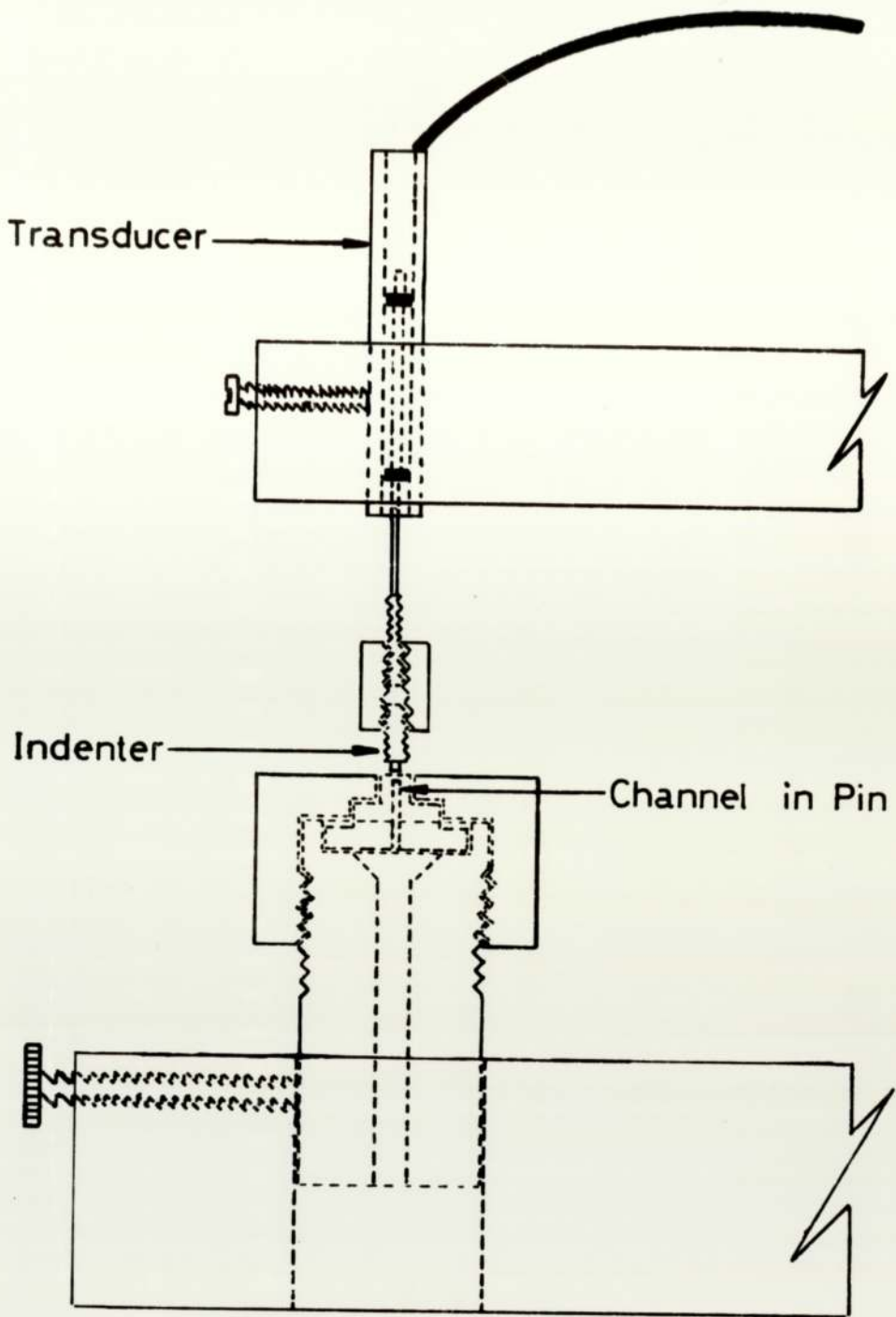


Fig.2.17 Practical Details of Indentation Tester.

thermocouple junction was unimpaired by the silver conducting paint. The results obtained from the indentation experiments are purely a comparison of the Glass Transition Temperature of unworn and worn pins and not absolute measurements, since the thermocouple does not measure the actual surface temperature.

The indenter was made from steel which is a good conductor of heat and expands when heated. This presented a problem; if the pin was heated and the indenter placed on top at a particular temperature, then not only was heat removed from the surface of the wear pin by the steel indenter (i.e. the measured temperature dropped), but the indenter also expanded due to the hot-air blower and the additional heat from the surface. This resulted in a 'negative' indentation being registered. This problem was overcome by raising the indenter a small distance above the surface of the pin as it was heated (2mm was sufficient). It was found, eventually, that the surface temperature stabilized and by this time the indenter's expansion had also reached an equilibrium. When the indenter was placed on top of the surface, there was no surface temperature measurement reduction and a positive indentation was obtained. Different surface pin temperatures were obtained by varying the distance of the hot-air blower from the surface of the pin.

2.5 X-Ray and Electron Diffraction

An X-Ray Diffraction pattern was obtained from a bulk sample of PPO. Glancing angle X-Ray diffraction was then attempted on worn surfaces of PPO to investigate any changes in crystallinity which may have occurred as a result of sliding. After varying the glancing angle, X-Ray voltages and currents, time of exposure, no acceptable diffraction pattern could be obtained.

There was also very little success in obtaining a transmission electron diffraction pattern. The problem encountered in this technique was in obtaining a sample thin enough to enable the electron beam to pass through. The optimum thickness of the

specimen is of the order $2,000\text{\AA}$. Although the polymer can be microtomed, uniform specimens of this thickness are difficult to produce.

2.6 Differential Thermal Analysis

An attempt was also made to measure the T_g of the surface layer by microtoming the polymer and using Differential Thermal Analysis. The mass of a $10\ \mu\text{m}$ disc of PPO microtomed from the surface is approximately 0.03mg . This is much smaller than the minimum sample size (10mg) of the D.T.A. used. The particular D.T.A. is thus far too insensitive for the microtomed sample.

CHAPTER THREE

EXPERIMENTAL RESULTS

3.1 Friction and Wear

3.1.1 Establishing Conditions for Boundary Lubrication

The divisions between the lubrication regimes of boundary, elastohydrodynamic and 'mixed' are ill-defined and somewhat controversial. The onset of hydrodynamic film formation will depend on the particular geometrical sliding configurations involved and the moduli of elasticity of the materials in contact. To identify the limits of the boundary lubrication regime for the present apparatus and materials, a series of experiments was made to determine the variation of friction with speed at different loads in silicone fluids of different viscosities. The results are shown in Fig. 3.1. In each experiment, the friction was allowed to stabilize; this usually occurred within a period of half an hour. A new pin and ring was used for each load/viscosity combination. The individual curves in Fig. 3.1, can be plotted on a single graph by using the dimensionless parameter ($\eta N/P$), as shown in Fig. 3.2, where η is the viscosity of the fluid in Nsm^{-2} , N is the angular speed in rev.s^{-1} , and P is the pressure in Nm^{-2} . Boundary lubrication conditions are assumed to occur where the coefficient of friction μ is more or less independent of the dimensionless parameter ($\eta N/P$). This occurs at values of the parameter less than 10^{-9} .

3.1.2 Measurements

Fig. 3.3 shows a graph of coefficient of friction against speed for a load of 11N and a silicone fluid viscosity of 10cs. The coefficient obtained during dry sliding is

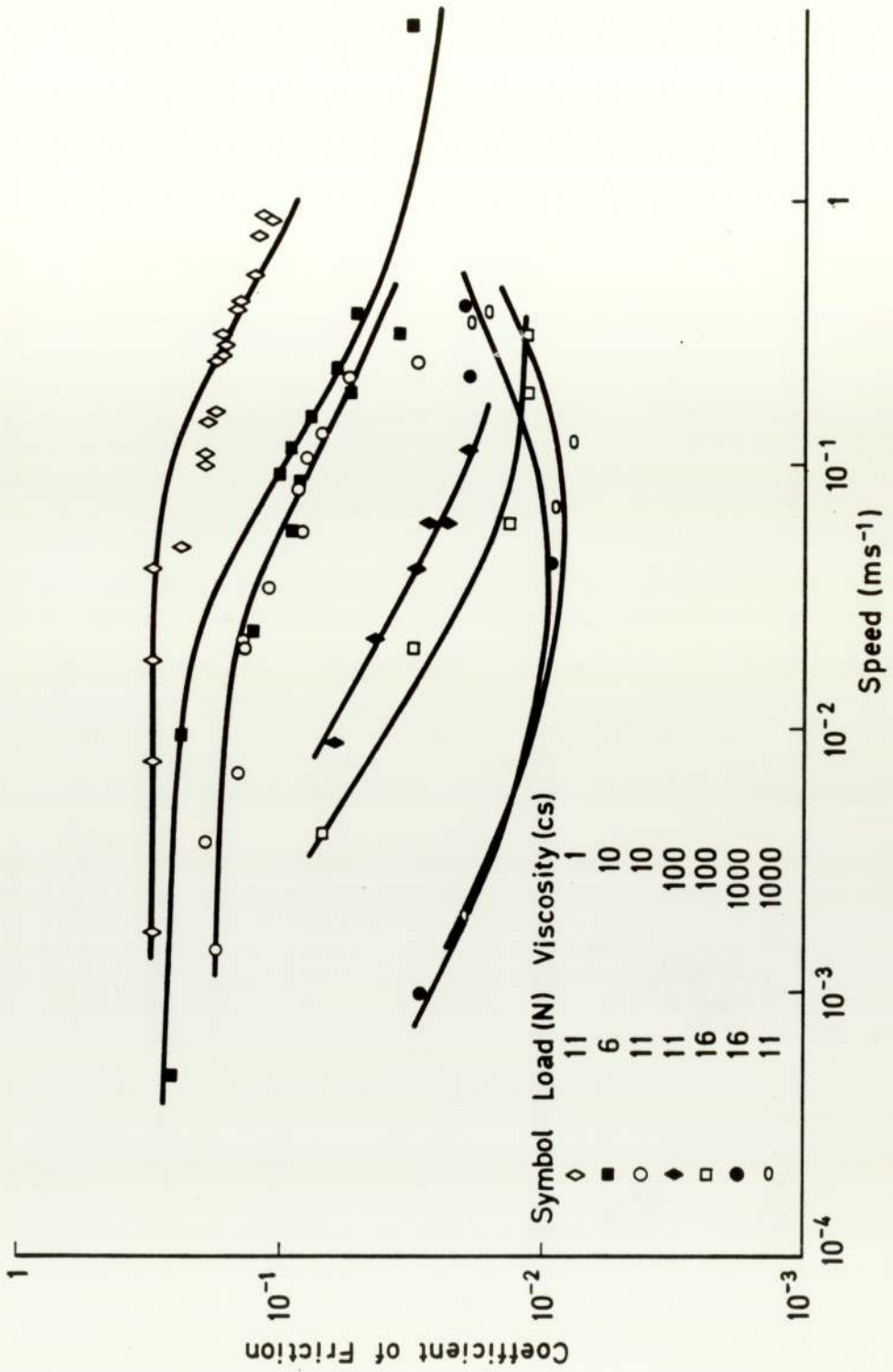


Fig.3.1 Variation of Coefficient of Friction with Speed for Different Loads and Viscosities.

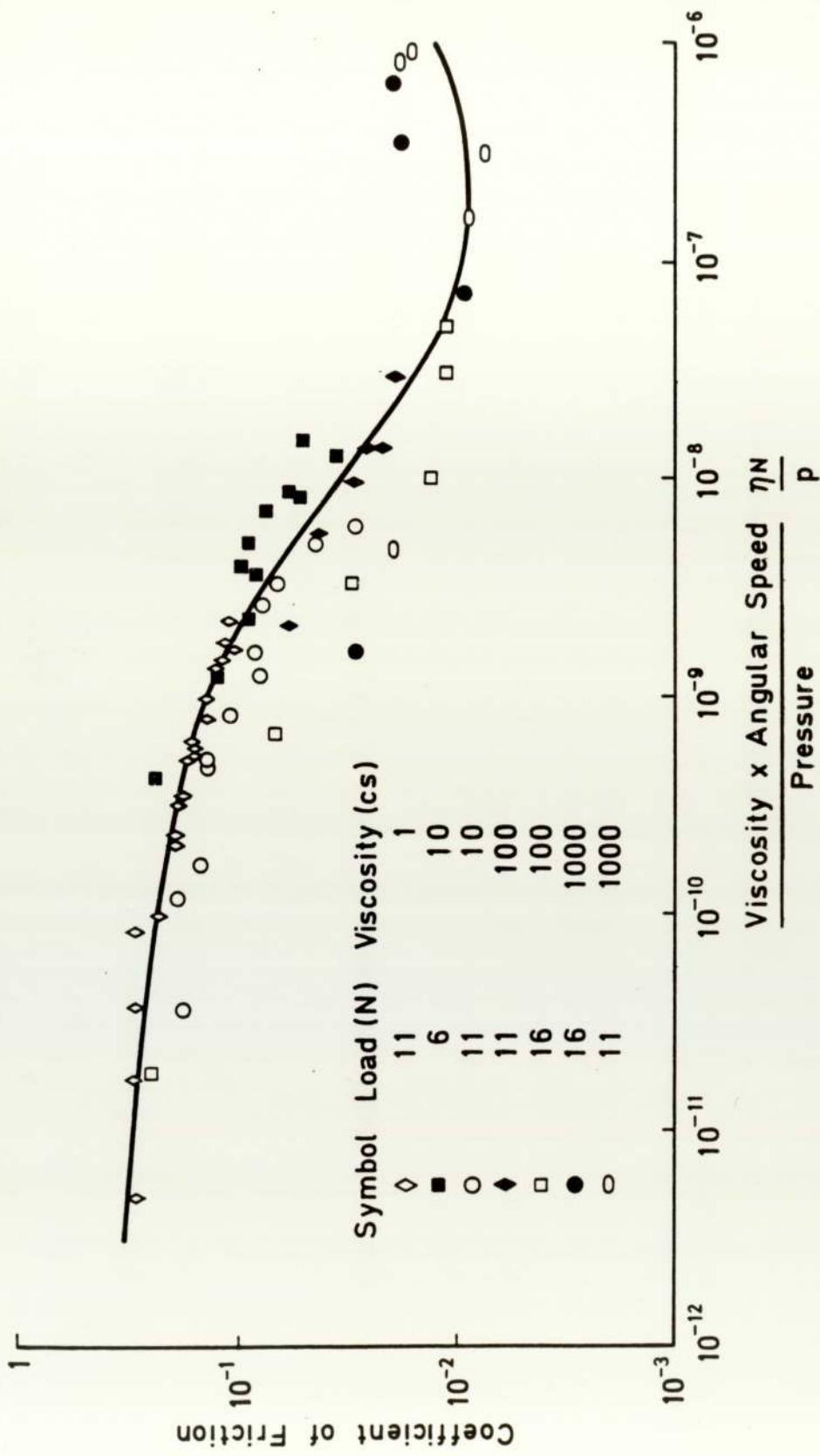


Fig.3.2 Variation of Coefficient of Friction versus the Dimensionless Parameter $\frac{\eta N}{p}$.

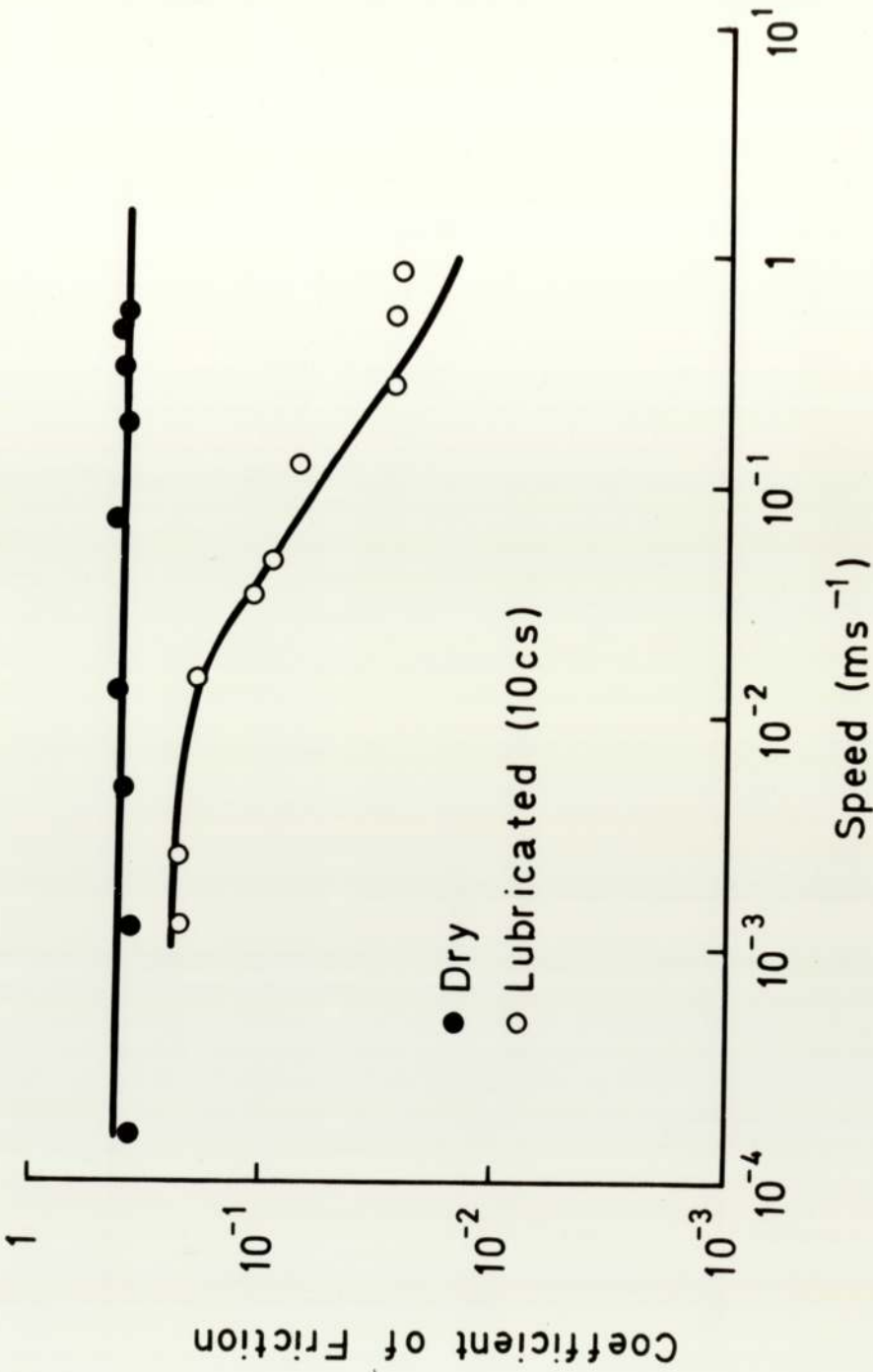


Fig.3.3 Coefficient of Friction versus Speed for a Load of 11N(Dry and Lubricated with 10cs Silicone Fluid).

shown also. By consideration of Fig. 3.1, Fig. 3.2 and Fig. 3.3, it is evident that by using a load of 11N and a viscosity of 10cs, experiments can be carried out in the boundary, mixed, and elastohydrodynamic regimes, merely by increasing the speed of sliding. Fig. 3.4 shows the wear rate versus speed graph for a load of 11N, under dry sliding conditions and when lubricated by 10cs viscosity silicone fluid. Wear rates were calculated from the slope of the wear trace after 1,000 revolutions of the wear disc, when steady-state conditions had been reached. A typical trace, showing both wear and friction, is given in Fig. 3.5. The dry and lubricated wear rates are quite similar at speeds within the boundary regime; differences only begin to occur at about the same speed as the friction starts to decrease, i.e. at approximately 0.025ms^{-1} (see Fig. 3.3).

There are two possible ways to detect any changes which may have occurred in the surface layers of the PPO during boundary lubrication; indirectly using the friction and wear apparatus, and directly, by using physical analytical techniques on the surface layers. The indirect approach was pursued first by wearing a pin under conditions of boundary lubrication for a certain number of revolutions of the disc. The polymer wear surface was then wiped with absorbent tissue to remove any excess fluid, the bath of lubricant was removed and the wear counterface replaced with a clean dry one having the same C.L.A. surface roughness value and same method of preparation. Sliding was then recommenced under the same load and speed as before, but now under nominally dry conditions. The result of this experiment was that the coefficient of friction still maintained a low value and under further examination, this value was found to be slightly lower than the coefficient of friction when the lubricant was present. (This observation is discussed in more detail in Ch. 4). However, after a certain depth of wear, the coefficient of friction rose quite sharply to the dry value. This type of experiment was performed at three different speeds; 0.0037ms^{-1} (well within the boundary regimes); 0.021ms^{-1} (more or less at the transition) and 0.25ms^{-1} (in the mixed lubrication regime). Results are shown in Fig. 3.6. This shows two typical chart

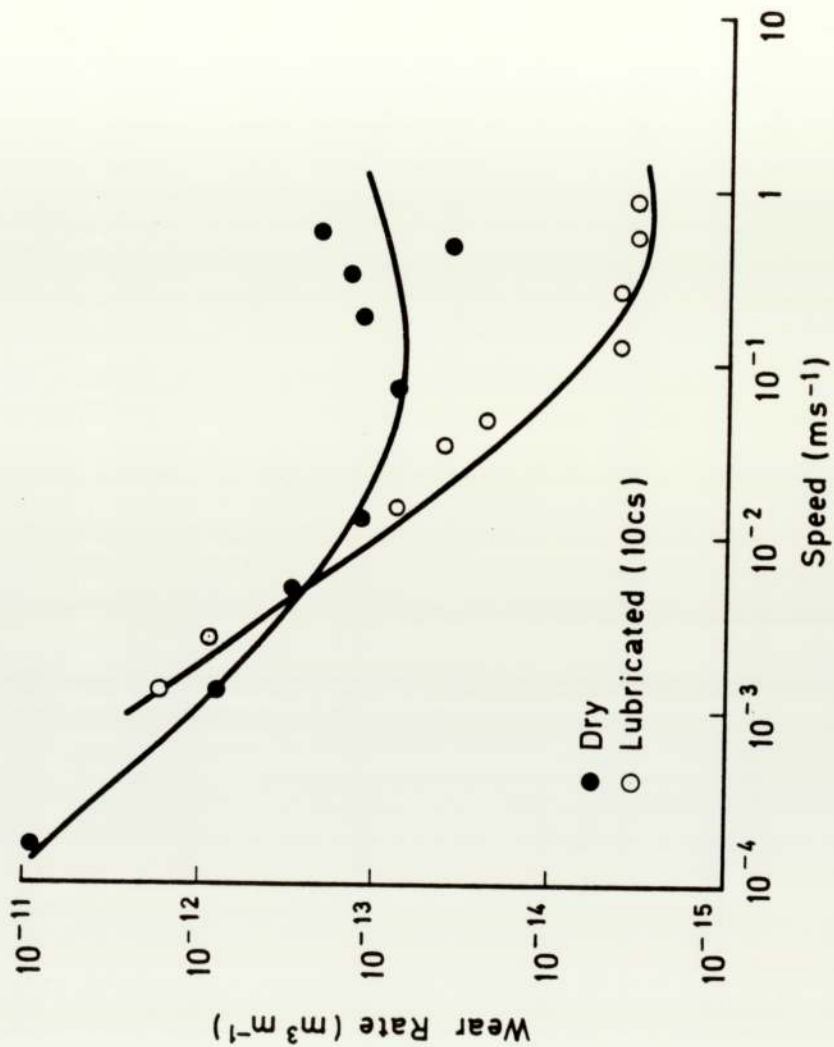
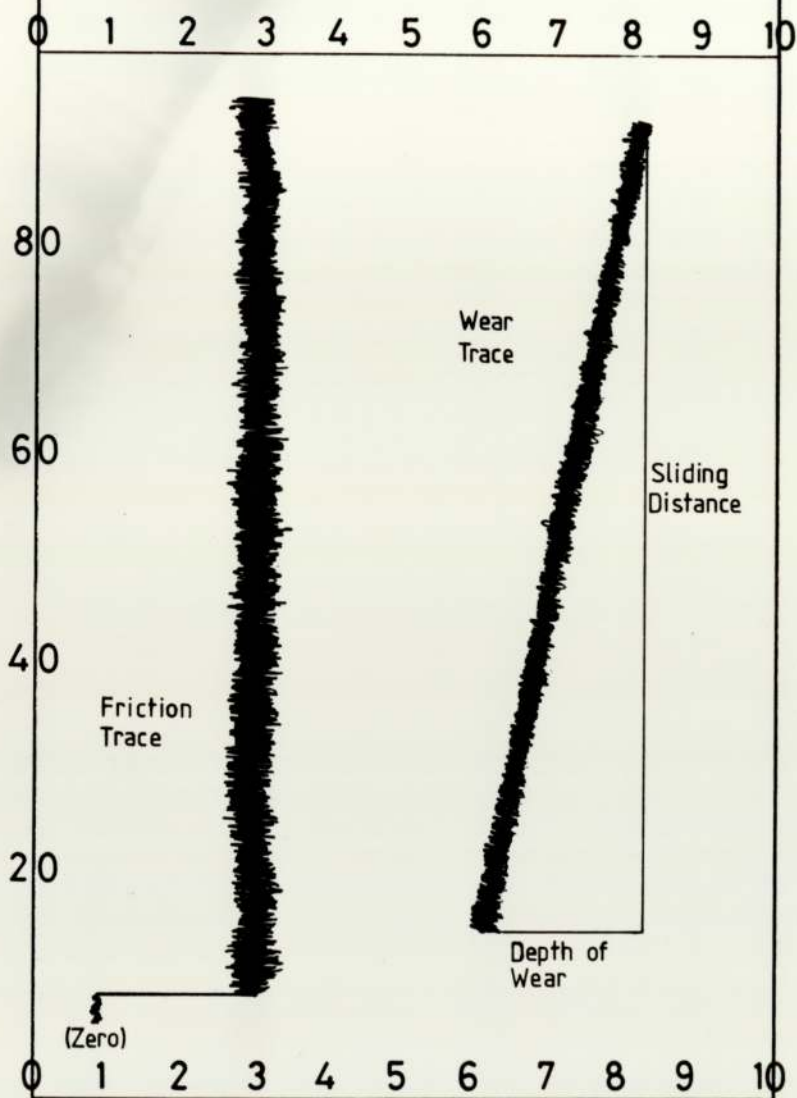


Fig.3.4 Wear Rates versus Speed for a Load of 11N, for Dry Conditions and Lubricated with 10cs Silicone Fluid.

The Chart Recorder paper is calibrated in microns to measure the Depth of Wear. Knowing the Chart Recorder Speed and Sliding Speed, the Sliding Distance and hence Wear Rate can be calculated.



The Chart Recorder paper is calibrated so that, for example $1\text{cm} \equiv 10\text{gm force}$. The Friction Force is multiplied by 3 to calculate μ , (See Ch.2.1.6).

Fig.3.5 Typical Chart Recorder Trace showing Friction and Wear.

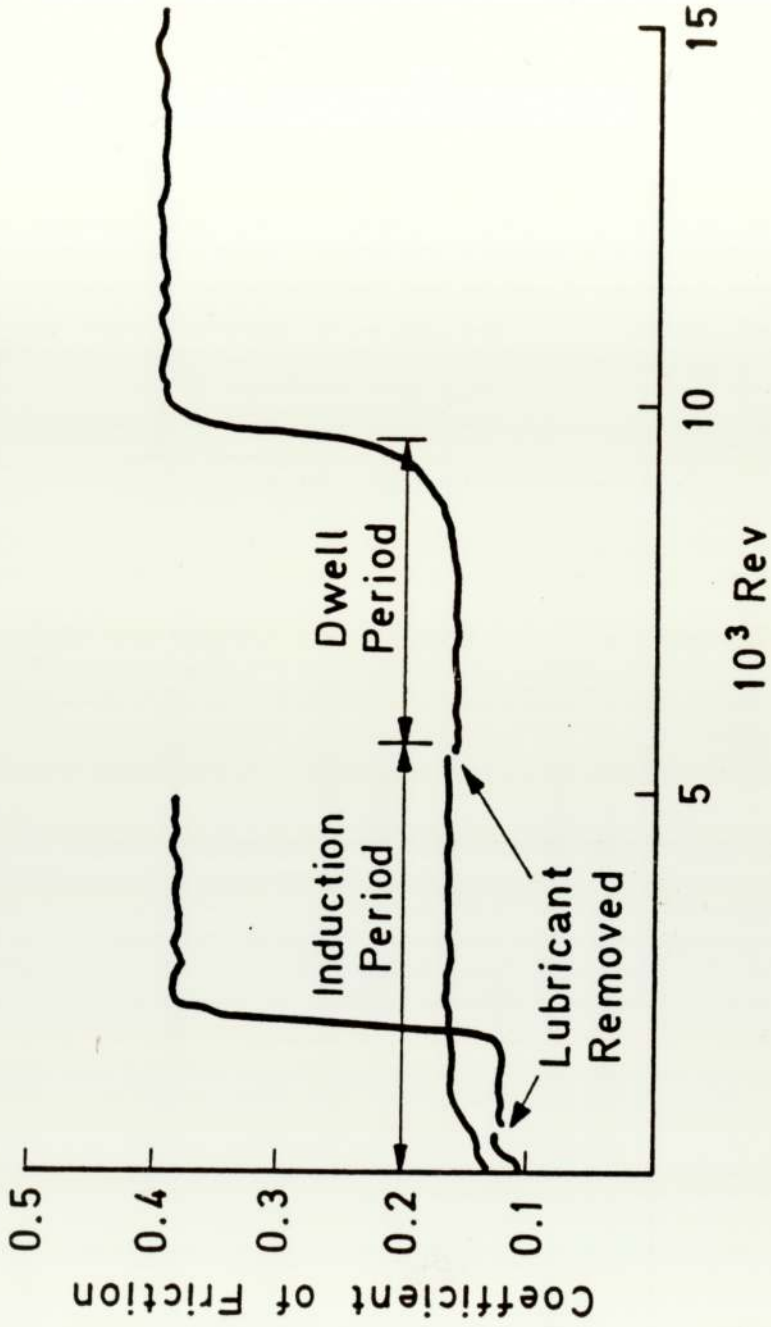


Fig.3.6 Two Typical Chart Recorder Traces for the Speed of 0.021ms⁻¹ showing Induction and Dwell Periods.

recorder traces (for the speed of 0.021ms^{-1}) from which it can be seen that a finite time (or number of revolutions of the wear disc) is needed after the removal of the fluid - a 'dwell time' - before the coefficient of friction rises to its characteristic dry value. It may therefore be concluded that sliding in silicone fluid leads to the formation of a surface layer on the polymer which differs in some way to that obtained during dry sliding. The time required for the friction to rise to its dry value can then be interpreted as the time needed to wear away this modified surface layer. To examine this aspect in more detail, the depth of polymer worn away during the dwell-time was determined for different induction times (or number of revolutions of the wear disc) of lubricated sliding. The results are shown in Fig. 3.7 for the three different speeds mentioned previously. Fig. 3.7 clearly indicates that a critical period of lubricated sliding is required to establish a modified surface layer (the critical period is shown by the sudden increase in depth of wear before μ rises). The critical number of revolutions for the speed of 0.0037ms^{-1} is approximately 2,500 and approximately 12,500 for the speed of 0.021ms^{-1} . These can be converted into critical times (17 hrs and 18 hrs for the speeds of 0.0037ms^{-1} and 0.021ms^{-1} respectively) and used to plot a graph of the time of critical period of lubricated sliding versus speed. Fig. 3.7 shows that for the speed of 0.25ms^{-1} , after 230,000 revolutions of lubricated sliding, no penetration had occurred. This experiment was repeated for the same speed, for an even larger number of revolutions, 900,000 (equivalent to a time of 109 hrs) and still no penetration occurred. The critical periods of lubricated sliding required to produce a modified layer versus sliding speed are shown in Fig. 3.8. It can be seen that the duration of the critical period of lubricated sliding is constant within the boundary regime, but tends to infinity outside this regime. In other words, it is impossible for the silicone fluid to penetrate at a speed of 0.25ms^{-1} , under conditions which are well outside the boundary regime.

One uncertainty over these results still remains. Because of the sensitivity of the friction and wear behaviour of polymers to the presence of very small amounts of

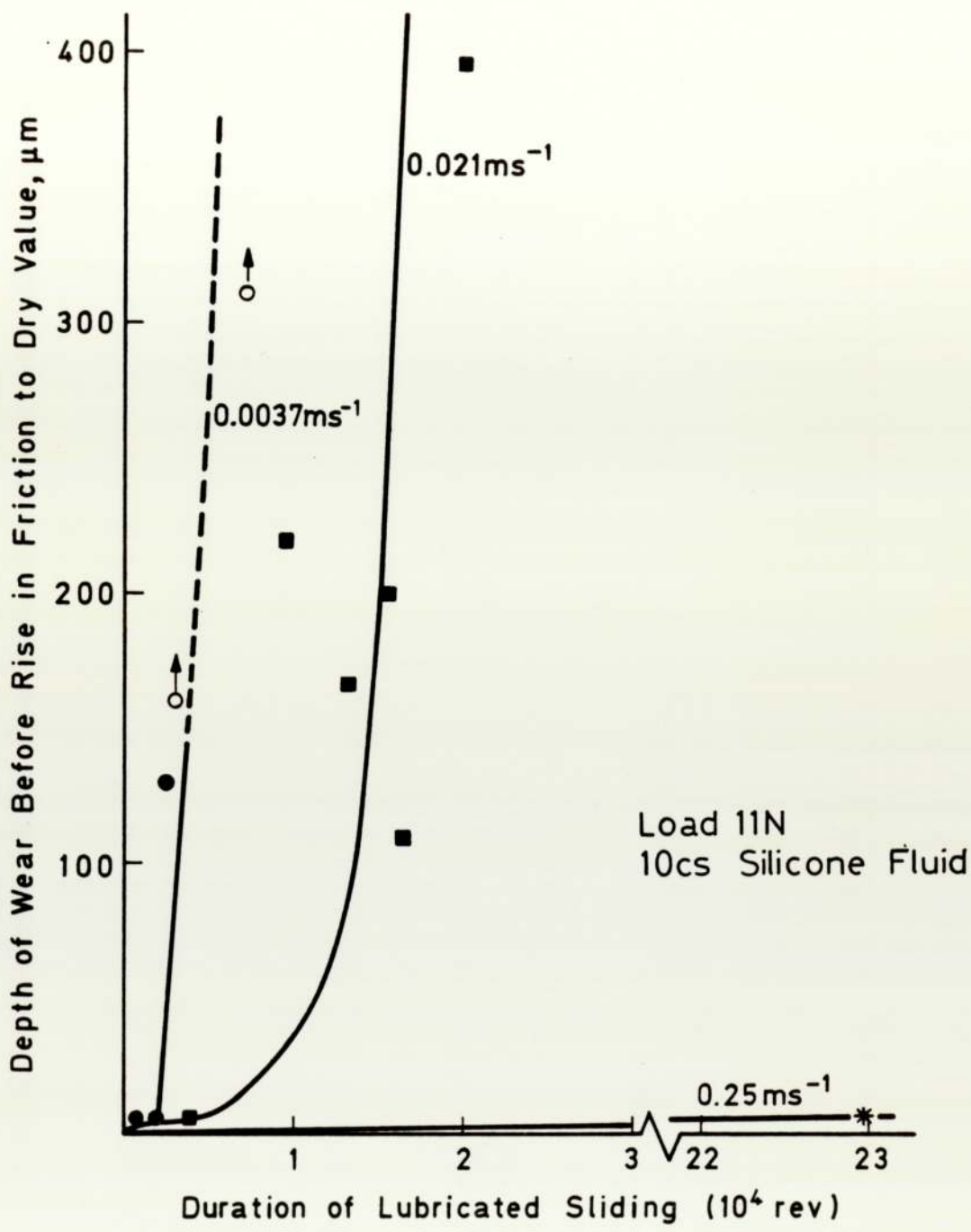


Fig.3.7 Depth of Wear before Rise in Friction to Dry Value versus Duration of Lubricated Sliding, for Three Different Speeds of Sliding, 0.0037ms^{-1} , 0.021ms^{-1} and 0.25ms^{-1} .

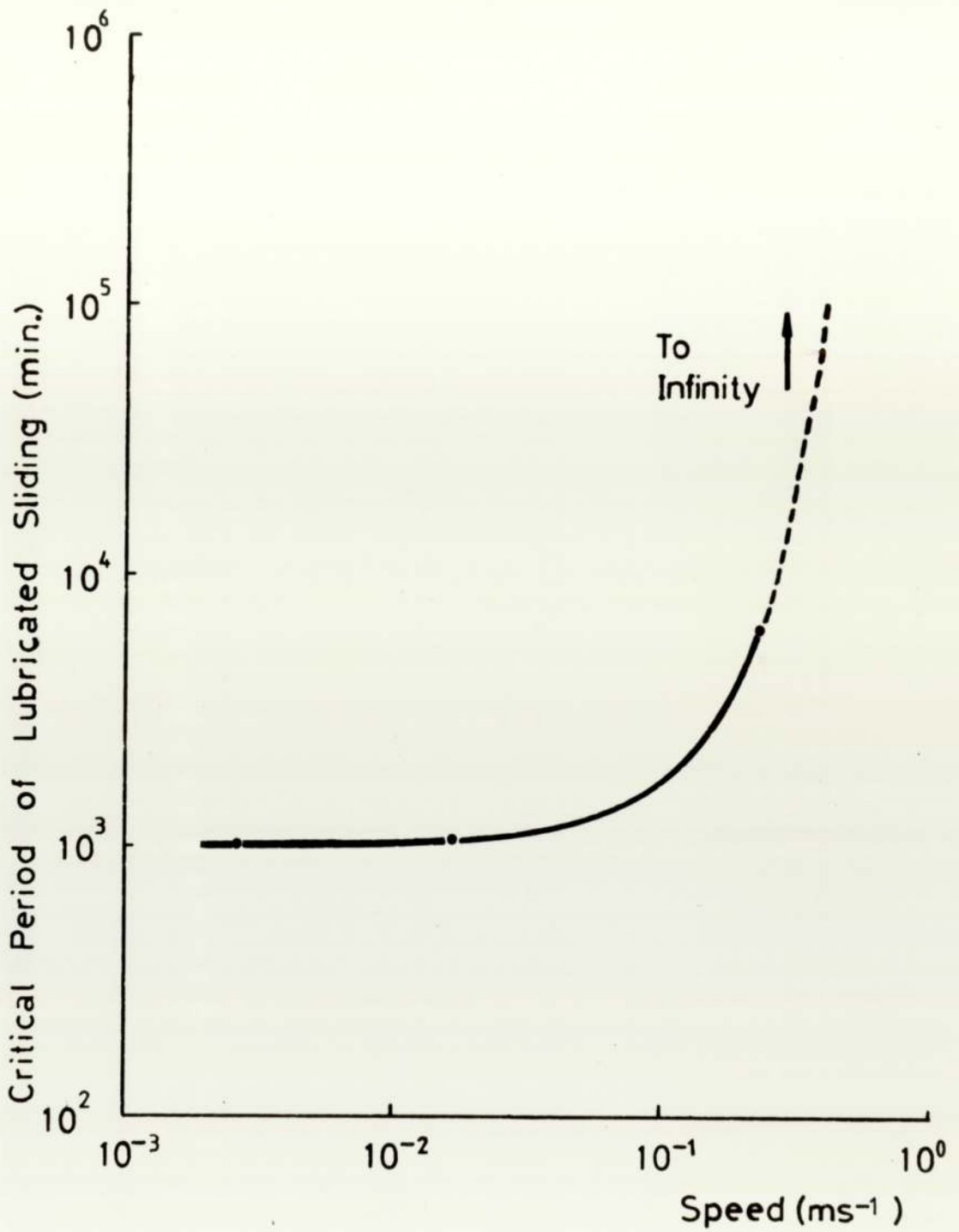


Fig.3.8 Critical Period of Lubricated Sliding versus Speed.

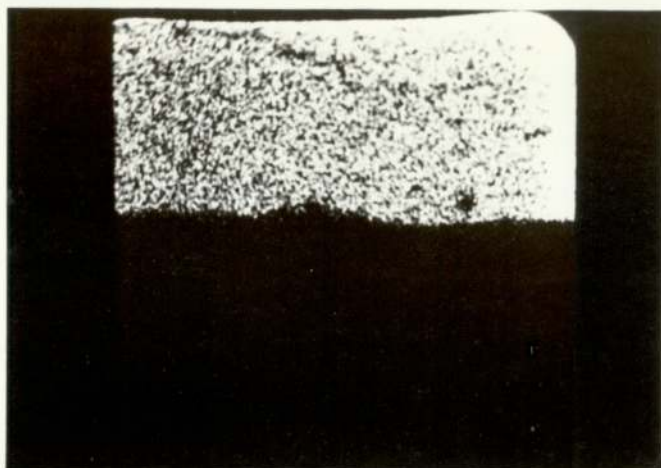
fluid, it is possible that the method of removal of the excess fluid at the end of the period of lubrication was insufficient to remove all traces of fluid. To examine this, a polymer pin was immersed in silicone fluid at room temperature for a few seconds and the excess fluid removed as previously. The pin was positioned on the apparatus and set in motion at a speed of 0.0037ms^{-1} with a clean dry wear counterface and no bath of lubricant. The coefficient of friction rose immediately to its dry value. It is evident, therefore, that the long dwell times obtained previously with the worn lubricated polymer could not have been attributable to residual traces of fluid. It seems reasonable to conclude, at this stage, that the long dwell times are a consequence of a modified surface layer produced under boundary lubrication conditions. The next section is concerned with the examination of the surface layers of the PPO using a more direct approach.

3.2 Electron Probe Microanalysis (E.P.M.A.)

Fig. 3.9 and Fig. 3.10 show X-Ray intensity pictures for the silver and silicon distributions and an electron micrograph of the transverse section of a pin of PPO worn under conditions of boundary lubrication - 0.0037ms^{-1} , 10cs viscosity silicone fluid and a load of 11N. Fig. 3.11 gives the same information except for a speed of 0.021ms^{-1} , 10cs viscosity silicone fluid and a load of 11N. These samples had been worn for a number of revolutions of the counterface appreciably greater than the limiting values of 2,500 for the speed of 0.0037ms^{-1} and 12,500 for the speed of 0.021ms^{-1} (see Fig. 3.7). The specimen edge is clearly defined by the silver X-Ray intensity picture, so that any Si present above this line must be in the polymer. As can be seen, the silver conducting paint also contains silicon, so to avoid any confusion, a portion of the mounting medium was removed from above the wear surface, as previously described. The results of this are shown in Fig. 3.12 and Fig. 3.13 for the same conditions as in Fig. 3.9, except that the pin was run for an even greater number of revolutions, 7,000. This larger period did not result in any further changes in the modified surface layer (i.e. no increase in the amount of Si

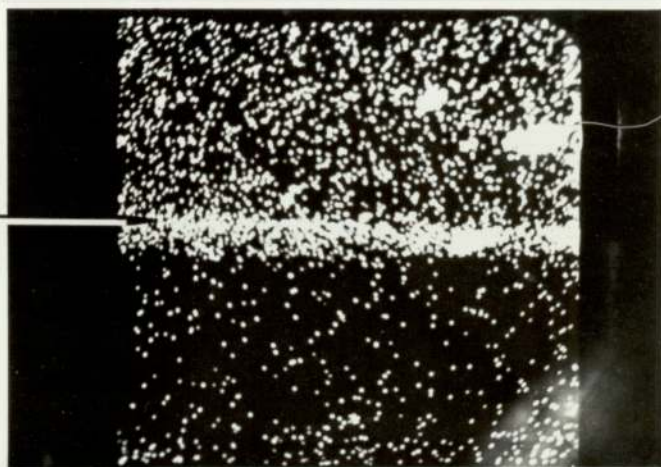
(a) X-Ray Distribution
of Ag

H10 μ m



(b) X-Ray Distribution
of Si

Specimen
Edge



(c) Electron Micrograph

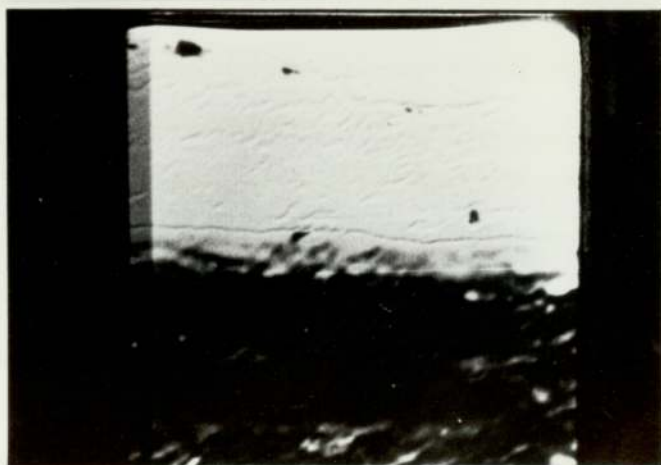


Fig. 3.9 (a),(b) and (c) X-Ray Distribution of Ag and Si and Electron Micrograph of the Transverse Section through a Polymer Pin Worn under Conditions of Boundary Lubrication (Speed 0.0037ms^{-1} , 10cs Viscosity Silicone Fluid, 11N Load), Magnification X1000.

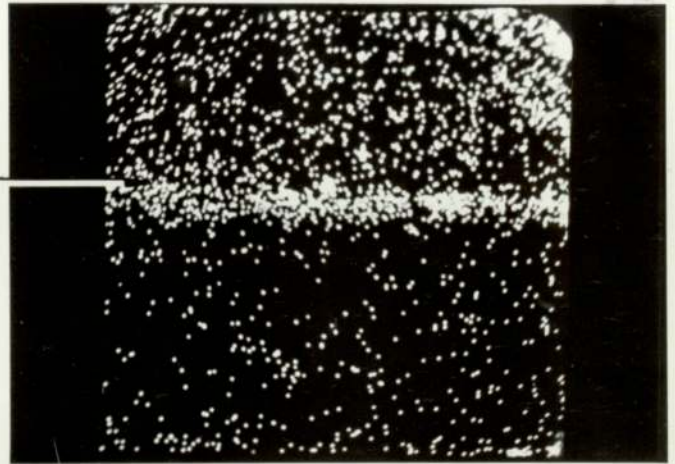
(a) X-Ray Distribution
of Ag

H 10 μ m



(b) X-Ray Distribution
of Si

Specimen
Edge



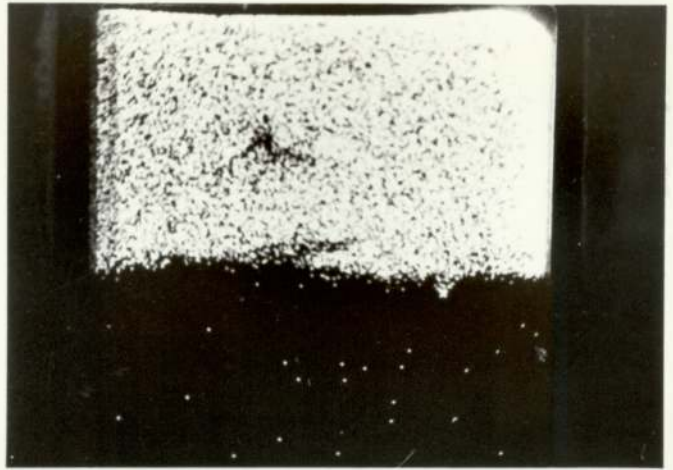
(c) Electron Micrograph



Fig.3.10 (a),(b)and(c) X-Ray Distributions of Ag and Si and Electron Micrograph of the Transverse Section through a Polymer Pin Worn under the same Conditions as in Fig.3.9, Magnification X1000.

(a) X-Ray Distribution
of Ag

H10 μ m



(b) X-Ray Distribution
of Si

Specimen
Edge



(c) Electron Micrograph



Fig.3.11 (a),(b)and(c) X-Ray Distributions of Ag and Si and Electron Micrograph of the Transverse Section through a Polymer Pin Worn under Conditions of Boundary Lubrication (Speed 0.021ms^{-1} , 10cs Viscosity Silicone Fluid, 11N Load), Magnification X1000.

(a) X-Ray Distribution
of Si

H 10 μ m

Specimen
Edge



(b) Electron Micrograph



Fig. 3.12 (a) and (b) A Typical Example of the X-Ray Distribution of Si and Electron Micrograph of the Transverse Section through a Polymer Pin Worn under the same Conditions as in Fig.3.9, except for 7,000 Revolutions of Lubricated Sliding, (using the later method of specimen preparation), Magnification X 1000.

(a) X-Ray Distribution of Si

10 μm

Specimen Edge



(b) Electron Micrograph

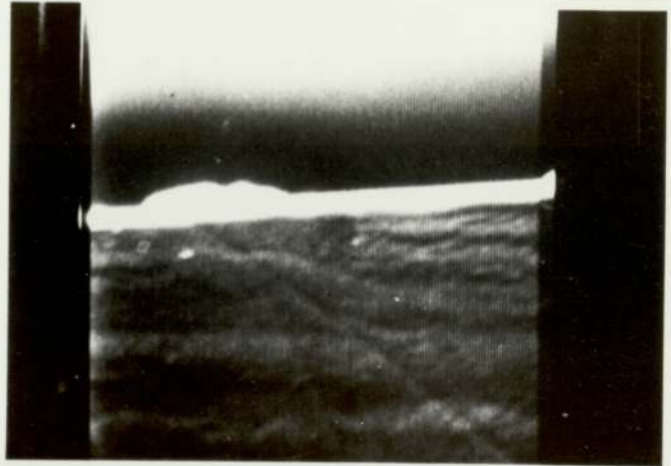


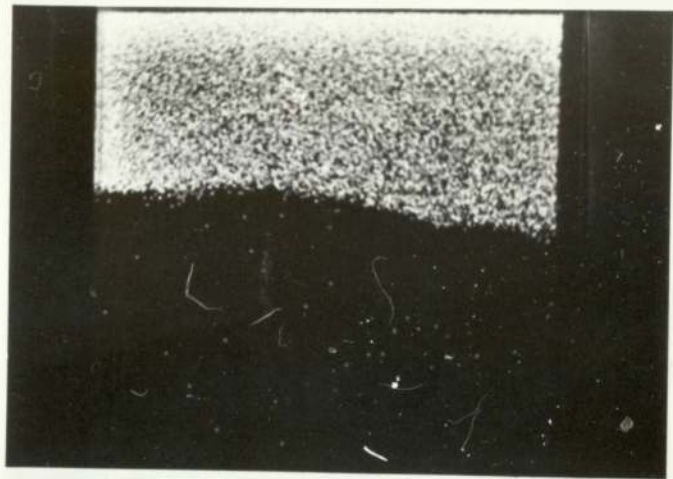
Fig.3.13(a) and (b) X-Ray Distribution of Si and Electron Micrograph of the Transverse Section through a Polymer Pin Worn under the same Conditions as in Fig.3.12, Magnification X1000.

present). Fig. 3.14 shows an area on the edge of the second tier of the wear pin used in Fig. 3.9, which had still been exposed to silicone fluid but not to sliding contact. This shows no concentration of silicon on the edge. Fig. 3.15 and Fig. 3.16 shows the top surface of an unworn pin, with the mounting medium removed. Again no silicon is present. The pictures in Fig. 3.14 were taken to show that Si was only present on the actual wear surface of the pin and had not been released to the other areas of the specimen during the mounting and polishing process. The results of Fig. 3.15 and Fig. 3.16 show that Si was not present in the polymer pin before wear.

Several of the E.P.M.A. silicon distribution maps suggest that superimposed on to a general, mean level of Si pick-up, there are isolated regions of higher concentration. This observation is supported by the line-profiles of Si across the centre of a worn pin as shown in Fig. 3.17 and Fig. 3.18. This pin was worn under conditions of boundary lubrication at a speed of 0.021ms^{-1} , 10cs viscosity silicone fluid, 11N load and 17,000 revolutions of lubricated sliding. The penetration of the electron probe beam is of the order of one micron. Fig. 3.18 shows an area of the profile at higher magnification. Two photographs of the area over which the line-profile was taken are shown in Fig. 3.19(a) and (b). They are at slightly different exposures. The rings on the polymer, arising from the rotation of the pin, are quite clear in the darker photograph, but an additional feature is visible in the lighter photograph - the appearance of material which has been raised from the surface of the polymer. (This is discussed later in this Chapter in the section on Scanning Electron Microscopy). A faint white line is visible in Fig. 3.19(a) showing the exact position of the line scan. The scanning is from top to bottom on the photograph and from right to left on the spectra. A general level of Si is shown on the surface of the pin, but with peaks on top, indicating regions of higher concentration. The total distance of scan in Fig. 3.17 is 0.8mm. The separation of the rings in Fig. 3.19(a) is therefore approximately 0.05mm ($50\ \mu\text{m}$), which agrees well with the separation of the two large peaks in the higher magnification line-scan shown in

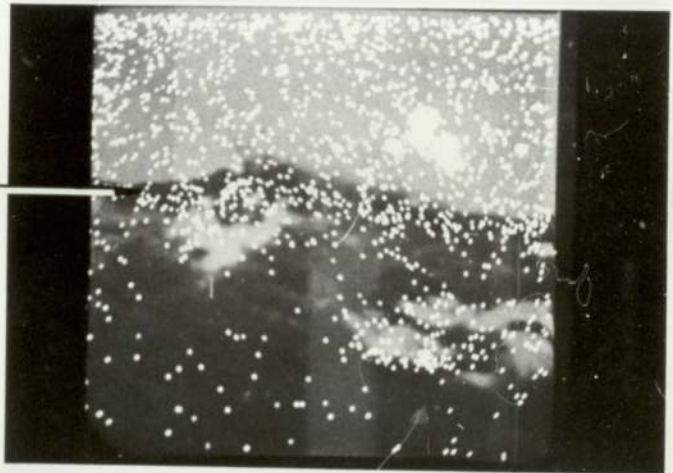
(a) X-Ray Distribution of Ag

H 10 μ m



(b) X-Ray Distribution of Si

Specimen Edge



(c) Electron Micrograph

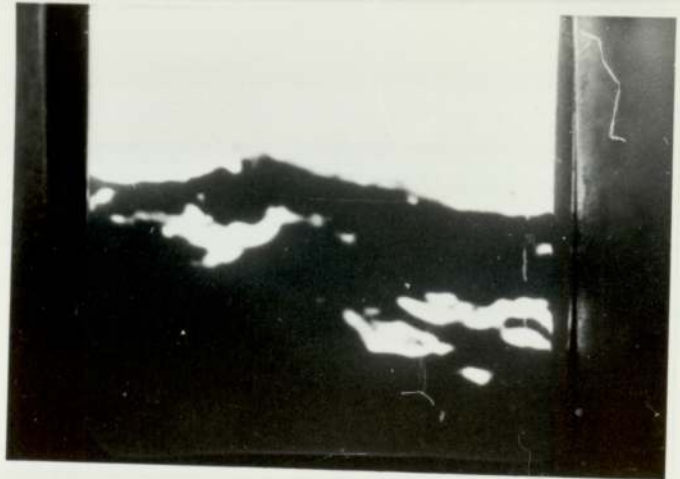
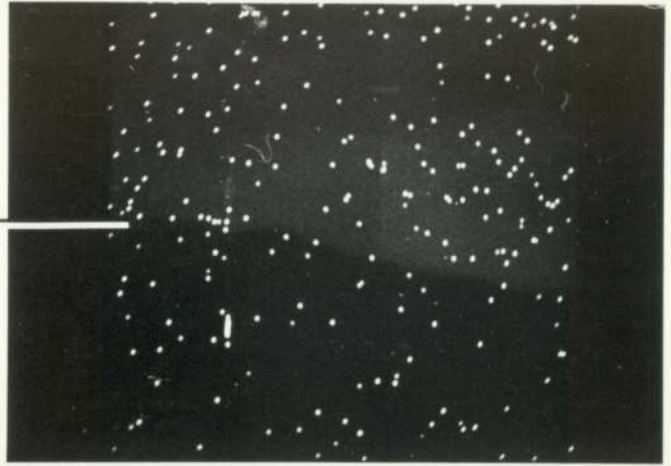


Fig.3.14 (a),(b) and(c) X-Ray Distributions of Ag and Si and Electron Micrograph from an Area on the edge of the Specimen used in Fig.3.9, which was not in Sliding Contact, Magnification.

(a) X-Ray Distribution
of Si

H 10 μ m

Specimen
Edge



(b) Electron Micrograph

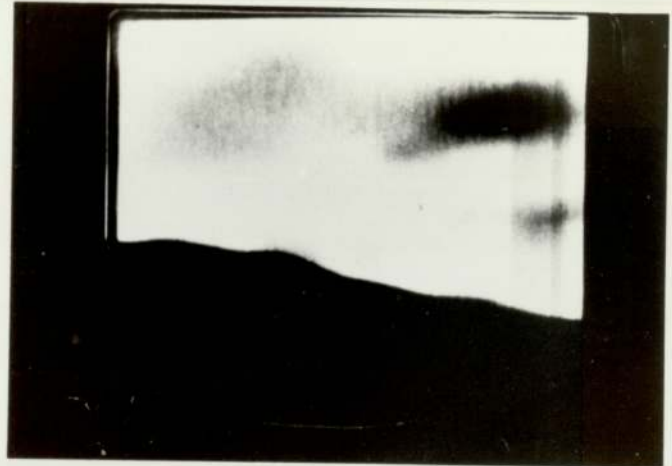
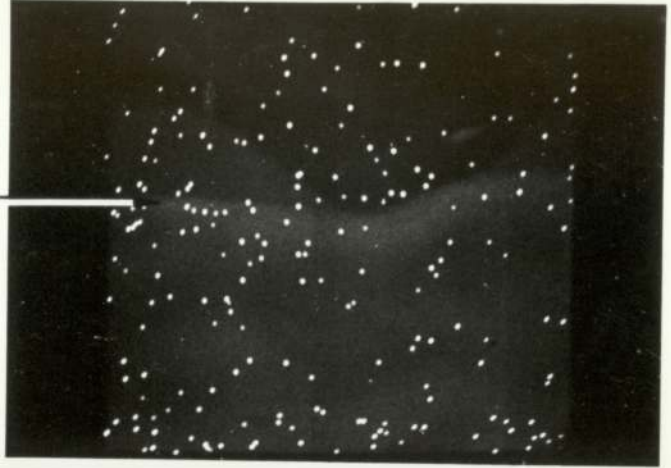


Fig.3.15 (a) and (b) A Typical Example of the X-Ray
Distribution of Si and Electron Micrograph for an
Unworn Pin, Magnification X1000.

(a) X-Ray Distribution
of Si

H 10 μ m

Specimen
Edge



(b) Electron Micrograph

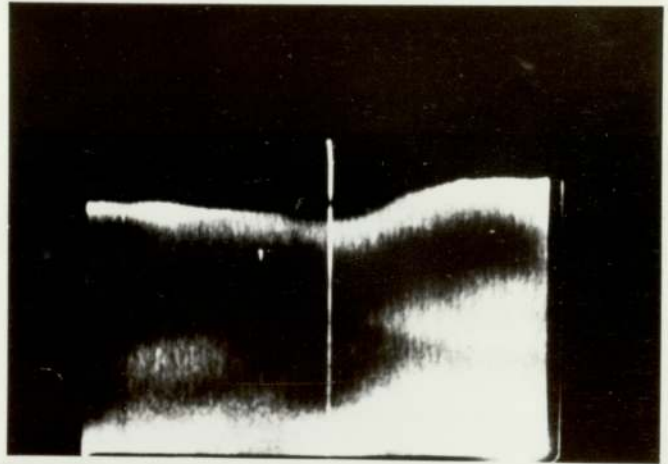


Fig.3.16(a) and(b) A Typical Example of the X-Ray
Distribution of Si and Electron Micrograph for an
Unworn Pin, Magnification X1000.

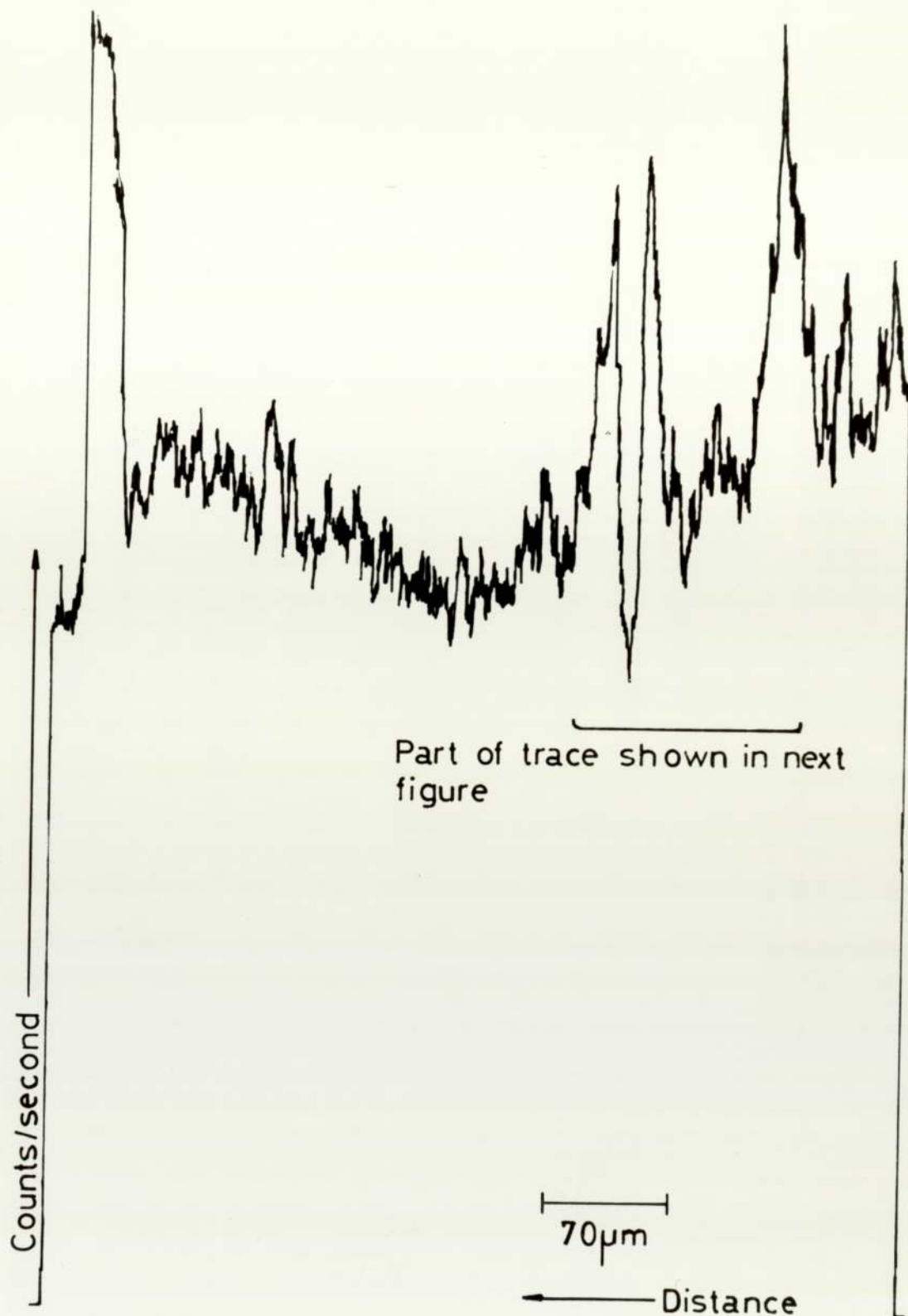


Fig.3.17 A Line-profile of Si across the Surface of a Polymer Pin worn under Boundary-lubricated Sliding Conditions (Speed 0.021ms^{-1} , 10cs Viscosity Fluid, 11N Load) Magnification $\times 120$, Total Distance of Scan is 0.8mm .

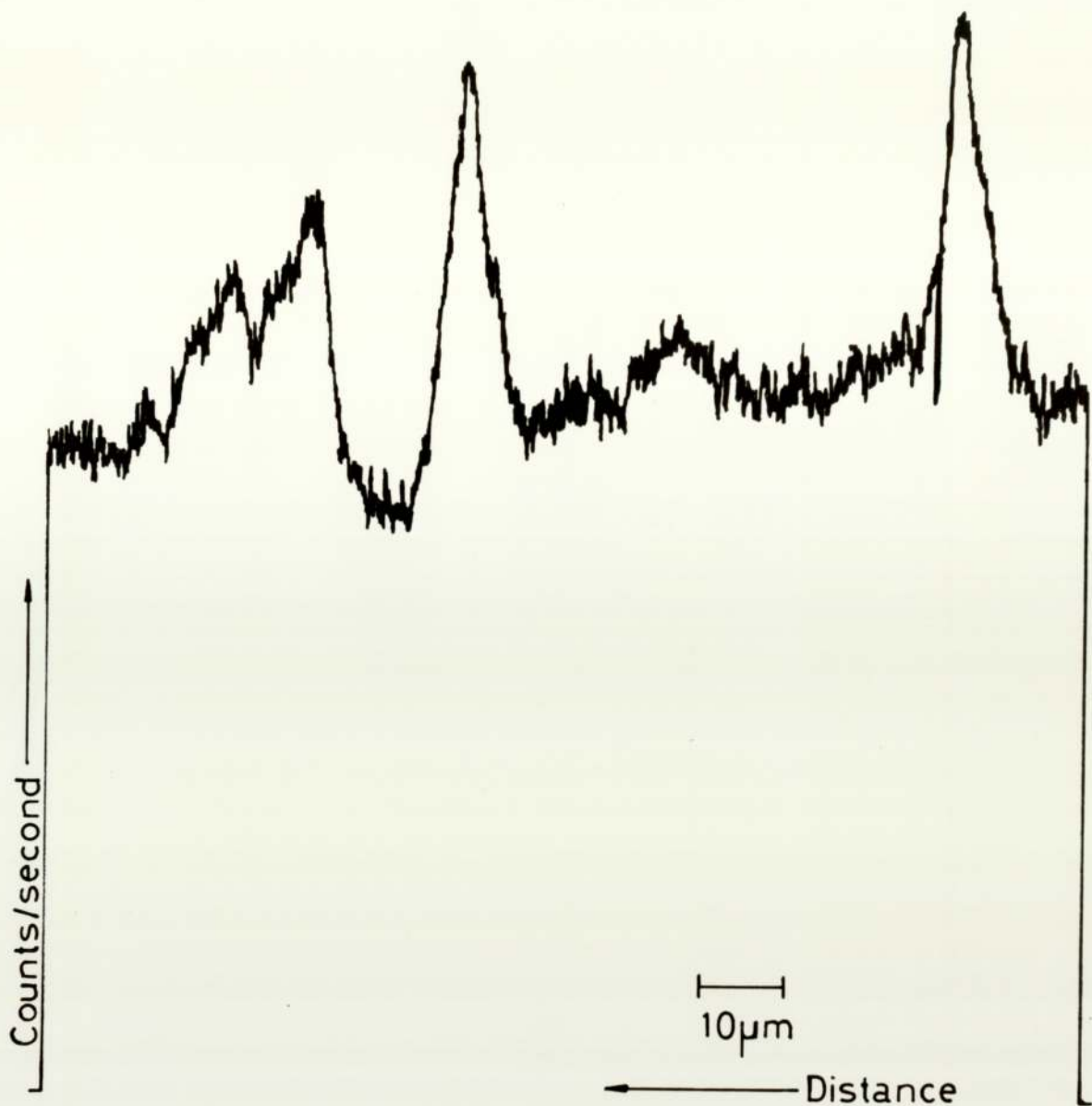


Fig.3.18 A Line-profile of Si across a Section of the same Pin as used in Fig.3.17 Magnification x750 . Total Distance of Scan is 0.14mm.

(a)



(b)



Fig.3.19(a)and(b) Two Electron Micrographs with Different Exposures of the Area over which the Line-profile was taken in Fig.3.17, Magnification X120.

Fig. 3.18.

Since a Si atom is present in the main chain of the silicone fluid, it may now be concluded that the silicone fluid penetrates into the polymer and is responsible for the modified surface layer.

As a consequence of this conclusion, it seems reasonable to postulate from the results shown in Fig. 3.7 and Fig. 3.8 that the silicone fluid only penetrates the PPO under conditions of boundary lubrication. To confirm that sliding contact is an essential element in the formation of the modified surface layer, some experiments were made to see if any penetration could be detected following static immersion of the polymer in silicone fluid. The effect of time on the penetration of silicone fluid into the polymer was investigated by immersion in 10cs viscosity fluid for periods of up to 4 weeks. When the excess fluid was removed and the pin set in motion on the apparatus, with a load of 11N and speed of 0.0037ms^{-1} , even after 4 weeks of immersion, the 'dwell-time' was very short and resulted in only $6\ \mu\text{m}$ of wear before the rise in friction to the dry value (c.f. depths of over $100\ \mu\text{m}$ in Fig. 3.7). The effect of temperature was investigated by immersing PPO pins in 10cs viscosity fluid at a temperature of 150°C (just below the volatilizing temperature of the fluid, 160°C) for approximately 36 hours. When the excess fluid was removed as before, and the pin placed on the apparatus, the friction rose immediately to its dry value. This is further evidence that the method of removal of excess silicone fluid by wiping with tissue, is quite adequate. These results therefore, show that static immersion and heated static immersion of PPO in silicone fluid are unable to produce any significant depth of modified layer.

So, the overall conclusion is that the modified layer produced during sliding in silicone fluid under boundary lubrication conditions, is the result of absorption of fluid into the polymer and that this absorption is primarily a consequence of the wear process itself.

With this type of 'dwell-time' experiment, it is possible that the fluid was released to the wear interface from the modified surface layer, as the layer was gradually worn away. If this occurs, the experiment would last for a much longer period of time. To avoid this, the wear pin was wiped with absorbent tissue as before, and the counterface replaced with a clean dry one, every twenty microns of wear.

The thickness of the layer of silicone fluid in the polymer, is approximately $7.5\mu\text{m} \pm 2.5\mu\text{m}$, estimated from the Si X-Ray intensity pictures. The thickness does not vary for the two speeds of 0.0037ms^{-1} and 0.021ms^{-1} , so it may be concluded that the thickness of the layer is independent of speed, provided the sliding conditions are confined to the boundary lubrication regime. The results from the Rutherford backscattering experiments (next section) also show the presence of Si under boundary lubrication conditions and also gives some information on the variation of silicon concentration with depth within the layer.

3.3 Rutherford Backscattering (R.B.S.)

3.3.1 Results

For a well-polished pure element (which is thicker than the range of the α -particles i.e. greater than $10\mu\text{m}$ in the case of silicon), the spectrum from an R.B.S. experiment would appear as in Fig. 3.20(a) with α -particle yield versus energy of the backscattered α -particle. The 'cut-off' energy is characteristic of the particular element involved. Particles penetrating the sample do so with a reduced energy, (due to inelastic collisions) and this results in more particles being involved in backscattering collisions. This is because the scattering cross-section is proportional to $1/E^2$, (where E is the energy of the α -particle before scattering occurs) so this quantity will increase as E is reduced. This results in the parabolic shape of the spectrum shown in Fig. 3.20(a). For a homogenous target of two

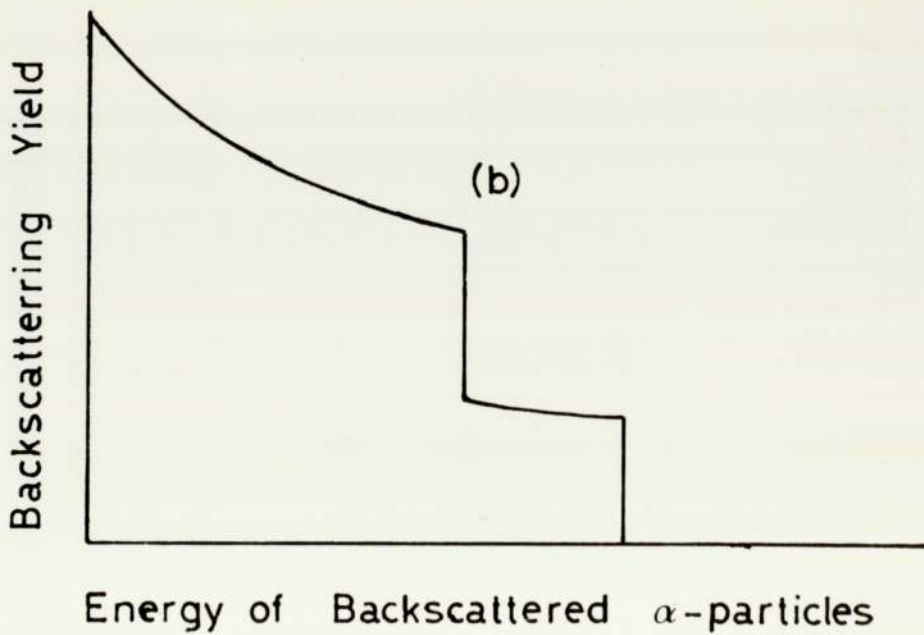
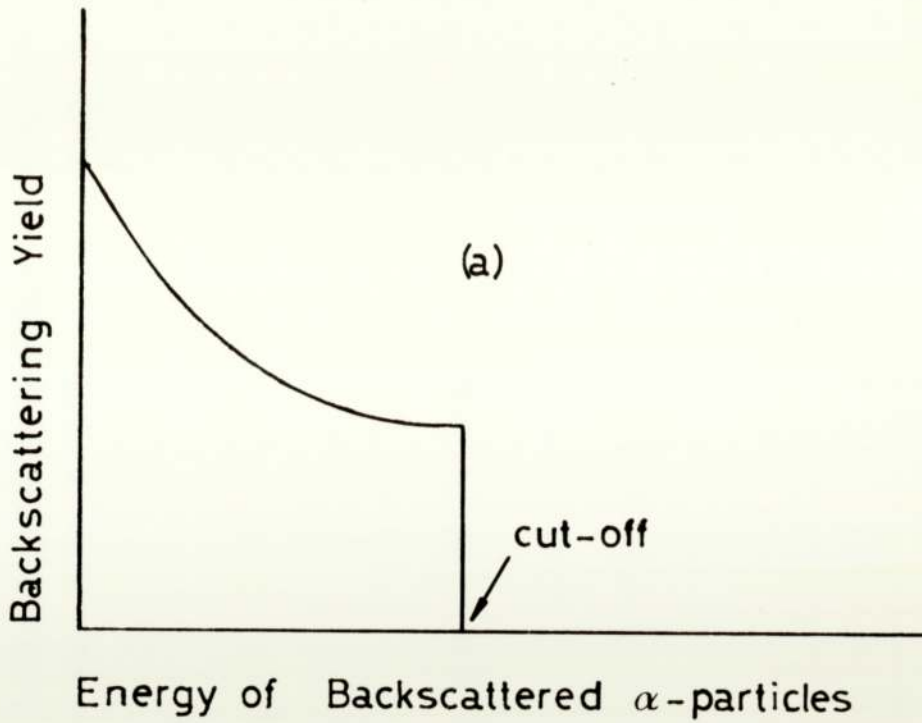


Fig.3.20 Two Ideal Spectra for a Single Element(a) and for Two Elements(b) from a Rutherford Backscattering Experiment.

elements, the spectrum would appear as shown in Fig. 3.20(b). Similar effects can be seen in the experimental spectra reproduced in Fig. 3.21 and Fig. 3.22. These show an unworn pin and a microtomed granule which was used for moulding the PPO used in the wear experiments. The granule of PPO was mounted in a resin compound and microtomed to avoid any surface contamination which might have arisen from handling whilst mounting. It was also used to verify that the PPO did not contain a significant level of silicon impurities. The peaks are all labelled on the two spectra with the particular elements present, namely, carbon, oxygen and silicon. The effect of the increased scattering cross-section can be seen quite easily with the carbon peaks showing a parabolic shape in both spectra. The parabolic shape is only beginning to appear with the oxygen peaks. For the unworn pin (Fig. 3.21) some contamination by silicon can be seen on the spectrum. However, there is no parabolic shape associated with this peak, and the contamination is therefore confined largely to the surface only. This contamination could have arisen from unavoidable handling in the machining of the pins. Approximate calculations from the width of the peak, indicate that the thickness of the contaminated surface layer is less than $0.1 \mu\text{m}$. (The horizontal energy scale corresponds to distance within the target, but it is not a linear dependence). The spectrum for the microtomed granule of PPO, Fig. 3.22 shows no silicon presence at all. To confirm that this depth of surface contamination is correct, a further experiment was made with an unworn pin from which about $0.1 \mu\text{m}$ had been removed from the surface by microtoming. Fig. 3.23 show the spectrum from this experiment. It can be seen that the surface contamination has been largely removed, as shown by the decrease in size of the Si peak. A background level is present on all R.B.S. spectra and consists of small quantities of the heavier elements. This is present even in the microtomed granule of PPO. The origin of the background level is uncertain, but could be attributed to secondary electrons from the sample and impurities in the sample. It should be remembered that the background level will also follow a parabolic distribution (due to the proportionality of the scattering cross-section with $1/E^2$), which is superimposed on

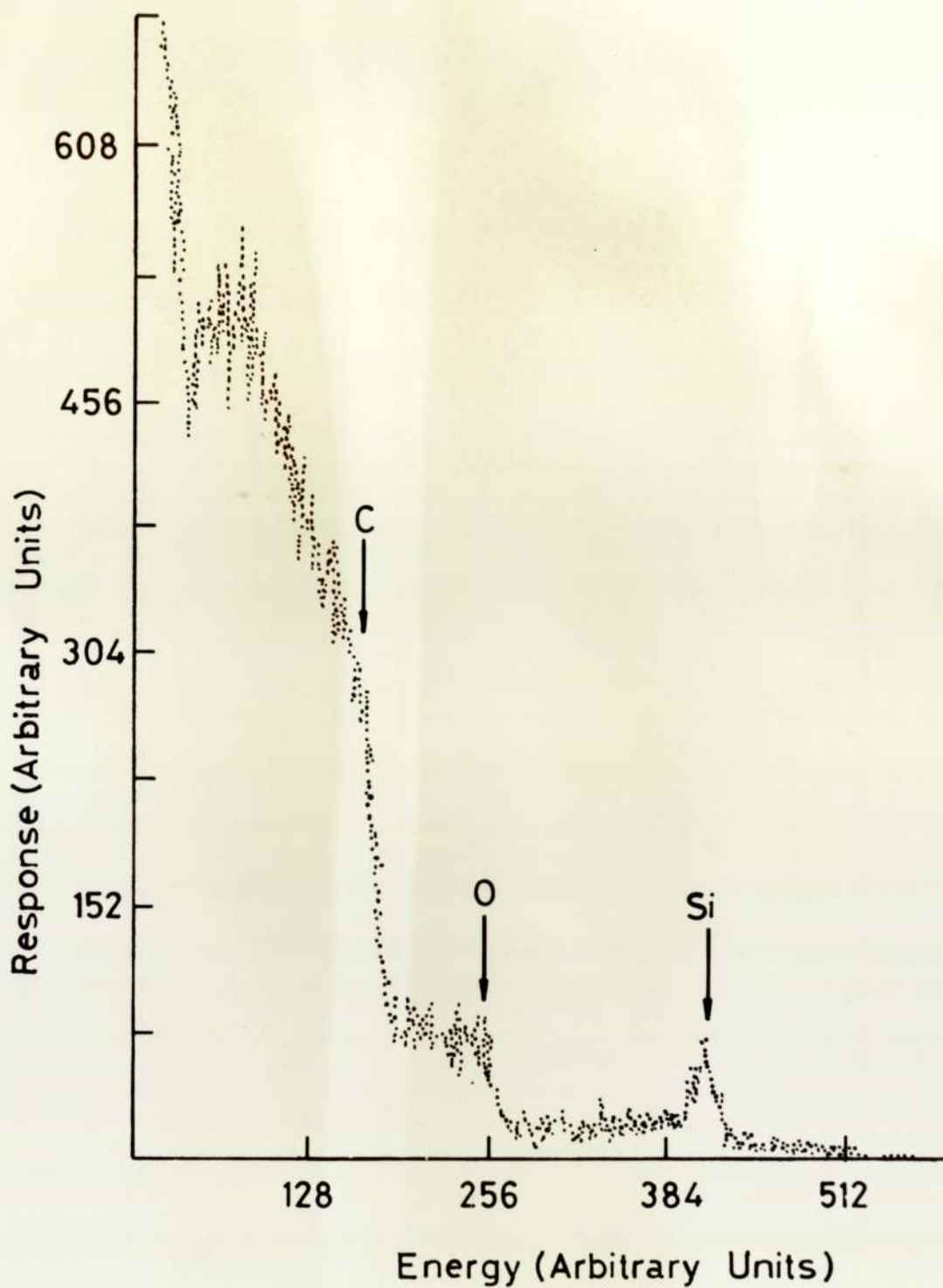


Fig.3.21 Rutherford Backscattering Spectrum for an Unworn Pin of PPO.

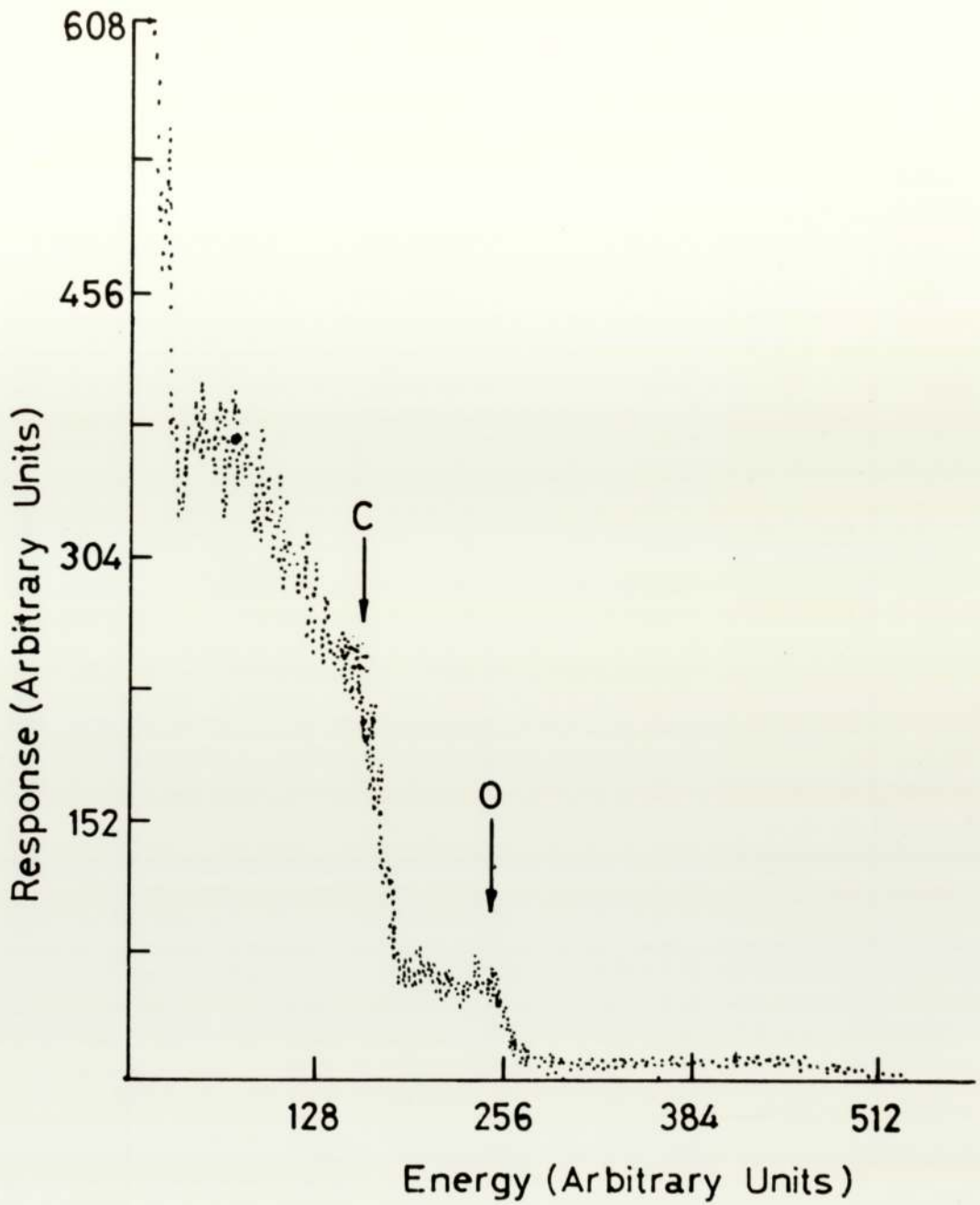


Fig.3.22 Rutherford Backscattering Spectrum from a Microtomed Granule of PPO.

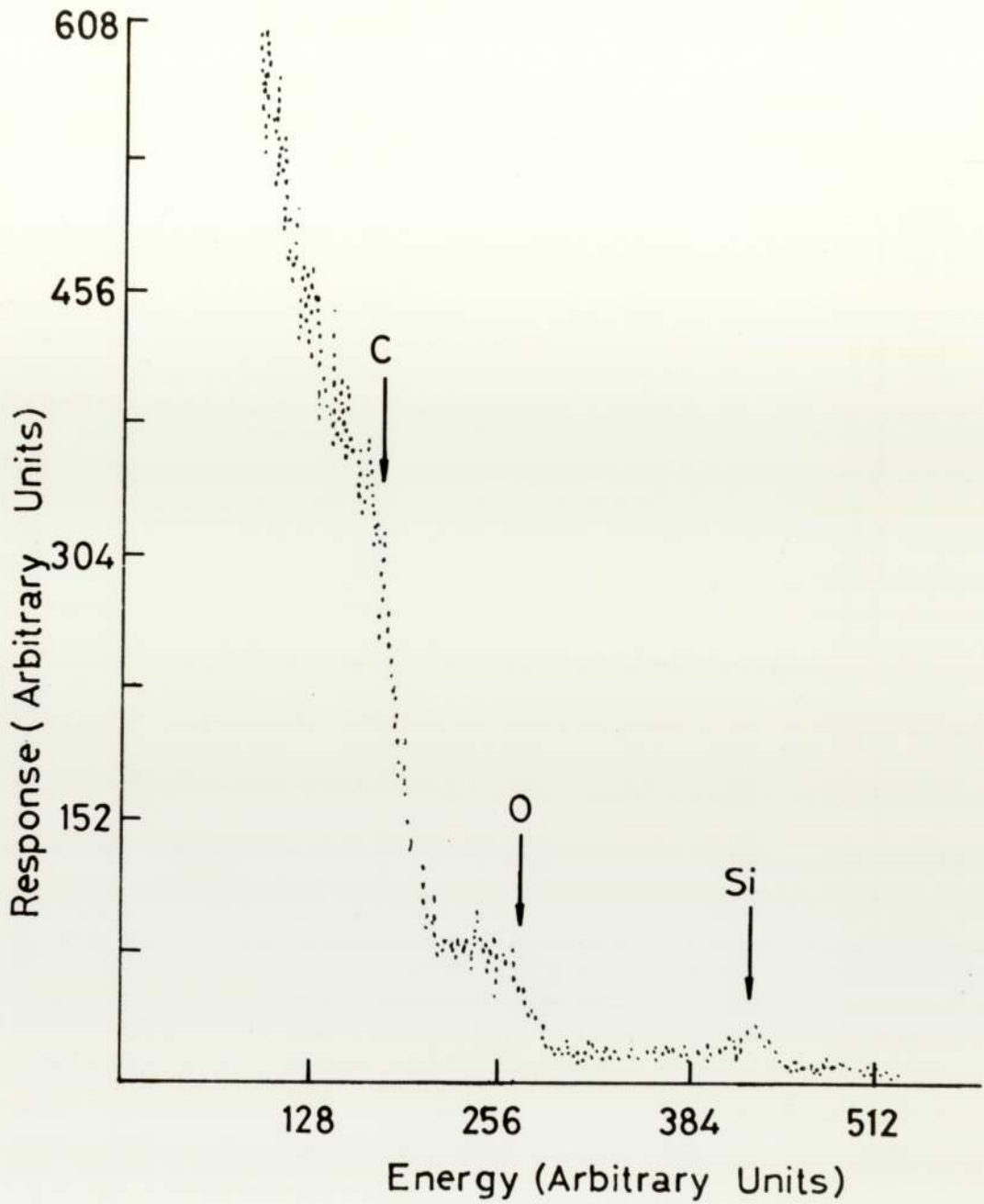


Fig.3.23 Rutherford Backscattering Spectrum from a Microtomed Unworn Pin of PPO.

the spectra. Recalling Fig. 2.15, these heavier masses can only be present in very small quantities. This is because only a small amount of these heavier elements result in a large yield of backscattered α -particles.

Fig. 3.24 shows the spectrum obtained for a worn pin, in the boundary regime at a speed of 0.0037ms^{-1} , 11N load, 10cs viscosity fluid and a number of revolutions of the counterface greater than 3,000 to ensure a reasonable depth of penetration of silicone fluid (see Fig. 3.7). Certain observations concerning the silicon response of the spectrum can be made. The large peak of Si indicates a high surface concentration on the target. After this peak, the response does not fall to the background level, indicating that Si continues to be present below the surface. The silicon response merges with the beginning of the oxygen response, before reaching the background level, so that the oxygen response is superimposed on that for the silicon. The silicon concentration is however, decreasing quite rapidly with decreasing energy (i.e. with decreasing distance into the polymer). This is concluded by the rapid departure from the parabolic distribution which would be obtained for a uniform concentration of a pure element.

3.3.2 Computer Simulation of Results

Fig. 3.25(a) and Fig. 3.25(b) show the results of applying a computer curve-fitting program to the experimental results for the pure granule of PPO and the worn pin. The program is based on an analytical solution to backscattering spectra (59). It takes into account, the energy loss on entering the target, the elastic scattering of the α -particle, energy loss back out of the target, the effect of α -particle straggle for thick targets, a method for deconvoluting merged peaks (using the additivity of stopping cross-sections), isotope effects, detector resolution, the energy loss of the α -particles in the detector surface metal layer, and the interdiffusion of two or more layers. Charged particles are subject to range straggling, so the α -particles will show a distribution of velocities about a mean value owing to the statistical

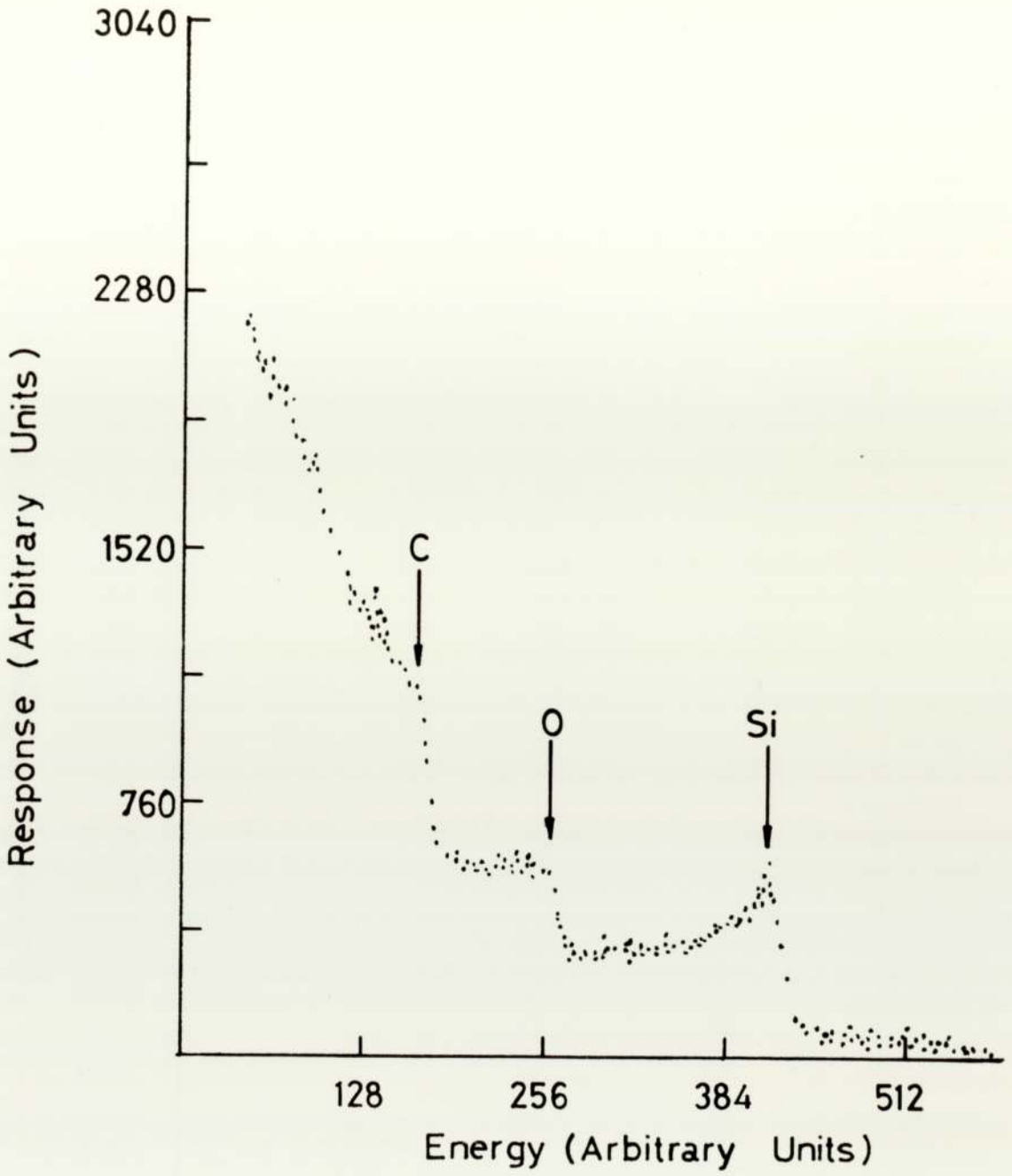


Fig.3.24 Rutherford Backscattering Spectrum from a Worn Pin of PPO (Speed 0.0037ms^{-1} , 10cs Viscosity Fluid, 11N Load).

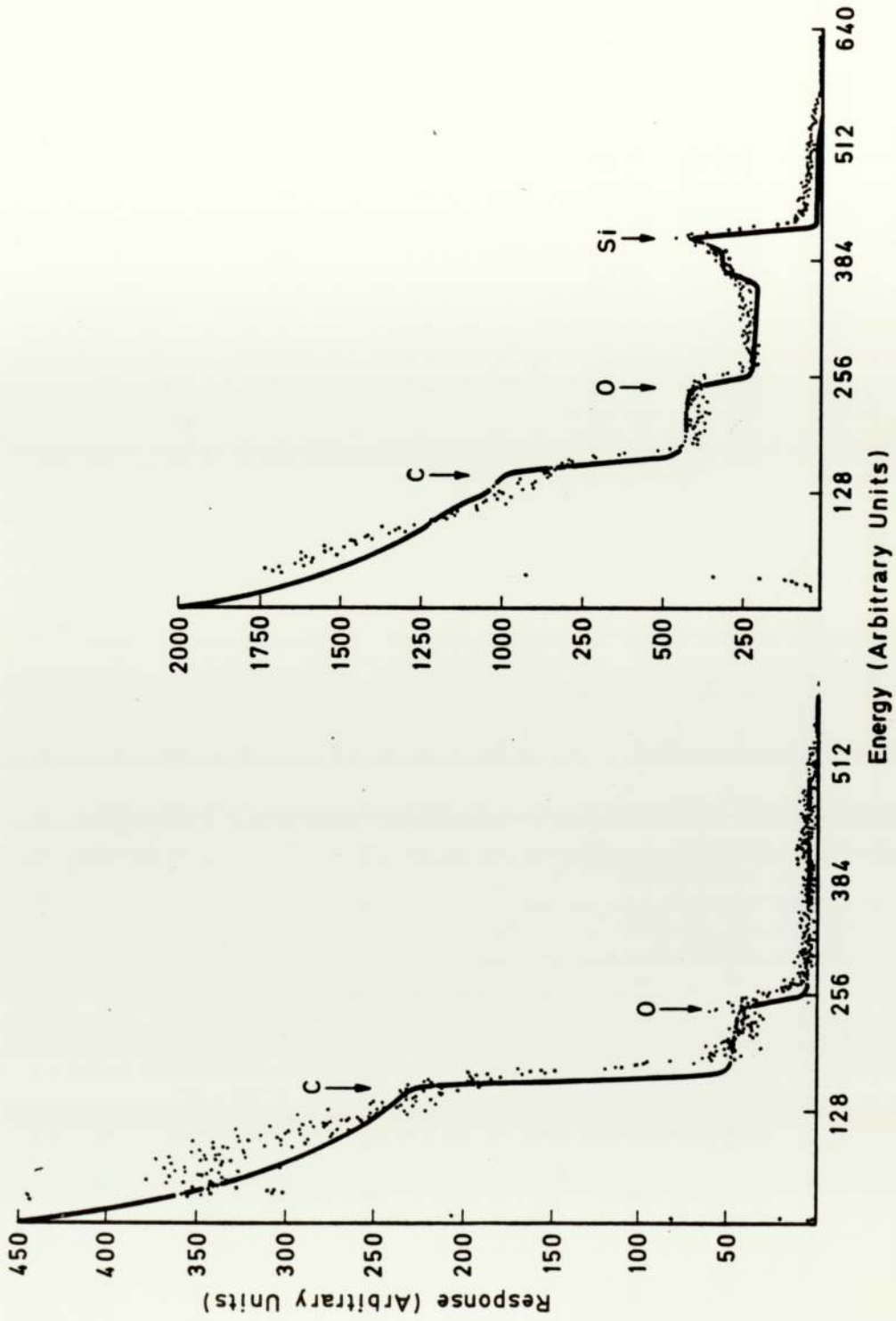


Fig.3.25(a) and (b) Two Computer Simulations of Rutherford Backscattering Spectra for (a) the Pure Granule of PPO and (b) the Worn Pin of PPO.

nature of the energy loss. Hence the ranges of the α -particles will be grouped about a mean value and since the number of collisions is large and they are independent processes, the range (or energy) distribution may be expected to be approximately Gaussian (60). The data needed to make backscattering calculations are described in Appendix 1.

The specimen whose spectrum is to be calculated is divided into layers, then this information is used to input the target elements as a function of depth (59).

The background level which appears in all these spectra must be taken into account in the computer simulation program. To determine which elements were present at background levels, an Energy Dispersive Analyser was used. This analyses the X-rays emitted from any given element. From the associated Bragg angle, the wavelength of the emitted X-ray can be found and hence the element identified. The result for a worn pin is shown in Fig. 3.26 and reveals the presence of titanium on the surface. Titanium appears also at the point at which the background begins on the R.B.S. spectra. So, a small amount of titanium extending throughout the sample was incorporated into the data of the program. This amount of titanium was less than 0.1% of the total number of atoms in the specimen. The input data for Fig. 3.25(a) used the exact chemical formula of the PPO and was adjusted for the actual number of atoms of each element present, to obtain the best simulation. The background was also taken into account, using the Ti, and the computer simulation gives a very good fit to the experimental results. For Fig. 3.25(b), the same data was used except additional layers of differing numbers of Si atoms (i.e. different concentrations) were added. Again, the fit can be regarded as very satisfactory. A diagram of the pin showing an interpretation of the various concentrations and depths of the computed layers, is shown in Fig. 3.27. Again, the presence of Si atoms is directly related to the concentration of silicone fluid within the polymer. It can be seen that there is a high concentration of oil on or near the surface, which decreases quite rapidly within the next 4,000^oÅ. The total depth of

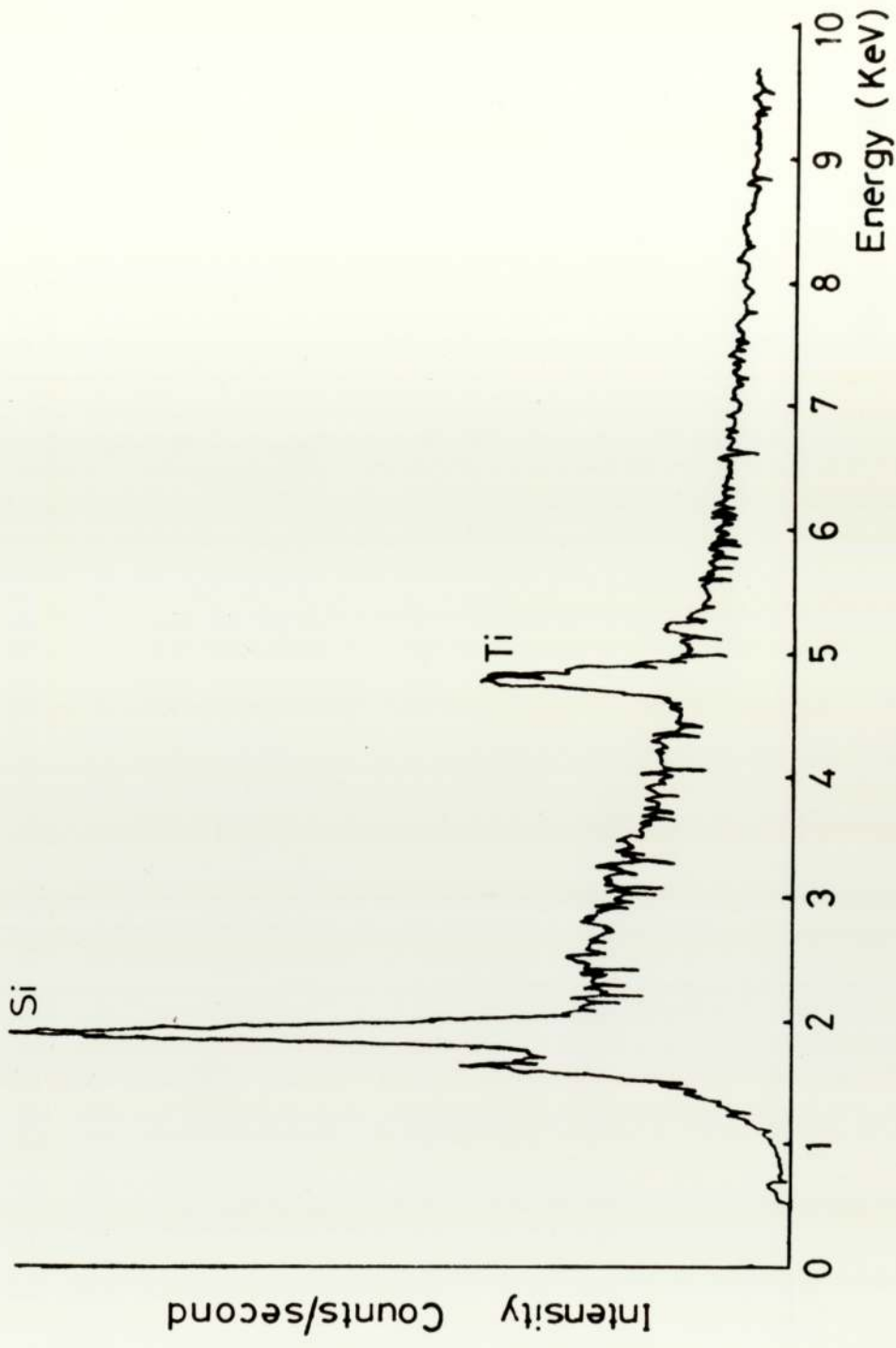


Fig.3.26 An Energy Dispersive Analysis of the Surface of
a Worn Pin of PPO.

Ratio of
Oil/Polymer

3:1

1:1

1:2

1:4

Polymer Surface

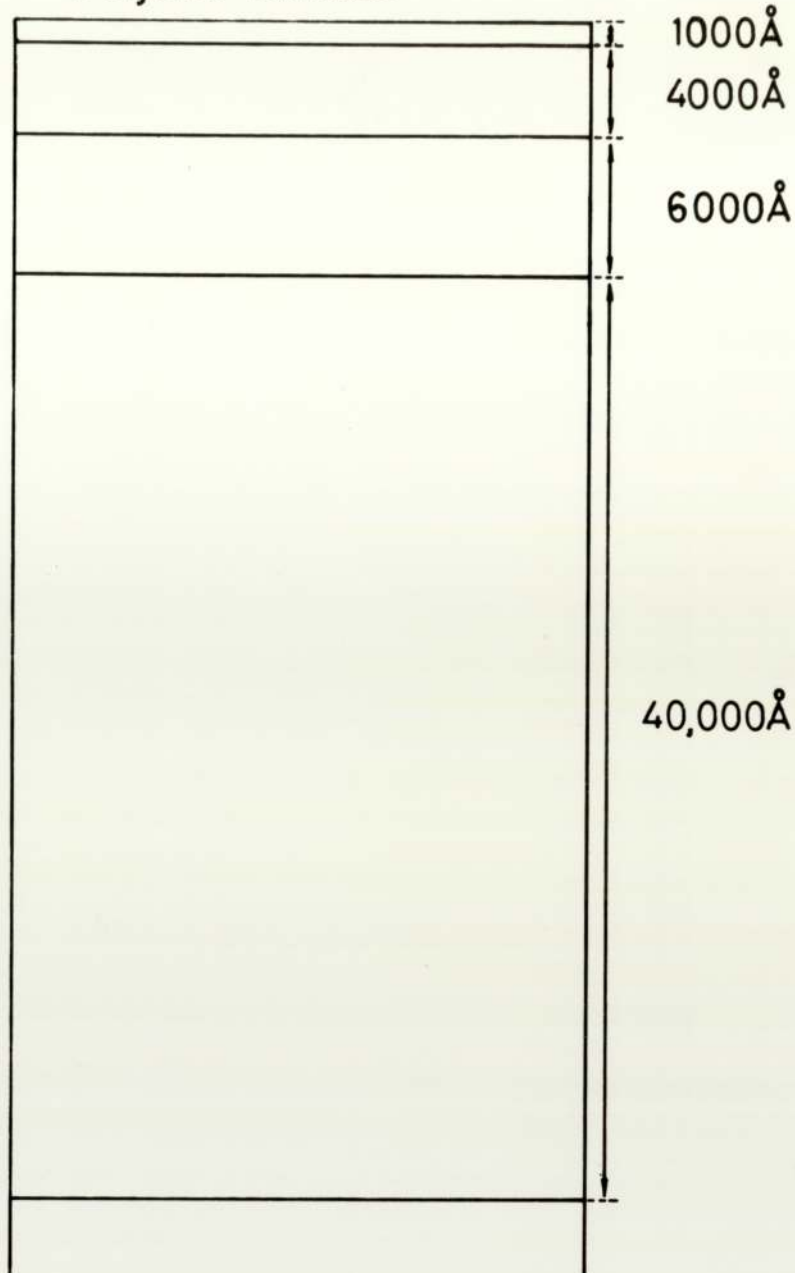


Fig.3.27 Representation of the Variation of the Ratio of Silicone Fluid to Polymer Molecules with Depth, derived from Rutherford Backscattering Computer Simulation Results.

computed layers is $5 \mu\text{m}$. To show that the silicone fluid penetrates no further than about $8 \mu\text{m}$ (as indicated by the E.P.M.A. results), a pin worn under conditions of boundary lubrication for a sufficient number of revolutions to ensure a modified surface layer, was microtomed to a depth of $8 \mu\text{m}$. The spectrum from this pin is shown in Fig. 3.28.

It is possible to compare spectra quite easily by expanding (or decreasing) the yield of backscattered α -particles for one spectrum to fit the heights of the oxygen response above the response of the previous element for the other spectrum. The two spectra of Fig. 3.23 and Fig. 3.24 have been superimposed in this way in Fig. 3.29. For the microtomed unworn pin, the difference in height is between the background level and oxygen level, but for the worn pin, the difference is between the silicon and oxygen levels. The oxygen level is chosen since its concentration is more or less constant within the target even though there is oxygen in the silicone fluid. By superimposing the spectrum for the pure granule of PPO, Fig. 3.22 onto the spectrum shown in Fig. 3.28 (as shown in Fig. 3.30), it can be seen that the response for Si has reached the background level, and it can therefore be concluded that no fluid penetrates further than a depth of about $8 \mu\text{m}$.

Any changes which the silicone fluid may have induced in the polymer surface need to be investigated. In order to do this, polymer pins worn under boundary lubrication conditions were examined in the Scanning Electron Microscope.

3.4 Scanning Electron Microscopy (S.E.M.)

The polymer pin is non-conductive, so a coating of gold-palladium was evaporated onto the wear pin to eliminate static charging. Fig. 3.31 shows an electron micrograph of the surface of a pin worn under conditions of boundary lubrication (0.0037ms^{-1} , 10cs viscosity silicone fluid, 11N load and 4,000 revolutions of sliding). Transverse features are visible (perpendicular to the direction of sliding)

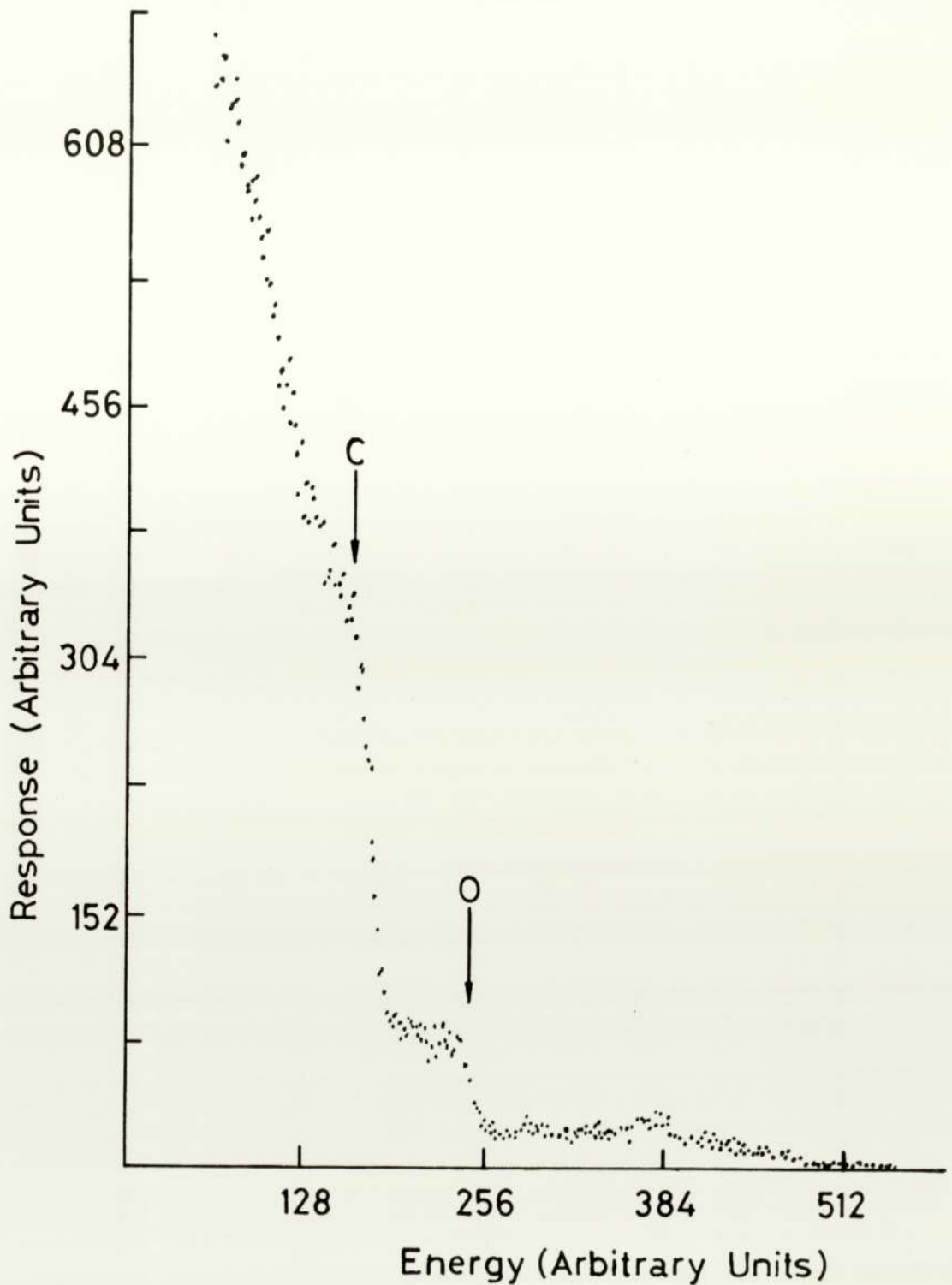


Fig.3.28 Rutherford Backscattering Spectrum from a Microtomed Pin of PPO, Worn under Boundary Lubrication Conditions (Speed 0.0037ms^{-1} , 10cs Viscosity Silicone Fluid, 11N Load). The Depth of Microtoming is approximately $10\mu\text{m}$.

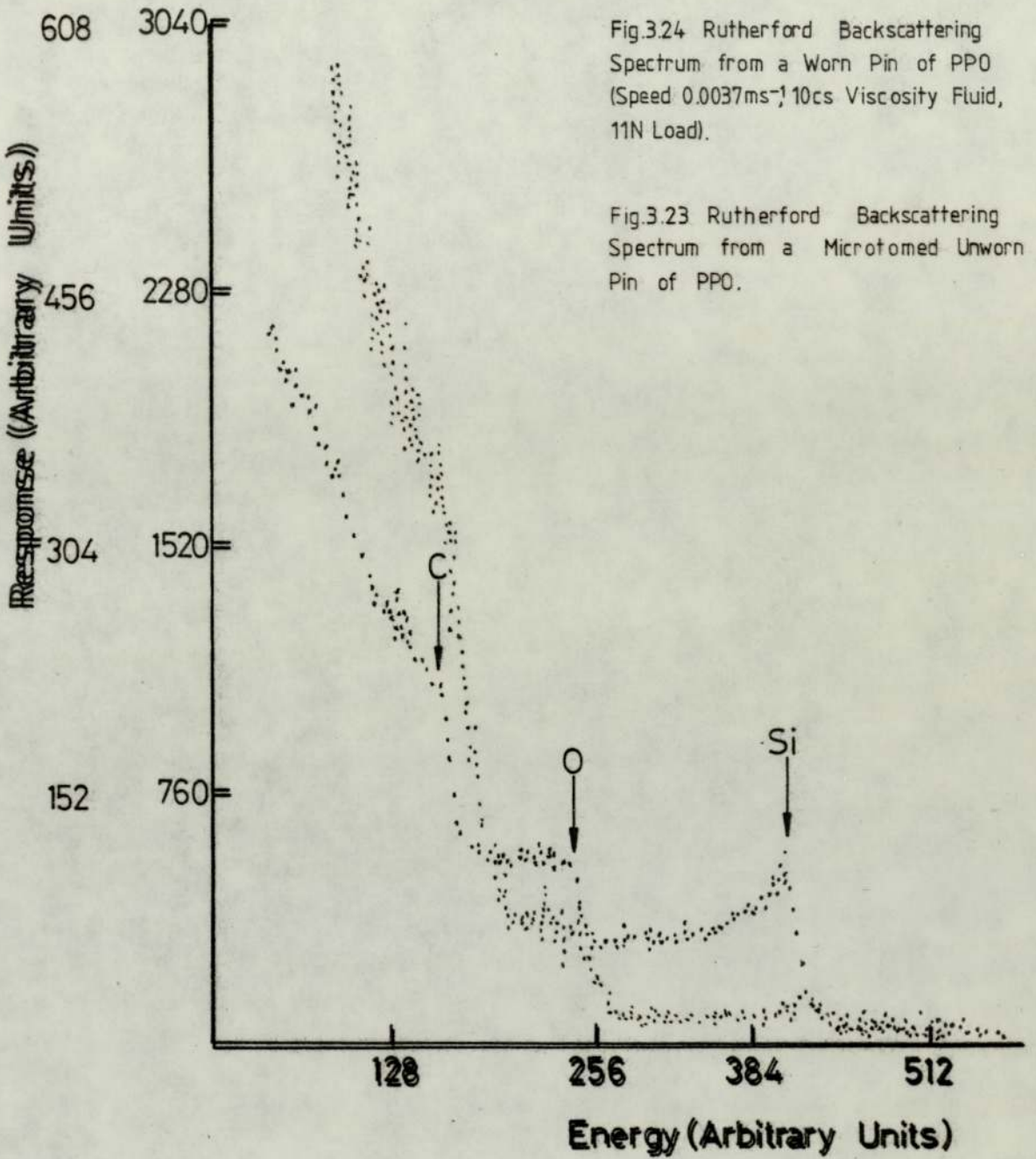


Fig.3.24 Rutherford Backscattering Spectrum from a Worn Pin of PPO (Speed 0.0037ms^{-1} , 10cs Viscosity Fluid, 11N Load).

Fig.3.23 Rutherford Backscattering Spectrum from a Microtomed Unworn Pin of PPO.

Fig.3.29 Fig.3.23 superimposed on Fig.3.24 .

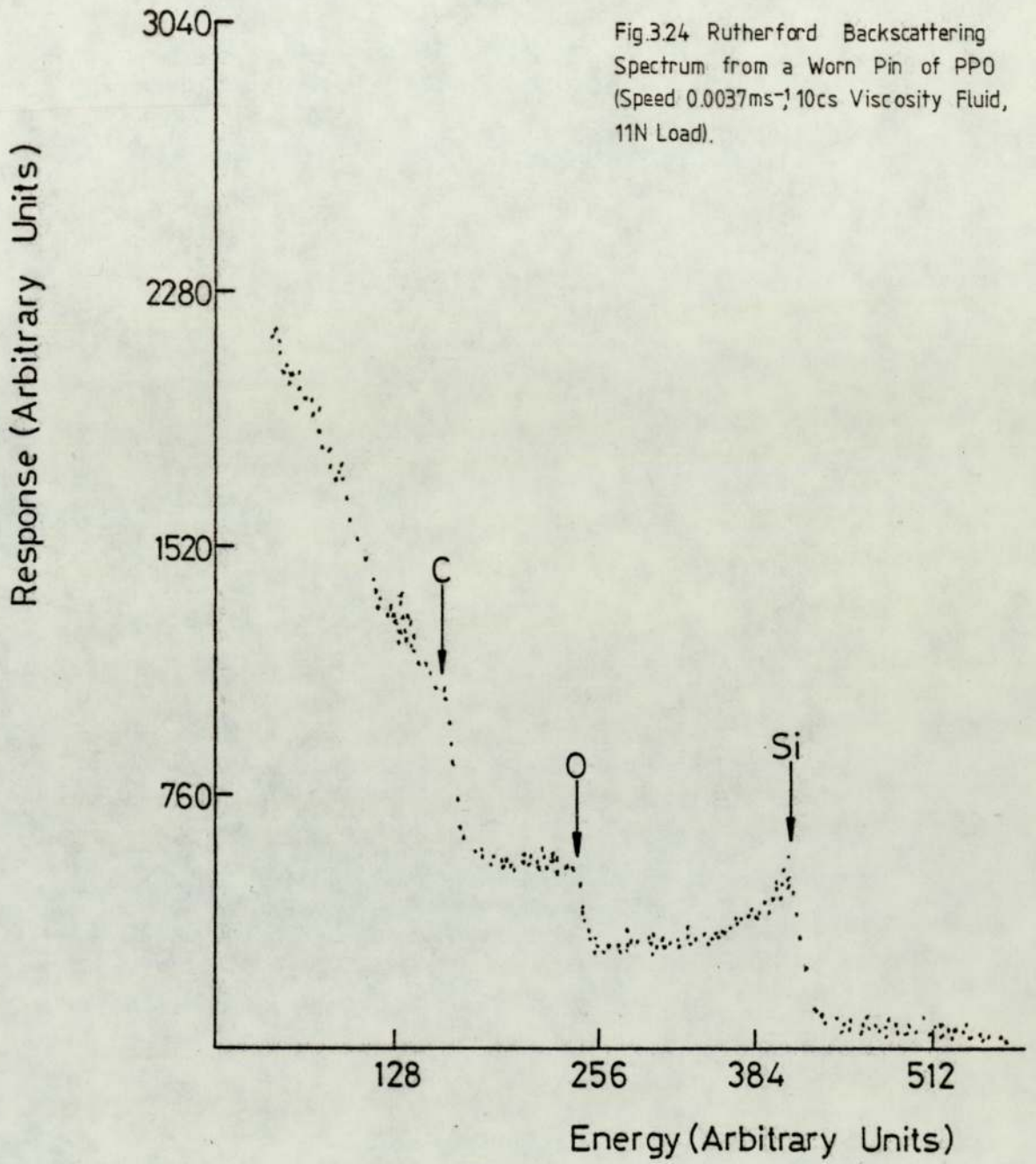


Fig.3.29

Fig.3.23 superimposed on Fig.3.24 .

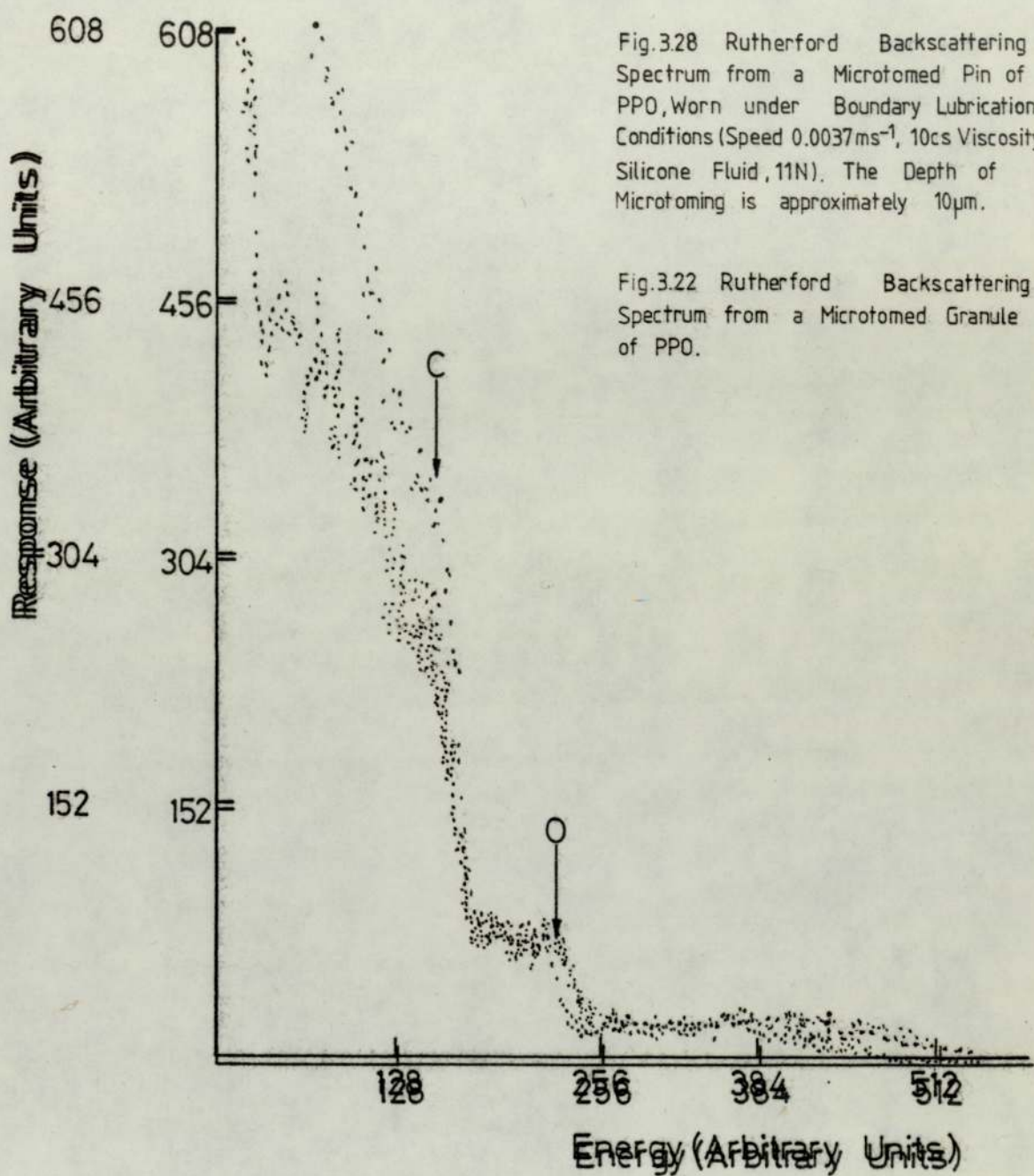


Fig.3.28 Rutherford Backscattering Spectrum from a Microtomed Pin of PPO, Worn under Boundary Lubrication Conditions (Speed 0.0037ms^{-1} , 10cs Viscosity Silicone Fluid, 11N). The Depth of Microtoming is approximately $10\mu\text{m}$.

Fig.3.22 Rutherford Backscattering Spectrum from a Microtomed Granule of PPO.

Fig.3.30 Fig.3.22 superimposed on Fig.3.28.

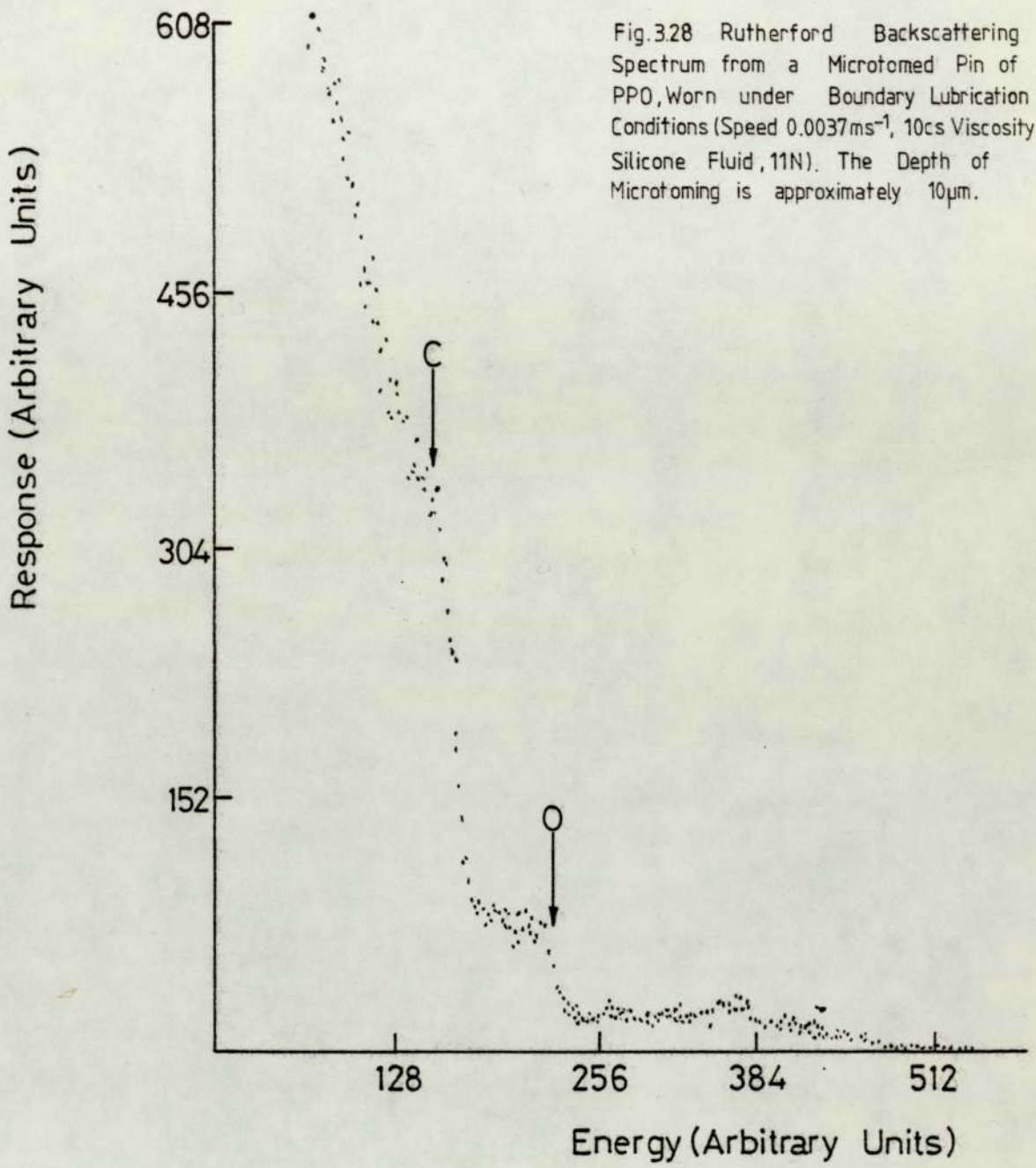


Fig.3.28 Rutherford Backscattering Spectrum from a Microtomed Pin of PPO, Worn under Boundary Lubrication Conditions (Speed 0.0037ms^{-1} , 10cs Viscosity Silicone Fluid, 11N). The Depth of Microtoming is approximately $10\mu\text{m}$.

Fig.3.30 Fig.3.22 superimposed on Fig.3.28.



Direction of Sliding

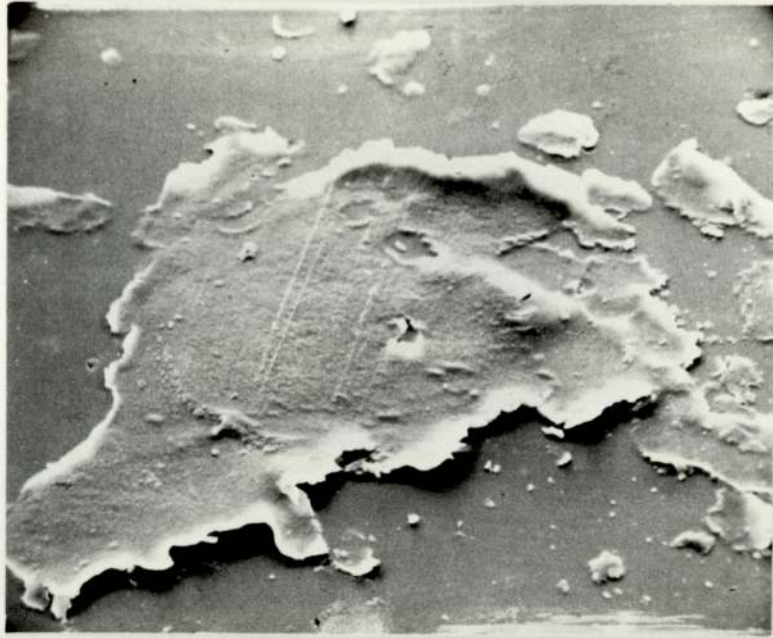


Fig.3.31 A Scanning Electron Micrograph of a Pin Worn under Boundary Lubrication Conditions, Magnification X1200.

on the surface, giving the impression that material has been raised. No cracks or features other than scratches are present along the direction of sliding. Very similar features have been observed by Evans (24), in experiments with PPO sliding under boundary lubrication conditions with silicone and other fluids. Fig. 3.19(b), the electron micrograph from the line-scan of Si, shows the presence of these transverse features with cracks also. The features are somewhat more severe than those in Fig. 3.31 and appear to follow the rings arising from the rotation of the pin. Fig. 3.32(a) shows an electron micrograph, from the surface of a pin worn under boundary lubrication conditions, of a large region, which appears to be completely raised from the surface of the polymer. An area within this raised region is shown in Fig. 3.32(b) at higher magnification. The direction of sliding is clearly visible and the surface has the appearance of being 'swelled' and softened.

Although it has been shown that fluid has been absorbed into the polymer during boundary lubrication, and various features have been observed on the surface as a consequence of this absorption, it is not known how the fluid is incorporated or if this absorption has altered the mechanical properties of the surface layers of the polymer. There are two possible mechanisms of fluid incorporation:-(i) the fluid may penetrate surface cracks producing a composite layer which is essentially a dispersion of fluid 'pockets' within the polymer surface layers or (ii) the fluid may diffuse uniformly into the surface layers with a concentration gradient determined by time, temperature and stress and leading to plasticisation of the polymer. By this last interaction, it is understood that the fluid chains separate the polymer chains and weaken the intermolecular bonding forces. In addition to this physical action, the bonding of plasticiser molecules to the polymer weakens the intermolecular bonding forces still further. The effect of plasticisation is to reduce the Glass Transition Temperature, T_g . The results of an indentation experiment are presented in the next section which was designed to find which mechanism of fluid incorporation occurs. The experiment investigates any change in T_g which may have occurred during boundary-lubricated sliding.

(a)



↙ Direction of Sliding

(b)

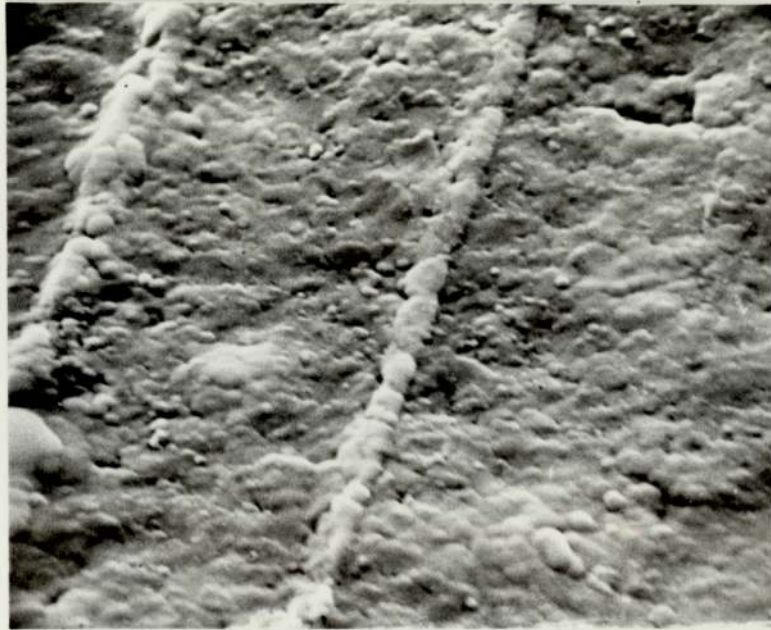


Fig. 3.32 (a) and (b) Two Scanning Electron Micrographs showing a Large Region of Plasticised Polymer, (a) Magnification X200 and (b) an Area within this Region, Magnification X4900.

3.5 Indentation Results

Fig. 3.34 shows typical traces obtained for indentations into the polymer for various temperatures with unworn pins. For each experiment, the expansion of the indenter was allowed to equilibrate before the indenter was placed on the surface of the pin. The indenter was allowed to settle before the load was applied. The application of the load is accompanied by a rapid indentation, shown by the straight vertical line in the traces. This gradually levels out, and another vertical line indicates the removal of the load when immediate elastic recovery occurs. The indenter does not return to its original level immediately, however, but gradually 'creeps' back showing a viscoelastic behaviour. Traces are shown for worn pins in Fig. 3.33 at more or less the same temperatures as in Fig. 3.34. All the worn pins used in this set of experiments were worn under boundary-lubricated conditions, at a speed of 0.0037ms^{-1} , 11N load, 10cs viscosity silicone fluid for a number of revolutions greater than 2,500, to ensure a modified surface layer. Comparisons of the shapes of the traces can be made. It can be seen that even at room temperature, the indentation produced when the load is applied, is greater for the worn pins. For the temperature of 120°C , the indenter alone produces an indentation of $6\ \mu\text{m}$ for the worn pin. The total indentation (i.e. depth of indentation produced for indenter alone added to the depth of indentation produced when load is applied) for the worn pin at this temperature is $17\ \mu\text{m}$. Comparisons of the two sets of results indicate a much softer surface for the worn pin. For temperatures below 140°C , with the unworn sample, the indentations produced were comparatively small. However, at 155°C , with just the indenter alone, a large indentation was registered. With the application of the load, the depth of indentation was far greater than at any previous temperatures. This occurred at a much lower temperature of 120°C for the worn pin. Fig. 3.35, curves B and C, show graphs of indentation versus temperature, where the circles represent total indentation for the apparatus described above. An additional indentation experiment was also performed with a conventional Rockwell Hardness Tester,

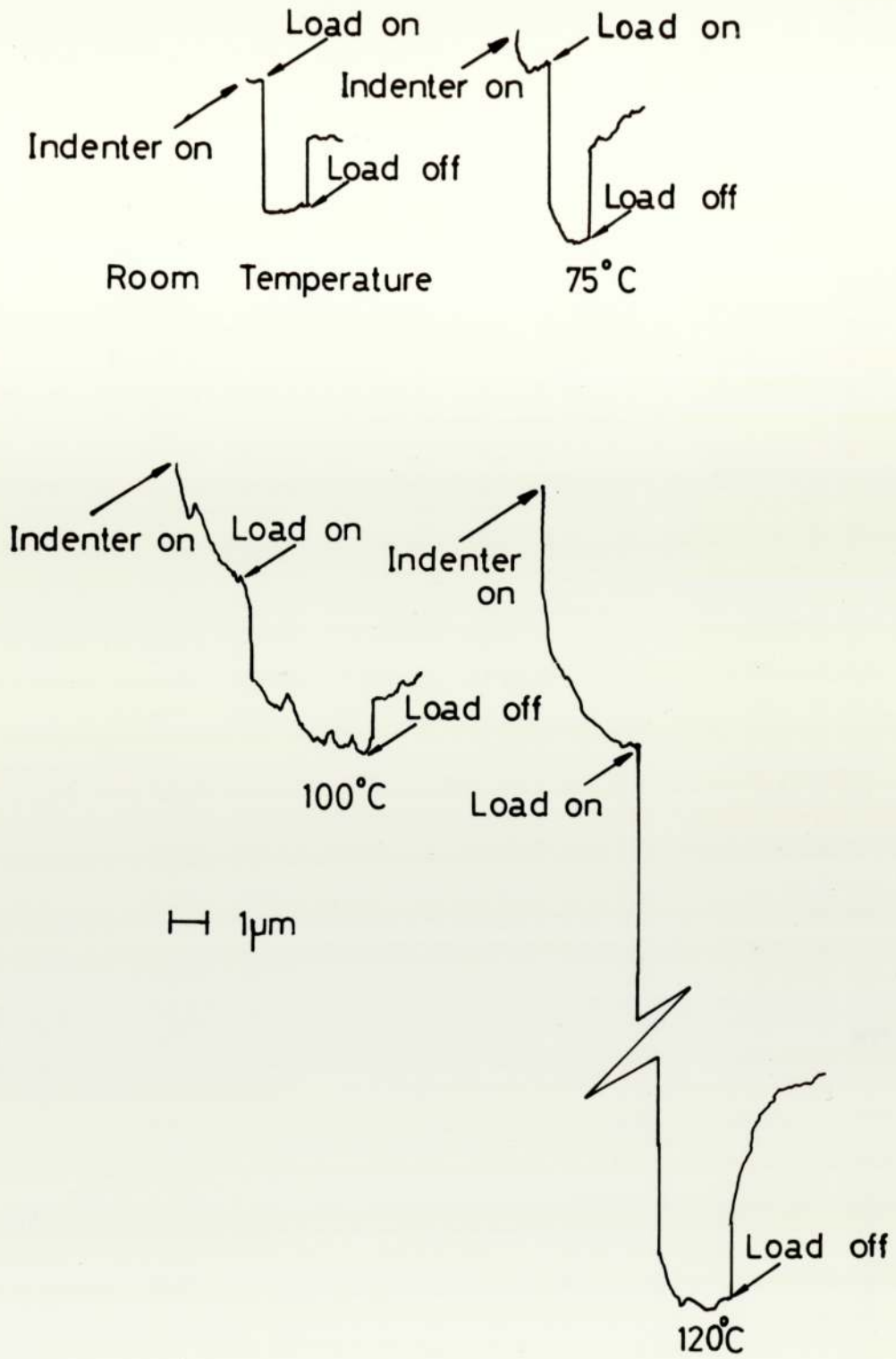


Fig.3.33 Results from Indentation Tests at Different Temperatures for a Worn Pin .

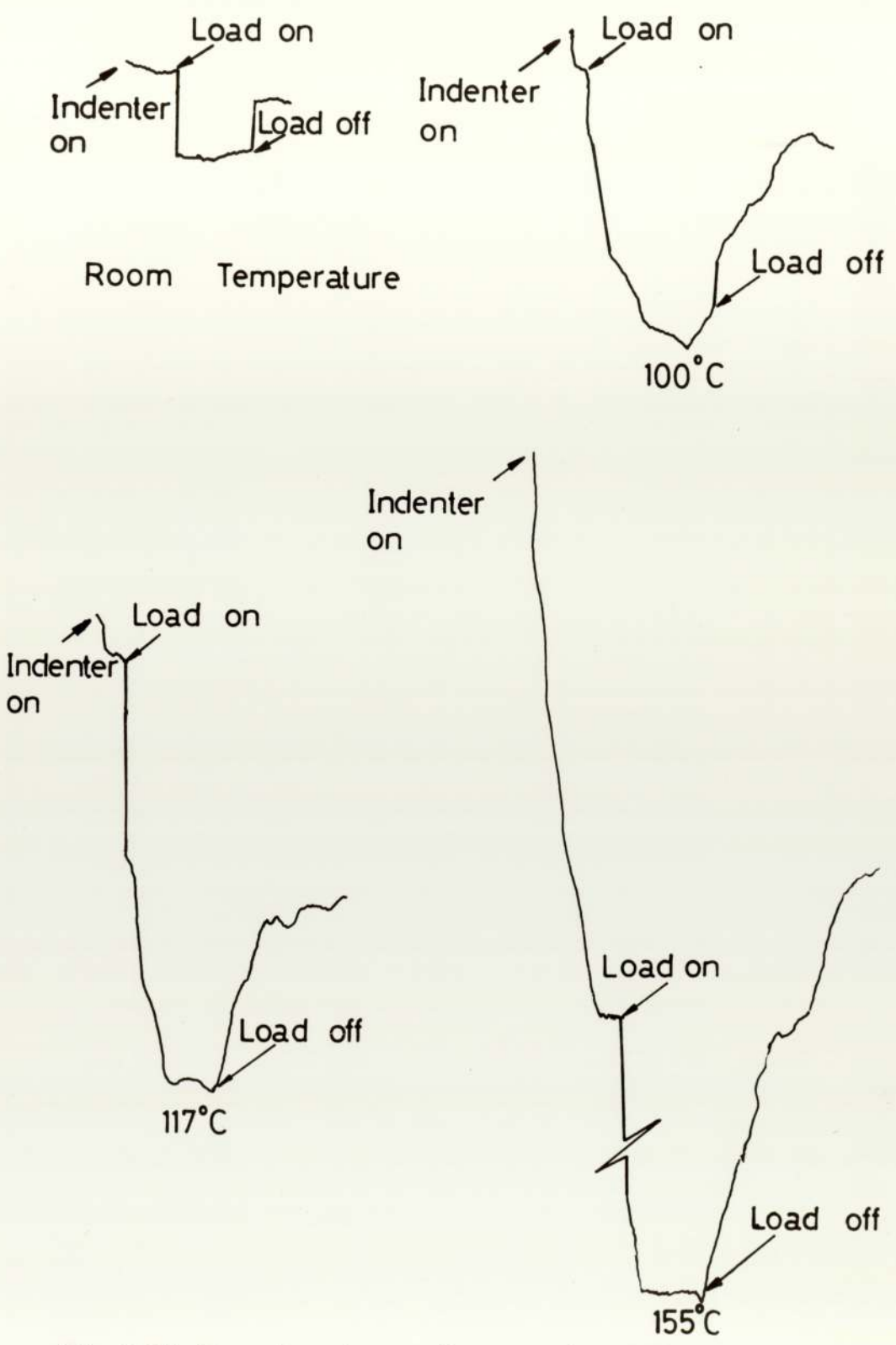


Fig.3.34 Results from Indentation Tests at Different Temperatures for an Unworn Pin.

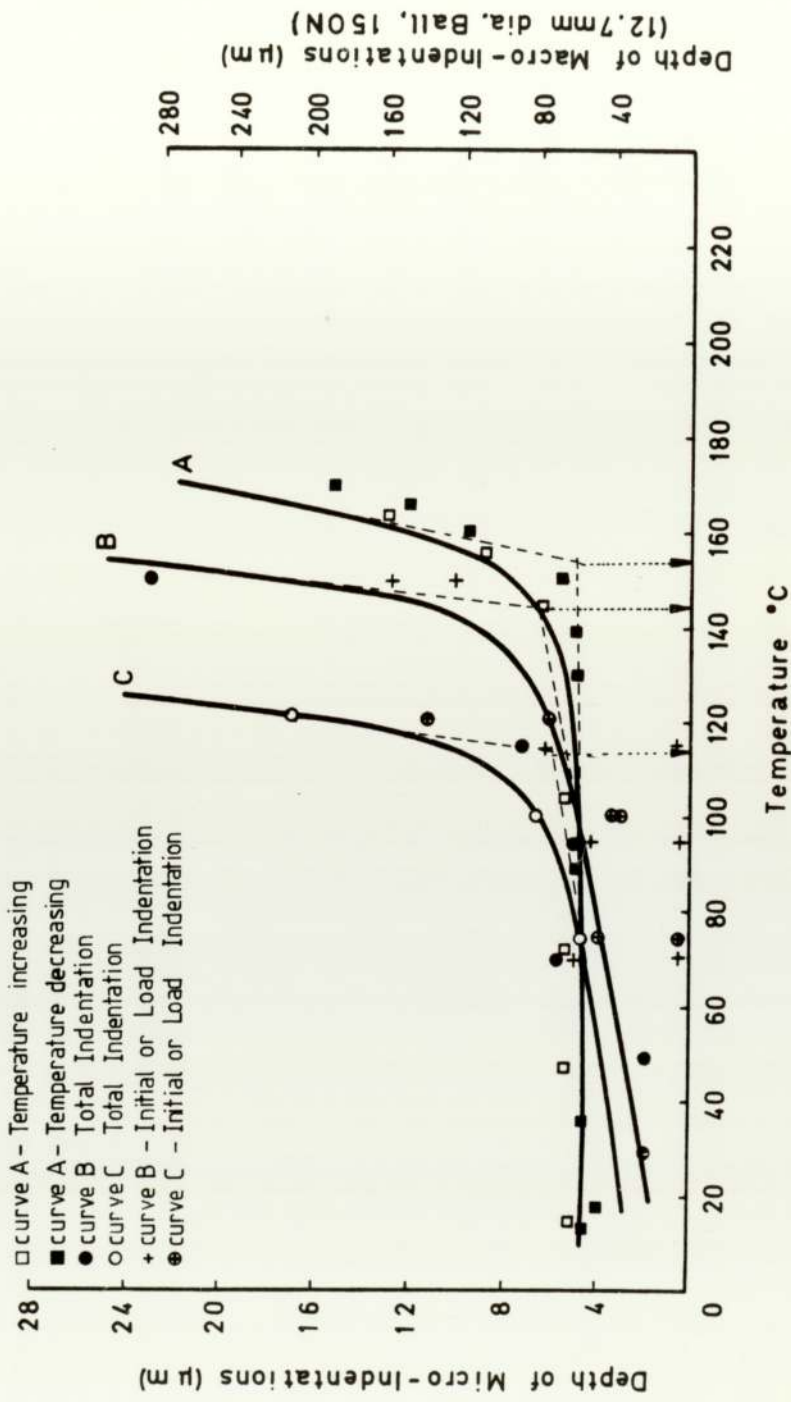


Fig.3.35 Indentation Depth versus Temperature, (A),(B)—Unworn Samples of PPO, (C)—Worn Pins (Speed 0.0037ms, 10cs Viscosity Fluid, 11N Load).

using a 12.7mm diameter ball, and a load of 150N on bulk, unworn PPO, and heated in a bath of silicone fluid. A silicone fluid was used as the heating medium because of its convenience and from the earlier experiments involving heated static immersion, it is known that this fluid has no effect on PPO. The results from the Rockwell Hardness Tester are also shown in Fig. 3.35 - curve A; the open squares signify results taken with the temperature gradually increasing whilst the closed squares relate to temperature decreasing. The temperature at which the depths of micro-and-macro-indentations starts to increase rapidly, can be extracted from the graphs, as shown in the Figure. The three Tg's estimated from the graph in this way, are 150°C and 143°C for the unworn PPO, curves A and B and 114°C for the worn pin of PPO, curve C. The temperature at which considerable softening occurs from the macro-indentation experiment is very close to that at which softening occurs with the micro-indentation experiment, confirming that the temperatures measured by the embedded thermocouple in the pins of PPO are fairly close to the actual surface temperature.

A Thermomechanical Analyser (Perkin-Elmer TMS-1) was also used to determine the softening point of a sample of PPO. The result from this is shown in Fig. 3.36 and the Tg by this method is $147^{\circ} \pm 1^{\circ}\text{C}$, which agrees well with the two previous estimates above.

It is apparent from these results that a reduction in Tg has occurred as a consequence of sliding under boundary-lubricated conditions. Since any reduction in Tg is indicative of plasticisation, it may therefore be concluded that the surface layers of PPO have been plasticised by silicone fluid during sliding conditions of boundary lubrication.

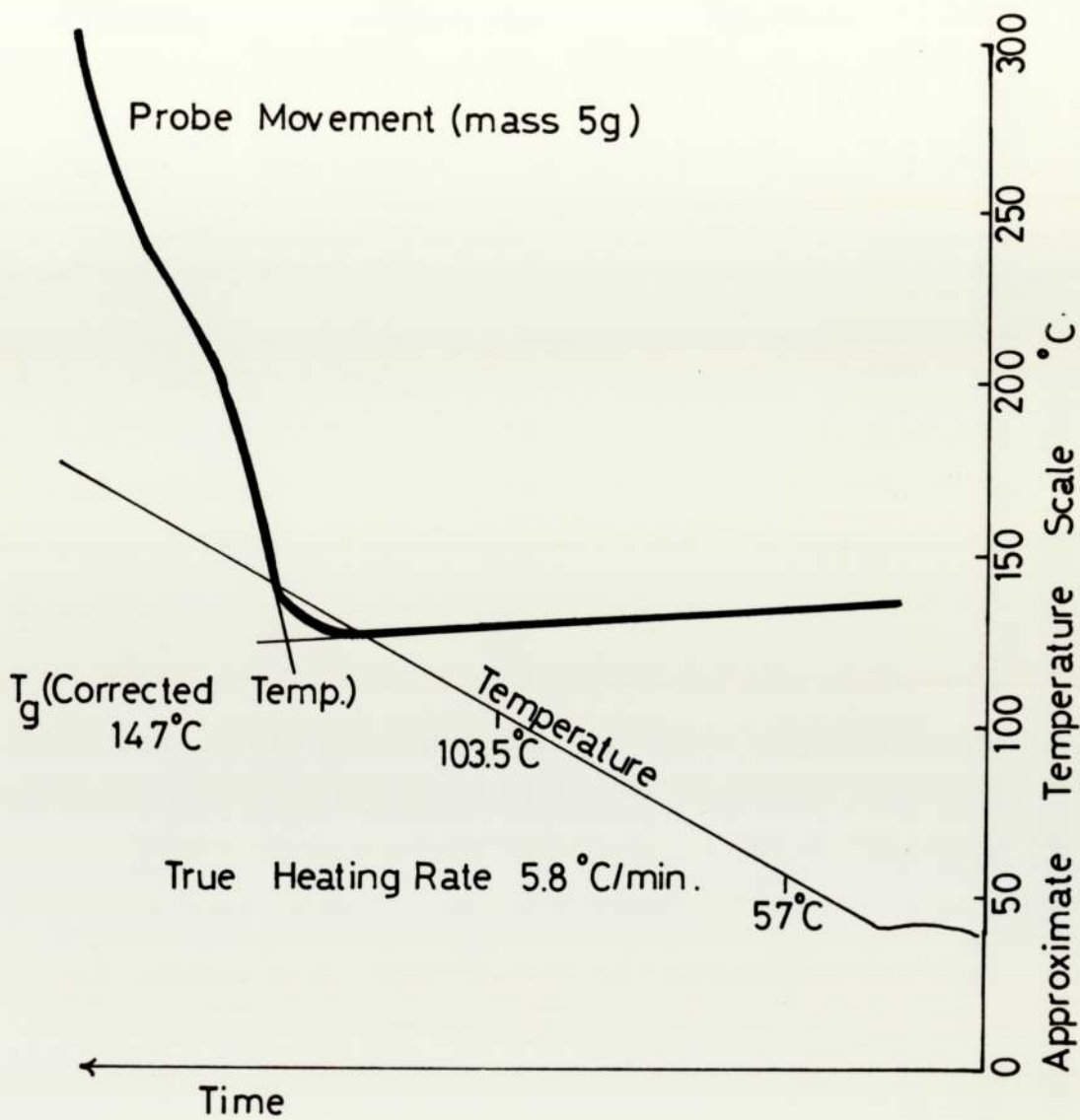


Fig.3.36 Result from Thermomechanical Analyser, giving a T_g of 147 °C.

CHAPTER FOUR

DISCUSSION

One of the most important results from the friction and wear measurements, is that after removal of lubricant from the surface of a pin worn under boundary lubrication conditions and exchange of the counterface for a clean dry one of similar surface roughness and preparation, the coefficient of friction still maintained a low value (Fig. 3.6). Experiments showed that all traces of surface fluid were removed by wiping with absorbent tissue, hence one is forced to conclude that the surface layer of the polymer has been modified in some way. In order to obtain more information concerning this modification of the polymer and the conditions under which it will occur, the sliding speed and number of revolutions of lubrication were varied. The results of these experiments may be conveniently summarized in Fig. 3.7 and Fig. 3.8. Fig. 3.7, for example, indicates that for a speed of 0.0037ms^{-1} , after sliding under boundary-lubricated conditions for 1,000 revolutions and subsequent removal of the lubricant, the coefficient of friction rose to its dry value after only a few microns of wear. However, after sliding under the same conditions for a number of revolutions greater than 2,500, the depths of wear before the friction rose, increased to over a hundred microns. This graph indicates not only the formation of a modified layer but also that there is a critical period of lubricated sliding before the layer is formed. Furthermore, the formation of this layer is confined only to boundary-lubricated sliding conditions, since at the speed of 0.25ms^{-1} under mixed lubrication conditions, even after 900,000 revolutions of sliding and subsequent removal of lubricant, the friction rose immediately to its dry value. The two observations concerning the critical period of sliding to form a modified layer and that a modified layer is not formed outside boundary lubrication conditions are emphasised in Fig. 3.8.

The depth of maximum shear stress, at which crack initiation might be expected, can be calculated from Hertzian elasticity theory (61). For two cylinders in contact, the contact band half-width is given by

$$b = \sqrt{\frac{4P'(K_1 + K_2) R_1 R_2}{R_1 + R_2}}$$

where P' is the load per unit length of the surface of contact,

$$K_1 = \frac{1 - \nu_1^2}{E_1} \quad \text{and} \quad K_2 = \frac{1 - \nu_2^2}{E_2}$$

where ν_1 and ν_2 are the Poisson's ratio for the two materials and E_1 and E_2 are the Young's moduli. R_1 and R_2 are the radii of the two cylinders. If it is assumed that the Young's modulus for steel is far greater than that of the polymer (the ratio is of the order 100/1), then it can be omitted from the equation. From the manufacturer's data, Poisson's ratio for PPO is 0.4, so the equation for the contact band half-width reduces to

$$b = 1.03 \sqrt{\frac{P'R}{E}} \quad \text{and} \quad P' = \frac{L}{l}$$

where L is the load = 1.1 kg

l is the pin diameter = 0.20 cm

and E is Young's modulus for PPO = $2.8 \times 10^4 \text{ kg/cm}^2$

This gives a value of $b = 190 \mu\text{m}$. The depth of maximum shear stress occurs at $0.78b$ which is about $150 \mu\text{m}$. This depth of maximum shear stress will decrease when tangential (frictional) forces are present (62), but even at a coefficient of friction of 0.25 it remains of the order of $0.5b$, which is about $100 \mu\text{m}$. All the coefficients for lubricated sliding were below 0.25. One may envisage that the depth of maximum shear stress at which crack initiation might be expected lies

within the modified layer. However, this cannot be the case, since the R.B.S. and E.P.M.A. results indicate the depth of the modified layer to be about $8 \mu\text{m}$. Hence, the fluid does not penetrate to any depth approaching that of bulk deformation. The penetration of the fluid into the surface must therefore be controlled by asperity deformation. For two balls in contact, from Hertzian elasticity theory, the radius of the area of contact is given by

$$a = \sqrt[3]{\frac{3 \pi P (K_1 + K_2) R_1 R_2}{4 (R_1 + R_2)}}$$

where P is the load = 1.1kg

K_1 and K_2 have the same meaning as previously, R_1 and R_2 are the radii of the two balls. Again, taking a value of $\nu = 0.4$ for PPO and assuming that Young's modulus of steel is far greater than that of the polymer, then this equation may be written

$$a = 1.08 \sqrt[3]{\frac{P R_1 R_2}{E (R_1 + R_2)}}$$

For the case of a hard hemisphere on a flat polymer surface, then R_1 must tend to infinity. Then the above equation reduces to

$$a = 1.08 \sqrt[3]{\frac{P R}{E}}$$

where R is now the radius of an asperity contact. Assuming that the depth of modified layer is commensurate with the depth of maximum shear stress, which neglecting friction is $0.5a$.

For steel abraded to a surface roughness value of $0.1 \mu\text{m C.L.A.}$, then the average radius of the asperities is $20 \mu\text{m}$ (63). Inserting this value, gives a depth of maximum shear stress of approximately $8 \mu\text{m}$ if it is postulated that the load is

supported equally over a distribution of, say, 25 hemispherical asperities. A number, which although not verified experimentally, is not unreasonable.

All the E.P.M.A. results on the worn surface show quite an abrupt end to the modified layer, with the X-Ray intensity for silicon dropping to the background level. Most show a higher concentration on the uppermost part of the surface and this is emphasised more in the R.B.S. results of Fig. 3.27, where a definite concentration gradient exists. The minimum detectable level of silicon is not known, so to check that no Si is present at any significant level, a worn pin was microtomed to a depth of approximately 10 μm . This spectrum is shown in Fig. 3.30, superimposed on the spectrum for the pure granule of PPO. No silicon peak is observed whatsoever, when the background levels are matched.

The results from the micro-and macro indentation experiments show that the fluid has plasticised the polymer, so the surface features shown in the electron micrographs can be regarded as direct effects of plasticisation. For example, the electron micrographs in Fig. 3.19 show plate-like areas raised up from the surface of the polymer. A larger area of raised material is shown in Fig. 3.32(a), and the area of swelling within this raised region (Fig. 3.32(b)) is caused by the diffusion of the fluid into the polymer. Plasticisation is primarily a diffusion-controlled process and depends upon time, temperature, stress and the molecular configuration of both the fluid and the polymer. All of these dependencies are present in a boundary - lubricated sliding system. It is known that some fluids are more 'compatible' than others in their ability to induce plasticisation of polymers. Compatibility can be characterised by their respective solubility parameters. The solubility parameter, δ , is defined as the square root of the cohesive energy density (3),

$$\delta = \left(\frac{\Delta E}{V} \right)^{\frac{1}{2}} \quad (\text{J}^{\frac{1}{2}} \text{m}^{-3/2})$$

where ΔE is the energy of vaporisation at zero pressure and V is the molar volume. The smaller the difference between the solubility parameters of the two substances, then the greater will be the possibility of plasticisation occurring. The solubility parameter for polydimethylsiloxane silicone fluids is $11700 \text{ J}^{\frac{1}{2}}\text{m}^{-3/2}$ and $18400 \text{ J}^{\frac{1}{2}}\text{m}^{-3/2}$ (64) for the PPO. These solubility parameters are not close enough to suppose that plasticisation would occur. Nevertheless, the experimental evidence presented here, suggests that plasticisation has occurred. Briscoe (65) has shown that for a polystyrene/silicone fluid system with monomer repeat units less than three, the fluid can plasticise the polymer. For the 10cs viscosity silicone fluid, the average number of repeat units is 8 (66). However, for silicone fluids, there is a broad distribution of molecular weights and hence number of repeat units. If this effect of plasticisation caused by the lower molecular weight fraction of the overall distribution is general, then one may suppose that plasticisation of the PPO is caused by the lower molecular weight component of the silicone fluid distribution.

Hence, one may say that when PPO slides in the presence of polydimethylsiloxane silicone fluid under boundary - lubricated conditions, a critical period of sliding is required to form a plasticised layer. Further, the depth of this layer is about $8 \mu\text{m}$. When all excess lubricant is removed, this layer gives depths of wear far greater than the $8 \mu\text{m}$ fluid penetration before the coefficient of friction rises to its dry value.

The question which may now be asked is, why should there be a critical period of lubricated sliding before the formation of a plasticised layer? In general, plasticisation will involve a reduction in strength of the surface layers. Initially, transverse features such as those in Fig. 3.31 may be formed on the softened surface of the polymer, as a result of the combination of adhesion and tensile stresses occurring at localised contacts during sliding. The shorter chain-length molecules are always present in the distribution of chain-lengths, but chain-scission

of the longer chain-length molecules could occur. This would effectively increase the concentration of shorter chain-length molecules and lead to further plasticisation. The process of chain-scission will also be time-dependent. Eventually the surface will become weaker and weaker, then fatigue at localised contacts, although always present, will become a more important component of the wear process. This will lead to a more disrupted layer such as that shown in Fig. 3.19(b). Cracks appear to follow the edge of the rings arising from rotation of the pin. The rings themselves consist of plasticised material, raised from the polymer, possibly as a result of adhesion to the counterface. Once crack-formation begins, fluid may be forced into the fissures during sliding. The X-Ray distribution for silicon (Fig. 3.13) indicates discrete areas of silicone fluid penetration. Furthermore, the rings in Fig. 3.19(b) coincide with silicon peaks in the line-scan of Fig. 3.18. The peaks are superimposed on a general level of silicon. The general level of silicon indicates plasticised polymer, and the peaks indicate penetration of the fluid into fissures. The fluid forced into fissures will weaken the surface still further, resulting in the raising of large areas of plasticised material such as that shown in Fig. 3.32. Previous work by Evans (24) for PPO sliding under boundary-lubricated sliding conditions show similar surface features, supporting the above mechanism. For example, with methanol, Fig. 4.1(a) and Fig. 4.1(b) show transverse features. In Fig. 4.1(a), these transverse features have been joined to form quite large fissures in the surface and again shows plate-like areas of plasticised material. In Fig. 4.1(b), a larger area of plasticised material is shown. Thus, the incorporation of the silicone fluid into the PPO involves two mechanisms. Initially, plasticisation, a diffusion process involving the shorter chains of the lubricant, occurs, followed by penetration of the fluid into surface cracks (after a sufficient weakening of the surface) involving the whole distribution of chain-lengths. Once the fluid begins to penetrate the surface fissures, then larger depths of wear before the friction rises to its dry value, will be obtained.

The next question which presents itself is 'why the depths of wear obtained in

(a)



(b)

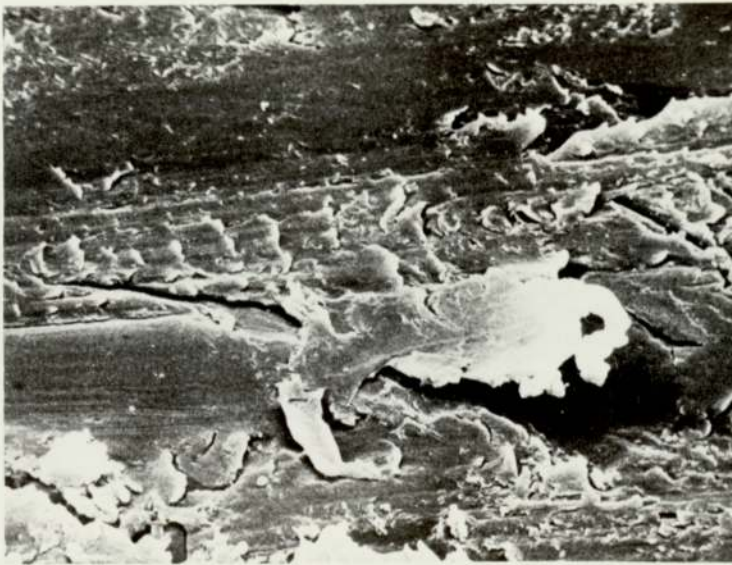


Fig. 4.1(a) and (b) Two Scanning Electron Micrographs of PPO sliding against Stainless Steel in the presence of Methanol under Boundary Lubrication Conditions , (a) Magnification X1500 and (b) Magnification X2000. (Reproduced from Evans(24)).

Fig. 3.7 are of the order of hundreds of microns, when the plasticised layer is only 8 μm in thickness?' The only explanation compatible with both sets of results, is that the layer gradually moves further into the polymer as wear occurs during the 'starved' lubrication period. Fluid which has penetrated the polymer via cracks and fissures during the critical period of lubrication will be trapped below the surface after removal of the excess lubricant, and thus provide a reservoir for a limited amount of continuing boundary lubrication. Of more importance, however, is the possibility that the retained fluid may plasticise the polymer as the uppermost plasticised layer is subsequently removed as a result of wear during the starved lubrication. This reservoir of silicone fluid will contain the whole distribution of chain-lengths, so again chain-scission of the layer chains may occur, thus enabling further plasticisation of the polymer. Eventually, when all the fluid in the layer is 'used up', high friction ensues.

An attempt is now made to quantify the changes in mechanical properties of the surface layer of the polymer which have occurred as a result of plasticisation during boundary-lubricated sliding. Bowden, Gregory and Tabor (25) have proposed an adhesive theoretical description for the boundary lubrication of metals and this was later modified by Rubenstein (41) to take into account changes occurring as a result of plasticisation of polymers during boundary-lubricated sliding. For metals under boundary-lubricated sliding conditions, the lubricant film is thought to break down at small localised regions, resulting in metallic contact. The force to shear these junctions constitutes part of the friction. The remainder of the frictional force is involved in shearing the lubricant film. Bowden et al. have used the following equation to describe the mechanism of the boundary lubrication of metals:-

$$F = A(\alpha S_0 + (1 - \alpha) S_L)$$

where F is the frictional force, A is the real area of contact, α is the fraction of

the real area of contact at which intermetallic contact occurs, S_o is the shear strength of the intermetallic contacts, S_L is the shear strength of the lubricant film. The hardness is given by

$$P_o = \frac{L}{A} \quad \text{so} \quad L = P_o A$$

$$\mu = \frac{F}{L} = \frac{A(\alpha S_o + (1 - \alpha) S_L)}{P_o A} \quad \text{therefore}$$

$$\mu = \frac{\alpha S_o}{P_o} + \frac{(1 - \alpha) S_L}{P_o}$$

Rubenstein applied this equation to the boundary lubrication of polymers, and similarly considered that (i) the frictional resistance arises from adhesion at polymer/metal contacts (ii) boundary lubrication is affected by an adsorbed layer of lubricant molecules. However, he introduced the additional assumption that the mechanical properties of the uppermost layer of the polymer could be changed, in contrast to the situation occurring with metal/metal contacts. He suggested that the mechanical properties of the polymer are affected by penetration of the lubricant molecules and so causes a reduction in hardness and shear strength of the polymer. This indeed is the case; the experimental results discussed earlier, show that the hardness of the polymer has decreased.

Referring back to Fig. 3.3, conditions of boundary-lubricated sliding were achieved for a speed of 0.0037ms^{-1} , a load of 11N and 10cs viscosity silicone fluid. At the onset of sliding, a coefficient of friction can be measured, μ_L^s , where 's' denotes the start of a lubricated experiment and 'L' denotes lubrication. At this point, plasticisation will not have occurred, since Fig. 3.7 and Fig. 3.8 indicate that a substantial amount of time is needed before a plasticised layer is formed. Hence,

$$\mu_L^s = \frac{\alpha S_o}{P_o} + \frac{(1 - \alpha) S_L}{P_o} \quad \text{eqn. 4.2}$$

At the end of a lubricated experiment, after plasticisation has occurred, then S_0 and P_0 will have been affected by the lubricant and changed to S and P , say. The coefficient of friction was measured again, μ_L^e , where 'e' denotes the end of a lubricated experiment. Therefore,

$$\mu_L^e = \frac{\alpha S}{P} + \frac{(1 - \alpha) S_L}{P} \quad \text{eqn. 4.3}$$

When the external lubricant is removed and sliding recommenced against a clean dry counterface, a coefficient of friction can again be measured. In this case $\alpha = 1$, (since no lubricant was present), the shear strength was still S and the hardness was still P . The coefficient of friction, μ_{-L} , where '-L' denotes removal of lubricant, can be written,

$$\mu_{-L} = \frac{S}{P} \quad \text{eqn. 4.4}$$

A coefficient of friction for dry sliding was measured at the same speed and load. Again $\alpha = 1$, and using 'D' to denote dry sliding conditions,

$$\mu_D = \frac{S_0}{P_0} \quad \text{eqn. 4.5}$$

Multiplying eqn. 4.3 by P and rearranging gives

$$(1 - \alpha) S_L = P \mu_L^e - \alpha S$$

substituting into eqn. 4.2

$$\mu_L^s = \frac{\alpha S_0}{P_0} + \frac{P}{P_0} \left(\frac{P \mu_L^e - \alpha S}{P} \right)$$

but $\frac{S_0}{P_0} = \mu_D$ and $\frac{S}{P} = \mu_{-L}$

therefore
$$\mu_L^s = \mu_D + \frac{P}{P_0} (\mu_L^e - \alpha \mu_{-L}) \quad \text{eqn. 4.6}$$

If the ratio $\frac{P}{P_0}$ can be estimated, then α can be found. From the graph Fig. 3.35 showing Micro-Indentation Depth versus Temperature, assuming that the hardness is inversely proportional to the indentation depth, then, for an unworn pin,

$$P_0 \propto \frac{1}{h_0}$$

where P_0 and h_0 are the hardness and indentation depth respectively. Therefore

$$P_0 = \frac{K}{h_0} \quad \text{eqn. 4.7}$$

where K is a constant of proportionality depending on the geometry of the indenter. For a worn pin,

$$P = \frac{K}{h} \quad \text{eqn. 4.8}$$

where P and h are the hardness and indentation depth respectively. From eqn. 4.7 and eqn. 4.8,

$$\frac{P}{P_0} = \frac{h_0}{h} \quad \text{eqn. 4.9}$$

For the temperature range from 23°C to 110°C, the average value for $\frac{P}{P_0}$ is $\frac{2}{3}$. This value is similar to that found by Cohen and Tabor (38) for nylon saturated with water, namely, $\frac{P}{P_0}$ is between $\frac{1}{2}$ and $\frac{1}{3}$. As a result of plasticisation of the surface layer of the PPO, the hardness of the polymer has decreased. Only an estimate of P_0 could be made from Vickers Hardness measurements since the deformation was not completely plastic. P_0 was estimated to be 18Kg/mm², and knowing the load

(1.1kg), the real area of contact was estimated to be 0.06mm^2 . Since the hardness of the polymer has decreased by a factor of $\frac{2}{3}$, then this implies an increase in the real area of contact by a factor of $3/2$, i.e. from 0.06mm^2 to 0.09mm^2 . The apparent area of contact can be calculated from Hertzian elasticity theory (61) using the following equation for a rigid cylinder pressing against a flat surface; the contact band half-width is given by:-

$$a = \sqrt{\frac{2}{\pi}} \left[\frac{WR (1 - \nu^2)}{E} \right]^{\frac{1}{2}}$$

where W is the load per unit length = 0.55kg/mm

R is the radius of the cylinder = 17.5mm

ν is Poisson's ratio and E is Young's modulus for PPO.

The calculated contact band width is equal to 0.4mm . If this is approximated to a rectangular contact area, then, multiplying by the diameter of the wear pin (2mm) gives an apparent area of contact of 0.8mm^2 . The real area of contact is thus about one ninth of the apparent area of contact.

Using the estimate of P_o and knowing α , then S and S_L can be found by substituting back into eqn. 4.3 and eqn. 4.4. By measuring the four coefficients of friction at different speeds within the boundary lubrication regime, the variation of α , S and S_L can be found with sliding speed. Table 4.1 shows these values at a load of 11N and 10cs viscosity silicone fluid. Fig. 4.2, Fig. 4.3, Fig. 4.4 and Fig. 4.5 show the variation of α , S, S_L and μ_L^e with sliding speed based on the values given in Table 4.1.

By choosing speeds at which no experimental data was acquired, values of α , S and S_L can be found from the graphs and substituted into eqn. 4.3 to find values of μ_L^e . For a speed of 0.01ms^{-1} , $\mu_L^e = 0.15$, for 0.001ms^{-1} , $\mu_L^e = 0.021$ and for 0.0001ms^{-1} ,

TABLE 4.1

VALUES FOR μ_D, μ_L^s, μ_L^e AND u_L FOR VARIOUS SPEEDS WITH A LOAD OF 11N AND 10CS VISCOSITY SILICONE FLUID

Speed (ms^{-1})	μ_D	μ_L^s	μ_L^e	μ_L
0.0014	0.38	0.2	0.21	0.19
0.0037	0.38	0.17	0.19	0.13
0.0068	0.38	0.13	0.15	0.12
0.021	0.38	0.1	0.13	0.09

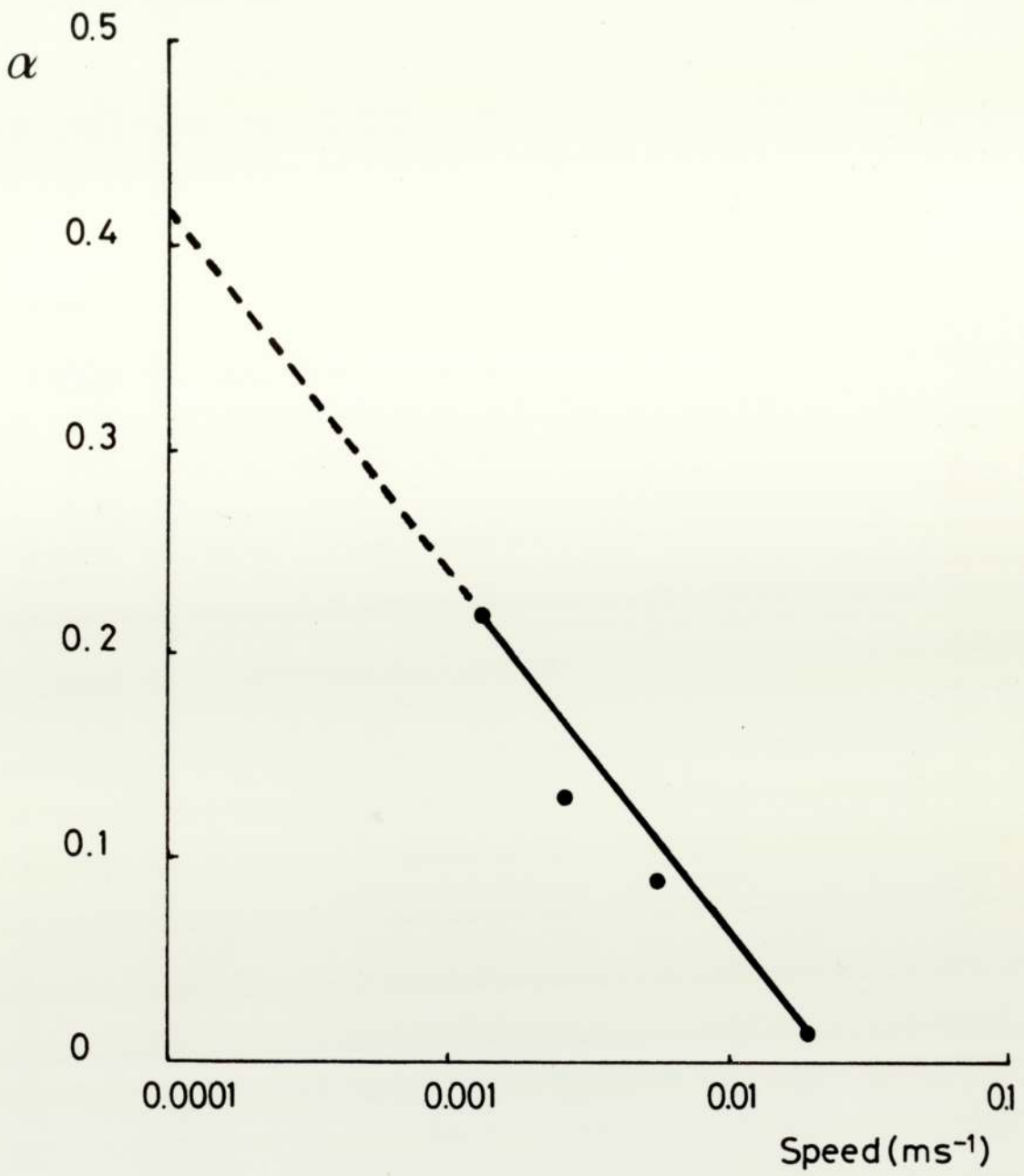


Fig. 4.2 Variation of α , (the Fraction of the Real Area of Contact at which Polymer/Metal Contact occurs) with Sliding Speed.

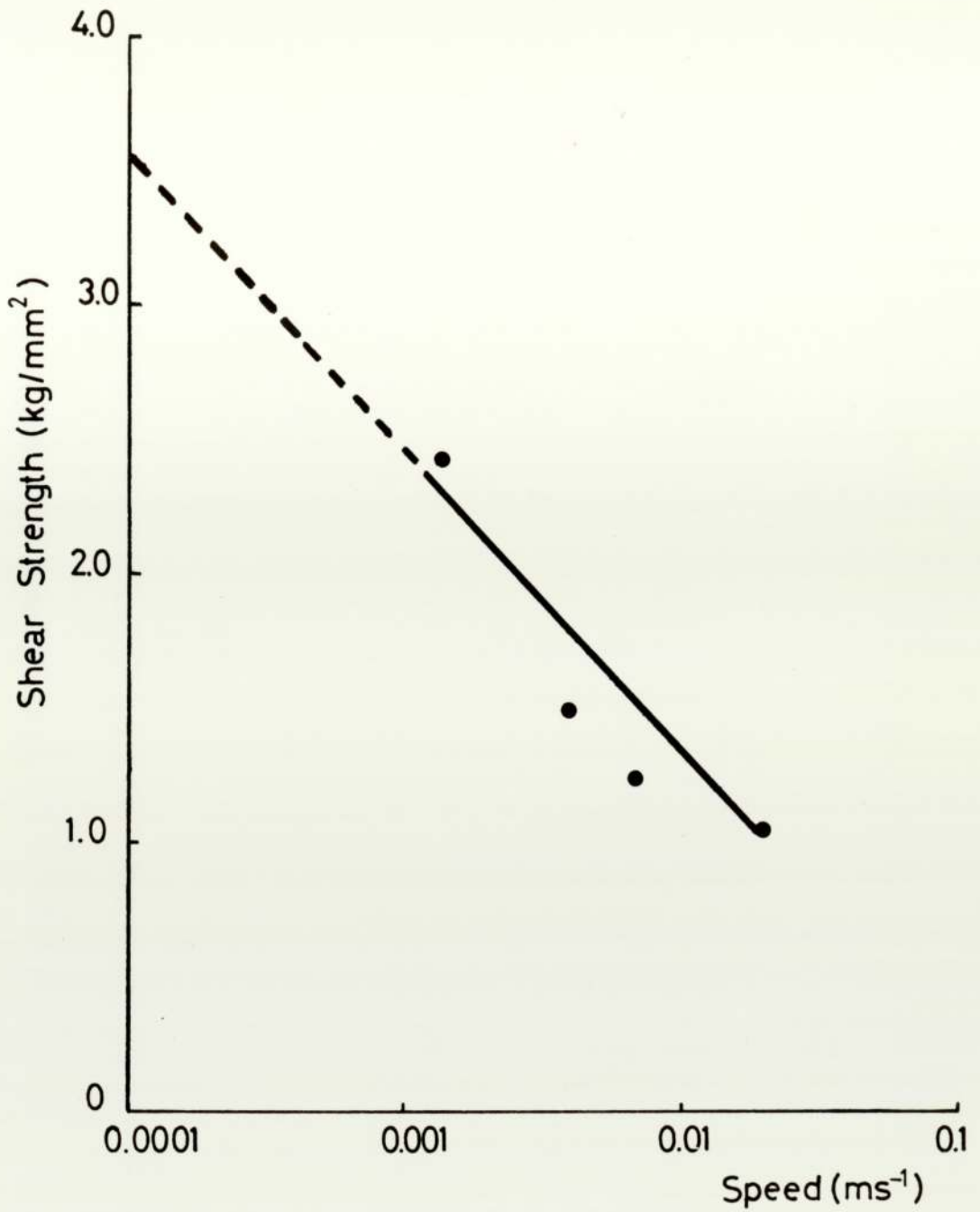


Fig.4.3 Variation of S_s (the Shear Strength of the Polymer) with Sliding Speed.

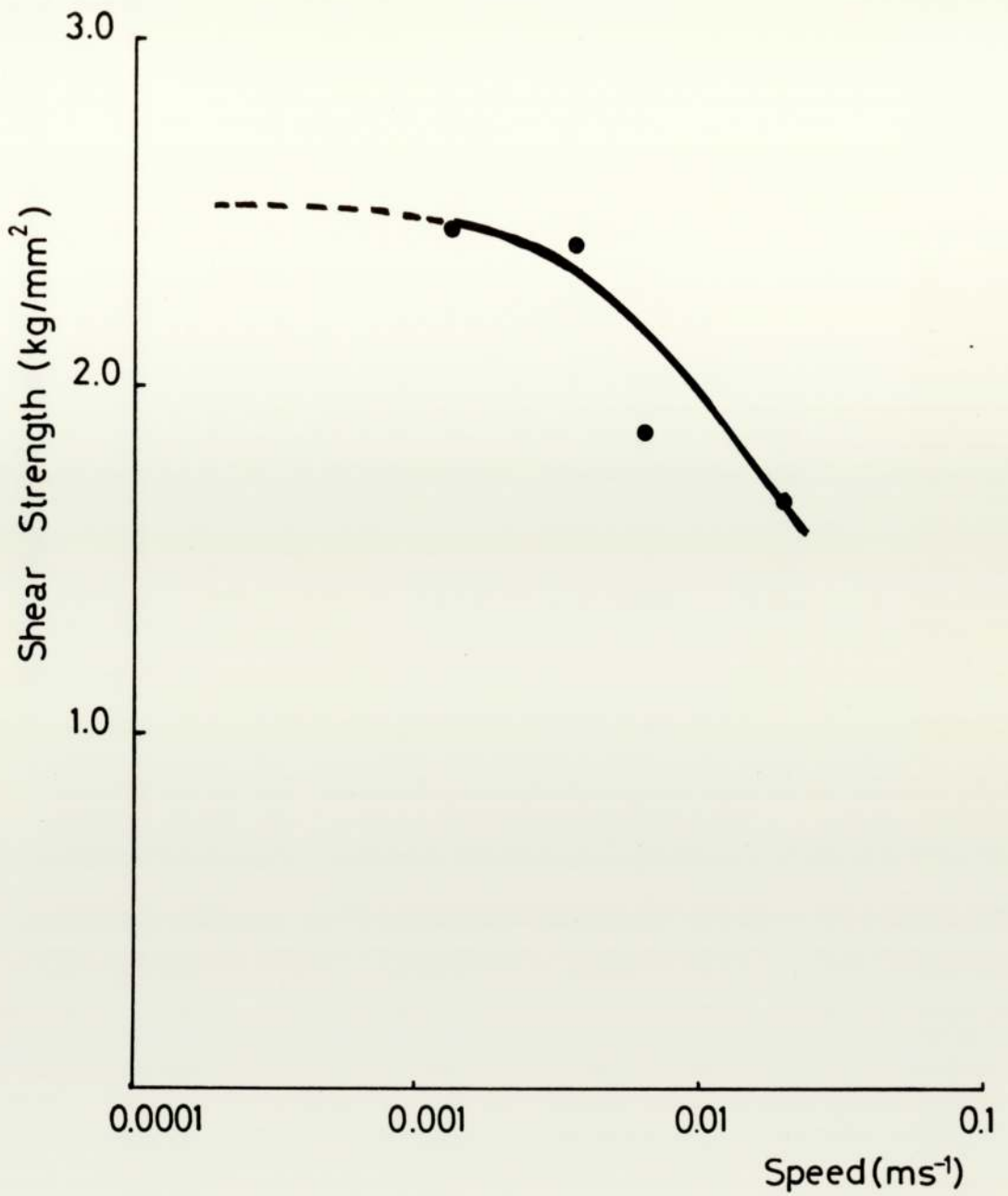


Fig.4.4 Variation of S_L , (the Shear Strength of the Lubricant) with Sliding Speed.

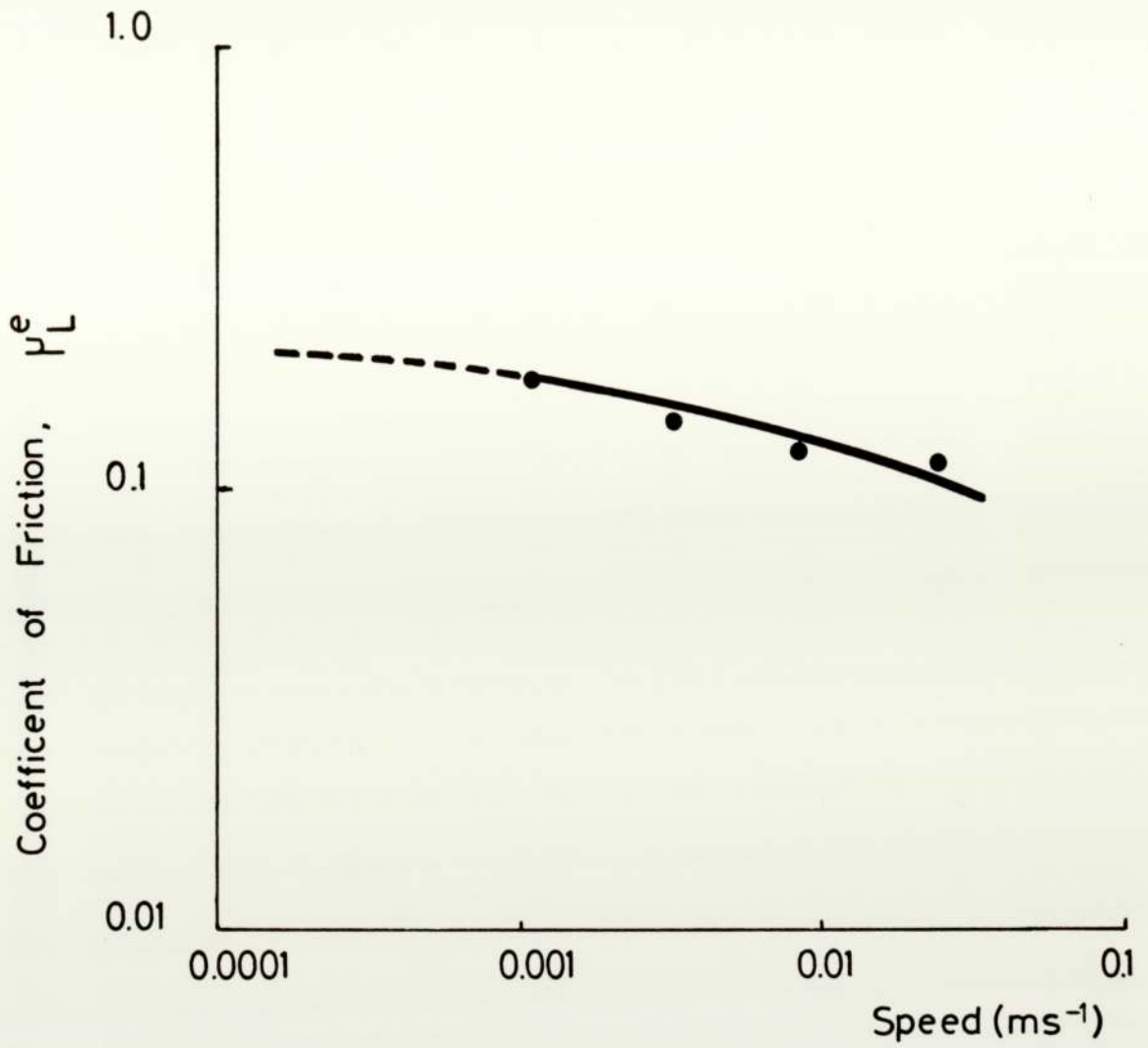


Fig. 4.5 Variation of μ_L^e , (the Coefficient of Friction at the end of a Lubricated Experiment) with Sliding Speed.

$\mu_L^e = 0.25$. These values are in good agreement with the experimental results shown in Fig. 4.5. Similar calculations can be made using eqn. 4.2 to predict μ_L^s . These values can be compared with the coefficients of friction in Fig. 3.3, which is effectively a graph of μ_L^s versus speed, since all these values were taken in the early stages of sliding after allowing enough time for running-in. For 0.01ms^{-1} , $\mu_L^s = 0.13$, for 0.001ms^{-1} , $\mu_L^s = 0.2$ and for 0.0001ms^{-1} , $\mu_L^s = 0.24$. Again, these values are in good agreement with those in Fig. 3.3.

If α is extrapolated back to the speed at which it approaches unity, it is interesting to note that S approaches the value of the bulk shear strength of PPO, 7.74kg/mm^2 (67). The bulk shear strength of the polymer is far greater than any of the shear strengths calculated here, verifying the suggestion by Rubenstein that a reduction in shear strength of the polymer occurs when a lubricant plasticises it.

From Fig. 4.4, it can be seen that the shear strength of the lubricant reaches a constant value at slower speeds within the boundary lubrication regime. This might be expected since the shear strength of the lubricant cannot increase indefinitely. The shear strength S_L , can be seen to vary logarithmically at higher sliding speeds, whilst in Fig. 4.2 and Fig. 4.3, the shear strength of the polymer, S , and α , the ratio of polymer/metal contact to the real area of contact, vary logarithmically at all sliding speeds. As the sliding speed decreases, α is increasing, in other words, a greater proportion of the load is supported by the polymer/metal contacts. This could lead to higher temperatures at these contacts but reduce the temperature at polymer/lubricant/metal contacts. A reduced temperature at the latter contacts will result in an increase in viscosity of the fluid (66) and hence an increase in shear strength of the lubricant.

The logarithmic decrease of shear strength of the polymer, S , with increasing sliding speed is difficult to explain. Briscoe (68) has predicted qualitatively either an increase or decrease in shear strength with sliding speed, depending on whether

the shear strength is dominated by the effects of strain rate or contact time. The effects of shear strain can be modelled by an Eyring activated rate process which yields a logarithmic relation between shear stress and strain. Because of the viscoelastic nature of polymers, the full effect of the pressure may not be realised when the contact time is decreased, i.e. velocity increased. The effective pressure is less than the applied pressure by a factor which is assumed to be an exponential function of velocity. The situation is made even more complex when the effect of temperature is considered also.

CHAPTER FIVE

CONCLUSIONS AND FURTHER WORK

An apparatus has been devised for measuring the friction and wear of polymer-metal combinations in conditions of boundary-lubricated sliding. Line-contact conditions are maintained continuously by slowly rotating a plane-ended, polymer cylinder against the curved surface of a rotating ring.

When polyphenylene oxide slides against hardened steel in the presence of polydimethylsiloxane fluids, a modified layer develops on the polymer which enables low friction to continue even after the removal of all excess fluid from the system. This layer is formed only under conditions of boundary lubrication. A critical period of sliding is required to produce the modified layer.

Surface examination by Rutherford backscattering of α -particles and electron probe microanalysis show that the depth of the modified layer is of the order of 8 μm . This depth does not vary with sliding speed within the boundary lubrication regime.

Estimates of the Glass Transition Temperature of the surface layer indicate that wear-induced plasticisation occurs rather than simple physical mixing.

The formation of the modified layer involves firstly plasticisation of the polymer by the fluid. Plasticisation will lead to a general weakening and reduction in strength of the surface layer. Scanning electron micrographs indicate a softer surface with the appearance of fissures. The fluid is then able to penetrate into the polymer via these surface cracks to a depth which is influenced by asperity rather than bulk deformation. It is thought likely that plasticisation of the polymer will involve the

lower molecular weight component of silicone fluid, initially present and/or formed by chain-scission. However, during penetration of the fluid into cracks, the whole distribution of molecular weights will be present.

The effects of the plasticised surface layer of the polymer on friction and wear in the absence of excess lubricant persist for much longer periods than its thickness would suggest. The only explanation of this consistent with results is that the mechanism by which this occurs involves migration of the fluid within the plasticised layer. The fluid which has penetrated the polymer through surface cracks will be trapped and can act as a reservoir of fluid to provide further plasticisation of the polymer.

Finally, applying a theory of boundary lubrication to polymers, the experimental results yield values of α , the fraction of polymer/metal contact to the real area of contact, S , the shear strength of the polymer and S_L , the shear strength of the lubricant. When making assumptions based on the premise that the friction is of an adhesive nature and that plasticisation causes a reduction in the mechanical properties of the surface layer of the polymer, then these parameters are shown to vary logarithmically with speed. These parameters can be used to calculate values of μ_L^s , the coefficient of friction at the start of a lubricated experiment and μ_L^e , the coefficient of friction at the end of a lubricated experiment. These are found to be in good agreement with the experimental values.

The mechanism of formation of the modified layer on the polymer requires further investigation. For a particular speed within the boundary lubrication regime polymer pins could be examined at regular intervals during the critical period using R.B.S., E.P.M.A., S.E.M. and Gel Permeation Chromatography (G.P.C.). R.B.S. and E.P.M.A. would show the build-up of the layer, whereas S.E.M. might show more extensive production of fissures towards the end of the critical period. G.P.C. could be used to find the molecular weight distributions of both the polymer and

fluid prior to sliding under boundary lubrication conditions. These could be compared with the molecular weight distributions of samples microtomed at regular intervals from different pins worn under boundary-lubricated sliding conditions during the critical period. If plasticisation does take place initially, by the lower molecular weights of the silicone fluid, then this should be reflected in the molecular weight distribution of the silicone fluid. Towards the end of the critical period, one might expect to find the higher molecular weights of the fluid present as well as the lower molecular weights. A suitable solvent is required for the use G.P.C., which will dissolve both the polymer and the fluid. Toluene would be a suitable solvent.

The technique described above would yield information concerning the lower molecular weights of the silicone fluid. However, it would not give any information concerning chain-scission of the higher molecular weights. The silicone fluid used in all these experiments can be mixed to produce different viscosities which are dependent on the relative amounts of the two viscosities initially present. Although 10cs viscosity silicone fluid can be supplied directly by the manufacturer it could be produced from say, a combination of a 1cs and a 100cs fluid or even, a 0.65cs and a 200cs fluid. This means that, although a 10cs fluid is produced, the distribution of molecular weight can be varied. Taking particular combinations of 2 fluids, their molecular weight distributions can be found initially using G.P.C. Then, a similar series of experiments could be carried out whereby the critical period of sliding is examined for each combination of fluid. If chain-scission does occur, then one may expect this to be a time-dependent process and therefore be reflected in the duration of the critical period.

Polymer pins could be immersed in the various molecular weight distributions of the 10cs silicone fluid and the effects of time, temperature and pressure examined using an autoclave. The contact pressure can be estimated from the calculations in the latter part of Chapter 4. Upon removal from the autoclave, various

experiments can be carried out. The surface of the pins can be wiped and a dwell-time test carried out. The pins can be weighed before and after to determine if there has been any absorption of fluid. The pins could also be analysed using G.P.C.

Having established the ways in which silicone fluid can influence the friction and wear of polyphenylene oxide, polymer-fluid combinations of greater practical importance should be examined. These should include polymers such as polyacetal, polyphenylene sulphide and PTFE. Composites, such as a reinforced phenolic resin and filled PTFE should also be examined. The fluids should include a mineral oil, a synthetic hydraulic fluid and water. The objective of this work would be to establish material combinations and conditions of sliding for which fluid contamination is either detrimental or advantageous to performance in a dry bearing.

APPENDIX 1

Target Information	[Table of Chemical Symbols
		Table of Atomic Numbers
		Table of Atomic Masses
		Table of Isotope Masses
		Table of Isotope Relative Abundances
		Table of Normal Densities (Atoms/cm ³)
Projectile Information	[Table of Stopping Cross-sections
Detector Information	[Table of Energy Loss in Detector Dead Layer
Experimental Information	[Projectile Atomic Number, Mass and Energy
		Target Tilt to the Beam
		Detector Angle, Solid Angle and Resolution (FWHM)
		Total Projectile Coulombs
		Multichannel Analyser (keV/Channel)

REFERENCES

1. Lancaster, J.K., "Dry Bearings : A Survey of Materials and Factors affecting their Performance." *Tribology*, 6, pp 219-252 (1973).
2. King, R.B., "Wear Properties of Dry Bearing Liners at Ambient and Elevated Temperatures - A Preliminary Survey". *Wear*, 56, pp 37-53 (1979).
3. Williams, D.J., *Polymer Science and Engineering*, Prentice-Hall, Inc., New Jersey (1971).
4. Israelachvili, J.N. and Tabor, D., "Van der Waals Forces : Theory and Experiment." *Progr. in Surface and Membrane Sci.*, 7, pp 1-55 (1973).
5. Lee, L-H., "Effect of Surface Energetics on Polymer Friction and Wear". *Advances in Polymer Friction and Wear*, (Lee, L-H., ed.), *Polymer Science and Technology Symposia Series*, Plenum Press, New York, Vol. 5A, pp 31-66 (1974).
6. Tabor, D., "Friction, Adhesion and Boundary Lubrication of Polymers". *Advances in Polymer Friction and Wear*, (Lee, L-H., ed.), *Polymer Science and Technology Symposia Series*, Plenum Press, New York, Vol. 5A, pp 5-30 (1974).
7. Lancaster, J.K., "Wear Mechanisms of Metals and Polymers." *Trans. Inst. Met. Fin.*, 56, pp 145-153 (1978).
8. Buckley, D.H. and Brainard, W.A., "The Atomic Nature of Polymer-Metal Interactions in Adhesion, Friction and Wear." *Advances in Polymer Friction and Wear*, (Lee, L-H., ed.), *Polymer Science and Technology Symposia Series*, Plenum Press, New York, Vol. 5A, pp 315-331 (1974).
9. Shooter, K.V. and Tabor, D., "The Frictional Properties of Plastics." *Proc. Phys. Soc.*, B65, pp 661-671 (1952).
10. Eiss, N.S., Warren, J.H. and Quinn, T.F.J., "On the Influence of the Degree of Crystallinity of PCTFE on its Transfer to Steel Surfaces of Different Roughnesses." *The Wear of Non-metallic Materials. Proc. of the 3rd Leeds-Lyon Symp. on Tribol.*, (Dowson, D., Godet, M. and Taylor, C.M., ed.), *Mech. Eng. Publ. Ltd.*, London, pp 18-24 (1978).
11. Rhee, S.H. and Ludema, K.C., "Transfer Films and Severe Wear of Polymers." *The Wear of Non-metallic Materials. Proc. of the 3rd Leeds-Lyon Symp. on Tribol.*, (Dowson, D., Godet, M. and Taylor, C.M., ed.), *Mech. Eng. Publ. Ltd.*, London, pp 11-17 (1978).
12. Tanaka, K. and Miyata, T., "Studies on the Friction and Transfer of Semi-crystalline Polymers." *Wear*, 41, pp 383-398 (1977).
13. Pooley, C.M. and Tabor, D., "Friction and Molecular Structure : the Behaviour of some Thermoplastics". *Proc. Roy. Soc. Lond. Ser. A* 329, pp 251-274 (1972).
14. Briscoe, B.J., "How Long Do Polymers Last in Service?" *P.R.I. Conf.*, London, Paper 9, Feb. (1977).
15. Tabor, D., "The Mechanism of Rolling Friction II. The Elastic Range". *Proc. Roy. Soc. Lond. Ser. A* 229, pp 198-220 (1955).
16. Rabinowicz, E., *Friction and Wear of Materials*, Wiley, New York, (1965).

17. Halliday, J.S., "Surface Examination by Reflection Electron Microscopy." Proc. Inst. Mech. Eng., 169, pp 777-787 (1955).
18. Greenwood, J.A. and Williamson, J.P.B., "Contact of Nominally Flat Surfaces." Proc. Roy. Soc. Lond. Ser. A 295, pp 300-319 (1966).
19. Evans, D.C. and Lancaster, J.K., "The Wear of Polymers". Treatise on Mat. Sci. and Tech. Vol. 13, Wear. (Scott, D., ed.), Academic Press Inc., New York, pp 85-139 (1979).
20. Ratner, S.B., Farberova, I.I., Radyukevich, O.V. and Lure, E.G., "Connection between Wear-resistance of Plastics and other Mechanical Properties." Abrasion of Rubber, (James, D., ed.), Maclaren, London, pp 145-154 (1967).
21. Lancaster, J.K., "The Formation of Surface Films at the Transition between Mild and Severe Metallic Wear". Proc. Roy. Soc. Lond. Ser. A 273, pp 466-483 (1963).
22. Lancaster, J.K., "Lubrication of Carbon Fibre-reinforced Polymers". Wear, 20, pp 315-334 (1972).
23. Caubet, J-C., Amsallem, C. and Cros, G., "Technologie du Frottement dans L'eau de Mer". Sciences et Techniques, 11, pp 27-38 (1967).
24. Evans, D.C., "Polymer-Fluid Interactions in Relation to Wear". The Wear of Non-metallic Materials. Proc. of the 3rd Leeds-Lyon Symp. on Tribol., (Dowson, D., Godet, M. and Taylor, C.M., ed.), Mech. Eng. Publ. Ltd., London, pp 47-55 (1978).
25. Bowden, F.P., Gregory, J.N. and Tabor, D., "Lubrication of Metal Surfaces by Fatty Acids". Nature, 156, pp 97-101 (1945).
26. Bowden, F.P. and Tabor D., The Friction and Lubrication of Solids, Part I, Oxford University Press, Oxford, (1950).
27. Dowson, D., "Transition to Boundary Lubrication from Elastohydrodynamic Lubrication". Boundary Lubrication-An Appraisal of World Literature. (Ling, F.F., Klaus, E.E. and Fein, R.S., ed.) A.S.M.E., pp 229-240 (1969).
28. Stribeck, R., "Characteristics of Plain and Roller Bearings". (in German), Zeit. V.D.I., 46, pp 1341-48, 1432-38, 1463-70 (1902).
29. Akhmatov, A.S., Molecular Physics of Boundary Friction, Israel Programme for Scientific Translations Ltd., (1966).
30. Allen, C.M. and Drauglis, E., "Boundary Layer Lubrication : Monolayer or Multilayer". Wear, 14, pp 363-384 (1969).
31. Bowers, R.C. and Murphy, C.M., "Status of Research on Lubricants, Friction and Wear." N.R.L. Rep. 6486 (1967).
32. Fort, T. Jr., "Adsorption and Boundary Friction on Polymer Surfaces." J. Phys. Chem., 66, pp 1136-1143 (1962).
33. Cudworth, C.J. and Higginson, G.R., "Friction of Lubricated Soft-surface Layers". Wear, 37, pp 299-312 (1976).
34. Archard, J.F. and Kirk, M.T., "Influence of Elastic Modulus on the Lubrication of Point Contacts". Proc. Inst. Mech. Eng. Labr. and Wear Convent., pp 181-189 (1963).

35. Matveevskii, R.M., "The Effect of the Polarity of Oil on the Friction of some Plastics". *Wear*, 4, pp 300-310 (1961).
36. Vinogradov, G.V. and Bezborodko, M.D., "Friction, Wear and Lubrication of Plastics". *Wear*, 5, pp 467-477 (1962).
37. Reh binder P., Lichtmann, V.I. and Mastenikov, V.M., "Deformation of Single Crystals of Metals as Facilitated by Absorption of Surface Active Substances." *C.R. Acad. Sci. URSS*, 32, pp 125-129 (1941).
38. Cohen, S.C. and Tabor, D., "The Friction and Lubrication of Polymers". *Proc. Roy. Soc. (Lond. Ser.) A* 291, pp 186-207 (1966).
39. Owens, D.K., "Friction of Polymer Films. I. - Lubrication". *J. Appl. Poly. Sci.*, 8, pp 1465-1475 (1964).
40. Senior, J.M. and West, G.H., "Interaction between Lubricants and Plastic Bearing Surfaces". *Wear*, 18, pp 311-323 (1971).
41. Rubenstein, C., "Lubrication of Polymers". *J. Appl. Phys.*, 32, pp 1445-1450 (1961).
42. Tanaka, K., "Friction and Wear of Semi-Crystalline Polymers sliding against Steel under Water Lubrication". *Wear of Materials*, (Ludema, K., Glaesar, W.A. and Rhee, S.K., ed.), A.S.M.E., pp 563-572 (1979).
43. Evans, D.C., "The Wear of Plastics Materials in Water and Aqueous Solutions". *R.A.E. Tech. Rep. TR 78061*, (1978).
44. Kambour, R.P., "A Review of Crazing and Fracture in Thermoplastics". *J. Poly. Sci. Macromol. Rev.*, 7, pp 1-154 (1973).
45. Booser, E.R., Scott, E.H. and Wilcock, D., "Compatibility Testing of Bearing Materials". *Proc. Inst. Mech. Eng. Lubr. and Wear Conf.*, London, pp 366-370 (1957).
46. Pratt, G.C., "Plastic-based Bearings". Chapter 8, *Lubrication and Lubricants*, (Braithwaite, E.R., ed.), Elsevier, pp 337-426 (1967).
47. Allen, A.J.G., "Surface Properties of Polyethylene : Effect of an Amphipathic Additive". *J. of Colloid Sci.*, 14, pp 206-221 (1959).
48. Briscoe, B.J., Mustafaev, V. and Tabor, D., "Lubrication of Polythene by Oleamide and Stearamide." *Wear*, 19, pp 339-414 (1972).
49. Bowers, R.C., Jarvis, R.C. and Zisman, W.A., "Reduction of Polymeric Friction by Minor Concentrations of Partially Fluorinated Compounds". *Ind. Eng. Chem. Prod., Res. and Develop.*, 4, pp 86-92 (1965).
50. Ikeda, H. "Plastic-based Anti-friction Materials". *Japanese Patent 75 101, 441* (1975).
51. Arkles, B.C. and Theberge, J., "Migratory Internal Lubrication of Thermoplastic Resins". *Lubr. Eng.*, 29, pp 552-555 (1973).
52. Hill, M.P.L., Millard, P.L. and Owen, M.J., "Migration Phenomena in Silicone Modified Polystyrene." *Advances in Polymer Friction and Wear*, (Lee, L-H., ed.), *Polymer Science and Technology Symposia Series*, Plenum Press, New York, Vol. 5B, pp 469-479 (1974).

53. Fearon, F.W.G. and Smith, R.F., "Wear Characteristics of Silicone Modified Polystyrene". *Advances in Polymer Friction and Wear*, (Lee, L-H., ed.), *Polymer Science and Technology Symposia Series*, Plenum Press, New York, Vol. 5B, pp 481-490 (1974).
54. Pascoe, M.W. and Dzhankmedov, A.K., "The Wear of Oil Filled Thermoplastics". *The Wear of Non-metallic Materials. Proc. of the 3rd Leeds-Lyon Symp. on Tribol.*, (Dowson, D., Godet, M. and Taylor, C.M., ed.), *Mech. Eng. Publ. Ltd., London*, pp 60-64 (1978).
55. Abouelwafa, M.N., Dowson, D. and Atkinson, J.R., "The Wear and Mechanical Properties of Silicone Impregnated Polyethylene". *The Wear of Non-metallic Materials. Proc. of the 3rd Leeds-Lyon Symp. on Tribol.*, (Dowson, D., Godet, M. and Taylor, C.M., ed.), *Mech. Eng. Publ. Ltd., London*, pp 56-59 (1978).
56. Hutchins, G.A., *Characterization of Solid Surfaces*, Ch. 8, (Kane, P.F. and Larrabee, G.B., ed.), *Plenum Press, New York*, pp 441-484 (1974).
57. Mitchell, I.V., "Rutherford Backscattering". *Physics Bulletin*, 30, pp 23-25 (1979).
58. Ziegler, J.F., "Material Analysis by Nuclear Backscattering". *New Uses of Ion Accelerators*, (Ziegler, J.F., ed.), *Plenum Press, New York*, pp 75-103 (1975).
59. Ziegler, J.F., Lever, R.F. and Hirvonen, J.K., "Computer Analysis of Nuclear Backscattering". *Ion Beam Surface Layer Analysis*, (Meyer, O., Linker, G. and Kappeler, F., ed.), *Plenum Press, New York*, Vol. 1, pp 163-183 (1976).
60. Burcham, W.E., *Nuclear Physics : An Introduction*, Longman, London (1973).
61. Timoshenko, S.P. and Goodier, J.N., *Theory of Elasticity*, McGraw-Hill, New York (1951).
62. Hamilton, G.N., *Stress in Hertzian Contacts*. Ph.D. Thesis, University of Reading (1965).
63. Hollander, A.E. and Lancaster, J.K., "An Application of Topographical Analysis to the Wear of Polymers". *Wear*, 25, pp 155-170 (1973).
64. *Polymer Handbook*, (Brandrup, J. and Immergut, E.H., ed.), Interscience, London, (1966).
65. Briscoe, B.J., Discussion on "The Influence of Polydimethyl Siloxane on the Friction and Wear of Polyphenylene Oxide under Boundary Lubrication Conditions". by Skelcher, W.L., Quinn, T.F.J. and Lancaster, J.K. To be Published, *A.S.L.E. Trans.* (1982).
66. M.S. Silicone Fluids, Technical Data Sheet, G1.
67. *Enc. of Polymer Science and Technology*, Vol. 10, Phenols, Oxidative Polymerization, Wiley, New York (1969).
68. Briscoe, B.J. and Smith A.C., "The Effect of Periodic Loading on the Shear Strength Properties of Thin Organic Polymeric Films". *A.S.L.E. Trans.*, 23, 3, pp 232-236 (1980).